

## ABSTRACT

Title of Dissertation: **BERRY PHASE AND TOPOLOGICAL RESPONSE  
IN INTERACTING QUANTUM SYSTEMS:  
FROM WEYL SEMIMETALS  
TO CHIRAL SUPERCONDUCTORS**

Shuyang Wang  
Doctor of Philosophy, 2025

Dissertation Directed by: **Professor Jay Deep Sau**  
Department of Physics

Topological responses rooted in the Berry phase play an important role in modern condensed matter physics. However, in interacting quantum systems, the robustness and observability of such responses require careful analysis and examination. This dissertation comprises two studies on how topological phenomena, namely the chiral anomaly and the anomalous Hall effect, emerge and are (un)renormalized in interacting quantum systems.

The first part investigates the robustness of the chiral anomaly in interacting systems through a mixed anomaly framework. The chiral anomaly is one of the robust quantum effects in relativistic field theories with chiral symmetry, where charges in the chiral sectors appear to be separately conserved. The chiral anomaly, which is often associated with a renormalization-invariant topological term, is a violation of this conservation law because of quantum effects. In condensed matter systems like Weyl semimetals, analogous phenomena emerge as charge pumping between Fermi pockets under electromagnetic fields. However, because the chiral charge is

defined in terms of low energy quasiparticles, most studies of the chiral anomaly in condensed matter apply to effectively non-interacting systems. We apply an approach in which the chiral symmetry in solid materials is viewed as a so-called emanant symmetry of the underlying space translation symmetry, a mixed anomaly between the charge  $U(1)$  and space translation. In this framework, the chiral charge is associated with total momentum, and we show that the corresponding chiral anomaly remains unrenormalized by interactions in contrast to other chiral charges in  $(1 + 1)D$  whose renormalization is dependent on regularization. In  $(3 + 1)D$ , is equivalent to the charge transferred between Fermi surfaces which can be measured through changes in Fermi-surface-enclosed volume. To measure this effect, we propose a pump-probe technique.

The second part turns to another Berry-phase-related response, the anomalous Hall effect in the phase-disordered regime of chiral superconductors. Motivated by recent experiments showing evidence for chiral superconductivity in an anomalous Hall phase of tetralayer graphene, we study the relationship between the normal state anomalous Hall conductivity and that in the phase-disordered state slightly above the critical temperature of the superconductor. Numerical simulations show that the Berry phase on the Fermi surface determines the charge asymmetry between vortices and antivortices, resulting in a nonzero Hall response that is close to the normal-state anomalous Hall response. However, using a gauge-invariant superconducting response framework, we find that while the vortex charge is screened by interactions, the screening charge, after a time delay, reappears in the longitudinal current. Thus, in this phase, the dc Hall conductivity aligns with the ac Hall conductance of the superconducting and normal phases, rather than with the screened vortex charge.

BERRY PHASE AND TOPOLOGICAL RESPONSE IN INTERACTING  
QUANTUM SYSTEMS:  
FROM WEYL SEMIMETALS  
TO CHIRAL SUPERCONDUCTORS

by

Shuyang Wang

Dissertation submitted to the Faculty of the Graduate School of the  
University of Maryland, College Park in partial fulfillment  
of the requirements for the degree of  
Doctor of Philosophy  
2025

Advisory Committee:

Professor Jay Deep Sau, Chair/Advisor  
Professor Sankar Das Sarma  
Professor Christopher Jarzynski  
Professor Victor M. Yakovenko  
Professor Mohammad Hafezi

© Copyright by  
Shuyang Wang  
2025

## Acknowledgments

I owe my deepest gratitude to my advisor, Professor Jay Deep Sau, for his support and supervision throughout my Ph.D study. He has always been generous with his time and patient with my questions and emails, especially in the early stages when I was still studying how to do my first Ph.D. research. I have learned a lot from him – not just technical tools, methods and experimental results, but also how to think clearly, develop and share ideas, and tackle problems with a structured and multi-perspective approach. I really appreciate his kindness, high standards, and the freedom he gave me to explore ideas and grow as a junior researcher.

I first met my advisor when he was assigned as my academic advisor during my first year. In that meeting, he gave me many suggestions on choosing the basic Ph.D. courses and how to enjoy the Ph.D. life, and also introduced me many of the topics he was working on, which left a strong impression on me and planted the seed of my interest in condensed matter theory.

After taking some core physics courses, I went back to him and asked about joining his research group. Instead of directly starting a project he already came up with, he encouraged me to explore the research landscape at CMTC (Condensed Matter Theory) and talk to other faculties and students to figure out what truly interested me. This really helped me to get a sense of many different subfields in this large research group and expanded my scope of condensed matter physics.

During that time, I had many inspiring discussions with Professor Victor Galitski's stu-

dents, Alireza Parhizkar and Colin Rylands. One of their projects, chiral anomaly, caught my attention. When I talked with my advisor, we realized it was a promising direction we were both interested in. That eventually led to my first research project, which became the beginning of my research life and the first part of this dissertation.

I also want to express my gratitude to my committee members – Professor Sankar Das Sarma, Professor Christopher Jarzynski, Professor Victor M. Yakovenko, and Professor Mohammad Hafezi – for generously making time in a busy August to attend my defense, and for their meaningful feedback and support about my dissertation.

I would also like to thank the CMTC community for creating such a friendly and helpful environment. In particular, I want to thank CMTC for organizing seminars that were extremely helpful and covered a wide range of topics across different subfields of condensed matter theory and experiment. I also want to thank Stuart Yi-Thomas, Yi-Ting Tu, and Doctor Katharina Laubscher for discussions and support. I also thank former CMTC members and friends Doctor Haining Pan, Doctor Huan-Kwang Wu, Rebecca Cawthorne, Erika Martin, Doctor Yi-Hua Lai, Doctor Haonan Xiong, Kaixin Huang, Doctor Zhiyu Yin, Doctor Mingshu Zhao, and Doctor Wance Wang for their help and friendship. You all made my time at Maryland a lot more fun and fulfilling.

Finally, I want to thank my family. To my mom, Hongmei Tuo, and my dad, Yun Wang, thank you for your endless support and encouragement. And to my wife, Yixin Wu, thank you for being there for me through everything. I could not have done this without you.

Thanks to everyone who helped me along the way.

## Table of Contents

Acknowledgements	ii
Table of Contents	iv
List of Figures	vi
List of Abbreviations	vii
List of Symbols	viii
List of Publications	xii
Chapter 1: Introduction	1
1.1 Berry Phase and Topological Phenomena . . . . .	4
1.1.1 Geometric Phase and Curvature . . . . .	4
1.1.2 Chern Number and Quantized Response . . . . .	5
1.2 Chiral Anomaly . . . . .	6
1.2.1 Chiral Anomaly in 1D Electron Systems . . . . .	7
1.2.2 Chiral Anomaly in Weyl Semimetals . . . . .	10
1.3 Anomalous Hall Effect . . . . .	13
1.4 Outline . . . . .	16
Chapter 2: Interaction Robustness of Chiral Anomaly in 1D	18
2.1 Regularization Dependence of the Chiral Anomaly . . . . .	18
2.1.1 Application to Interacting Spin-orbit Coupled Fermions . . . . .	23
2.1.2 Relativistic Anomaly in Condensed Matter Systems . . . . .	24
2.2 Momentum-based Chiral Anomaly from a Mixed Anomaly Approach . . . . .	28
2.2.1 Application: Chiral Charge Conservation between LLs with Different $K$ . . . . .	34
2.3 Discussion and Summary . . . . .	37
Chapter 3: Interaction Robustness of Chiral anomaly in 3D	38
3.1 Momentum-based Anomaly . . . . .	39
3.2 Luttinger Volume-based Chiral Charge . . . . .	42
3.3 Chiral Kinetic Theory . . . . .	45
3.4 Chiral Anomaly in the Landau Level Regime . . . . .	50
3.4.1 Non-interacting Weyl Model Under a Magnetic Field . . . . .	50
3.4.2 Momentum-based Chiral Charge . . . . .	51

3.4.3	Interaction Effects . . . . .	53
3.5	Measuring the Luttinger-volume-based Chiral Anomaly . . . . .	54
3.6	Discussion and Summary . . . . .	56
Chapter 4:	Anomalous Hall Effect from Screened Vortex Charge in Phase-Disordered Superconductors	58
4.1	Effective Action of a Hall Superconductor . . . . .	59
4.2	Electromagnetic Response . . . . .	61
4.3	Vortex Charge in an Anomalous Hall Superconductor . . . . .	64
4.4	Hall Response of the BKT Phase . . . . .	67
4.5	Vortex Charge Screening . . . . .	69
4.6	Discussion and Conclusion . . . . .	71
Appendix A:	Details of Bosonization	73
A.1	Lorentz-invariance-constrained Chiral Anomaly . . . . .	73
A.2	Chiral Anomaly with Non-Lorentz-invariant Point-splitting Regularization . . . . .	75
Appendix B:	Current $j$ v.s. Chiral Charge $\rho_{c, sb}$	78
Appendix C:	Kinetic Stress-energy Tensor $K^{\mu\nu}$ and Its Gauge-invariance	81
Appendix D:	Chiral Magnetic Effect Current in Chiral Kinetic Theory	86
Appendix E:	Second-order Term of the ac Hall Conductivity in the Chern Insulator	90
Bibliography		94

## List of Figures

2.1	Illustration of the Chiral Anomaly in the Sine-Gordon Model . . . . .	26
3.1	Schematic of a scattering pattern around the Fermi surface at finite $T$ . . . . .	44
3.2	Band structure of Weyl model with a small spin-orbit coupling under a magnetic field . . . . .	51
4.1	Schematic for the Origin of Anomalous Hall in a 2D Superconductor Above the BKT Transition . . . . .	58
4.2	Charge Difference and Hall Conductivity as Functions of Chemical Potential in a Lattice Model . . . . .	65
E.1	Second order conductivity $\sigma_{xy}^{(2)}$ v.s. the parameter $m$ . . . . .	93

## List of Abbreviations

1D	One-Dimensional
3D	Three-Dimensional
AQH	Anomalous Quantum Hall
BKT	Berezinski-Kosterlitz-Thouless
BZ	Brillouin Zone
CI	Chern Insulator
CME	Chiral Magnetic Effect
CSC	Chiral Superconductor
DOS	Density of States
FL	Fermi Liquid
FQH	Fractional Quantum Hall
FS	Fermi Surface
IQH(E)	Integer Quantum Hall (Effect)
IR	Infrared
LL	Luttinger Liquid
QED	Quantum Electrodynamics
QPC	Quantum Point Contact
QWZ	Qi-Wu-Zhang
RHS	Right hand Side
RPA	Random Phase Approximation
SC	Superconductor
TKNN	Thouless, Kohomoto, Nightingale and den Nijs
TL	Tomonaga-Luttinger
UV	Ultraviolet

## List of Symbols

$A_\alpha$	Electromagnetic gauge field
$A_\alpha(k)$	Cross-sectional area in momentum space
$\mathcal{A}(\lambda)$	Berry connection in parameter space
$B_T$	Transverse magnetic field
$C$	Chern number
$C^{\mu\nu}$	Stress-energy tensor correction
$C_1$	Superfluid compressibility
$C_2$	Superfluid stiffness
$C_3$	Gradient term coefficient
$C_4$	Chern-Simons term coefficient
$C_5$	Chiral conductivity term
$D_\mu$	Covariant derivative
$\Delta$	Superconducting gap
$\Delta Q_v$	Vortex charge difference
$\Delta\mu$	Chemical potential difference
$\Delta_0$	Zero-temperature gap
$E(\omega)$	Electric field
$E_F$	Fermi energy
$E_T$	Transverse electric field
$\tilde{E}_v$	Effective electric field for vortices
$F_{\mu\nu}$	Electromagnetic field strength
$\tilde{\mathcal{F}}_{\mu\nu}$	Berry curvature 2-form
$\tilde{f}$	Modified distribution function
$G$	DC conductance
$G(k, \omega, \mu)$	Green's function
$G_{\mathbf{k}}$	Phase-space factor
$\gamma_n$	Berry phase
$\gamma_\alpha$	Chirality of Weyl node
$\gamma^\mu$	Gamma matrices
$\gamma_5$	Chirality matrix
$\Gamma$	Spin-orbit coupling strength
$g$	Coupling constant in Sine-Gordon model
$g_2, g_4$	Luttinger model couplings
$H(\lambda)$	Hamiltonian with parameter $\lambda$

$H_{1DEG,approx}$	1DEG low-energy approximate Hamiltonian
$H_{csc,0}$	Normal-state Hamiltonian of chiral superconductor
$H_{csc,BdG}$	Bogoliubov–de Gennes Hamiltonian of chiral superconductor
$H_K$	Hamiltonian for junction with varying $K$
$H_{QWZ}$	Qi–Wu–Zhang model
$H_{soc}$	Spin-orbit-coupled Hamiltonian
$H_{soc,int}$	Interaction part of spin-orbit-coupled Hamiltonian
$H_{Weyl}$	3D Weyl Hamiltonian
$H_{Weyl,R}$	Rashba-driven Weyl Hamiltonian
$\hbar = 1$	Planck’s constant set to unity
$I_{coll}$	Collision integral
$\tilde{I}_{coll}$	Collision integral with phase-space factor
$j$	Electric current density
$j_0$	Charge density
$j^{5\mu}$	Chiral current 4-vector
$j_{mb}^{5\mu}$	Momentum-based chiral current
$j_{mb}^{5\mu,3D}$	3D momentum-based chiral current
$j_{c,mb}$	Momentum-based chiral current density
$\mathbf{j}_c^{3D}$	3D chiral current density
$\mathbf{j}_{CME}$	Chiral magnetic effect current
$j_{H,\alpha}$	Hall current component
$j_{L/T}$	Longitudinal/Transverse current
$j_{L,0}$	Initial longitudinal current
$j_v$	Vortex current density
$\tilde{j}_{\nu-,in}(0)$	Instantaneous current of incoming pulse
$\tilde{j}_{\nu-,rf}(0)$	Instantaneous current of reflected pulse
$\tilde{j}_{\nu+,out}(0)$	Instantaneous current of transmitted pulse
$K$	Luttinger parameter
$K_{\pm}$	Luttinger parameters on each side of junction
$K^{(\alpha,\beta)}$	Response kernel in effective action
$K^{\mu\nu}$	Kinetic part of stress-energy tensor
$K_0^{\mu z}$	Weyl point kinetic momentum tensor
$k_0$	Half the separation between Weyl nodes
$k_{max}$	Maximum momentum cutoff
$k_B$	Boltzmann constant
$k_F$	Fermi wavevector
$\vec{K}$	Stress tensor
$\vec{K}_0^z$	Weyl point stress tensor along the $z$ direction
$l_B$	Magnetic length
$L_z$	System size in $z$ direction

$\Lambda$	Chiral charge transfer
$\Lambda_{predict}$	Predicted chiral charge transfer
$\mu$	Chemical potential
$\mu_B$	Bohr magneton
$\mu_{R/L}$	Chemical potential of right/left sector
$N(0)$	Density of states at Fermi level
$N_\alpha$	Number of electrons in Fermi pocket
$N_{s(\bar{s})}$	Number of solitons/antisolitons
$\nu$	Filling factor
$\nu_\pm$	Edge sector filling factors
$\omega$	Angular frequency
$\omega_B$	Cyclotron frequency
$\Omega(\lambda)$	Berry curvature in parameter space
$\mathbf{P}$	Momentum density vector
$\Phi$	Bosonic field in bosonization
$\Phi_0$	Flux quantum
$\Pi$	Canonical conjugate momentum
$\psi_{R/L}$	Right/left fermion field operators
$\Psi$	Dirac spinor field
$q_{\nu_-,in}$	Incoming charge on $\nu_-$ edge
$q_{\nu_-,rf}$	Reflected charge on $\nu_-$ edge
$q_{\nu_+,out}$	Transmitted charge on $\nu_+$ edge
$Q_c$	Total chiral charge
$Q_{c,\nu_-,in}$	Incoming chiral charge
$Q_{c,\nu_-,rf}$	Reflected chiral charge
$Q_{c,\nu_+,out}$	Transmitted chiral charge
$Q_\pm$	Vortex/antivortex charge
$\mathbf{Q}^H$	Anomalous Hall momentum
$Q_z^H$	$z$ -component of Hall momentum
$R$	Range cut-off
$S_{1DEG}$	1DEG action
$S_{1DEG,0}$	Non-interacting 1DEG action
$S_{1DEG,h}$	1DEG action with high-order corrections
$S_{LL}$	Luttinger liquid action
$S_{LL,0}$	Free Luttinger liquid action
$S_{LL,bs}$	Backscattering term of Luttinger liquid
$S_{LL,int}$	Interaction term of Luttinger liquid action
$S_{sg}$	Sine-Gordon action
$S_{sc,eff}$	Effective action of superconductor
$\sigma_{xy}$	Hall conductance

$\sigma_H$	Anomalous Hall conductivity
$\sigma_H^{ab}$	Hall conductivity tensor component
$\sigma_{LL}$	Longitudinal conductivity
$\sigma_{LT}, \sigma_{TL}$	Off-diagonal conductivities
$\sigma_{TT}$	Transverse conductivity
$\sigma_v$	Vortex conductivity
$\sigma_{zz}(B)$	Longitudinal conductivity in magnetic field
$T$	Temperature
$T^{\mu\nu}$	Stress-energy tensor
$T_{BKT}$	BKT transition temperature
$T_{K-,K+}$	Transmission coefficient
$\tau$	Scattering time
$\tau_a$	Axial charge relaxation time
$\theta_{(r)}$	Phase of the order parameter at radius $r$
$\Theta(t)$	Heaviside step function
$u$	Renormalized velocity
$u_{\pm}$	Renormalized velocities in junction
$v$	Rashba coupling constant
$v_F$	Fermi velocity
$v_s$	Sound velocity
$\hat{V}(\mathbf{r})$	Pairing potential operator
$\xi$	Coherence length
$\zeta$	minimum highest-level momentum of soliton pairs
$\wedge$	Wedge product

## List of Publications

This dissertation is based on the following publications.

- [1] J. D. Sau and S. Wang, Theory of anomalous hall effect from screened vortex charge in a phase disordered superconductor, [arXiv:2411.08969 \(2024\)](#).
- [2] S. Wang and J. D. Sau, Interaction robustness of the chiral anomaly in weyl semimetals and luttinger liquids from a mixed anomaly approach, [arXiv:2401.09409 \(2024\)](#).

## Chapter 1: Introduction

Over the past two decades, the discovery of topological phases of matter has significantly deepened our understanding of condensed matter physics. One of the key insights in the study of topological phases is that certain physical responses, such as the quantized Hall conductance, are not governed by local order parameters, but rather by topological invariants: robust quantities that remain invariant under perturbations and disorder.[3, 4]. Among the earliest yet most profound examples is the Integer Quantum Hall Effect (IQHE), in which the transverse electrical conductance is quantized in units of  $e^2/h$  due to the presence of a bulk Chern number and chiral edge modes on the boundary [5, 6].

One of the key theoretical concepts that emerged from these studies is the Berry phase, an adiabatic geometric phase acquired by a quantum state upon cyclic evolution in parameter space. Berry curvature, its field strength, plays a crucial role in determining many observable topological effects, such as anomalous velocity, Hall conductivity, and orbital magnetization [7]. Significantly, the Berry curvature establishes a crucial connection between topology and physical response functions, particularly through the topological properties of energy bands, often captured in topological field theories such as Chern-Simons theory.

A particularly rich platform for exploring such topological responses is provided by Weyl semimetals. These materials have band-touching points (Weyl nodes) that serve as monopoles of

Berry curvature in momentum space [8]. The low-energy quasiparticles near these nodes obey the Weyl equation, giving rise to relativistic phenomena similar to the high-energy physics such as the chiral anomaly, the nonconservation of chiral current in the presence of parallel electric and magnetic fields. The chiral anomaly manifests itself as a non-trivial and rich topological response: a charge current proportional to  $\mathbf{E} \cdot \mathbf{B}$ , which has been interpreted semiclassically through the Berry curvature [9] and microscopically through quantum field approaches [10, 11].

Despite the success of non- or weakly interacting models in describing such topological effects, many realistic materials are subject to strong electron-electron interactions. This raises fundamental questions: How do interactions modify the topological responses predicted by single-particle theories? Do the topological invariants and associated response coefficients remain quantized and unchanged in the presence of interactions, or do new emergent features arise? These questions are far from trivial, particularly when anomalies - usually thought of as exact and robust[12] - interplay with interactions, even preserving the chiral symmetry.

In addition to Weyl semimetals, another prominent class of systems in which the Berry phase plays an essential role is in materials exhibiting the anomalous Hall effect (AHE). In these systems, a transverse Hall response arises in the absence of an external magnetic field, typically as a result of broken time-reversal symmetry[13]. The AHE has been widely observed in ferromagnets and topological materials, where it is often interpreted as a momentum-space analog of the quantum Hall effect, but without the presence of Landau levels. The toy model for AHE is the well-known Chern insulator, which is inherently connected to the Berry curvature.

Recently, multilayer graphene has shown evidence of a number of novel topological phases that can be tuned by gate voltage, magnetic field, temperature, and displacement field. These phases include several superconducting phases in twisted systems [14–24] and also in non-twisted

systems [25–27], some of which are spin triplet. More interestingly, a recent experiment [28] has provided evidence of chiral superconductivity in an anomalous Hall metal phase, which is quite close to systems that have shown an AHE as well as fractional quantum anomalous Hall phases [29].

The occurrence of superconductivity in close proximity to correlated phases has led to many theoretical proposals for the mechanism of superconductivity, some based on strong correlation [30, 31] and others based on the proximity to correlated topological states [32–34]. While this is an interesting question and has been speculated on, we will avoid delving into the mechanism itself and instead focus on the phenomenology of the chiral superconducting phase.

Given the close connection between Berry curvature and anomalous Hall conductance in the normal state [35–37], a natural question arises: how would such an anomalous Hall conductance manifest in a chiral superconducting phase? Furthermore, it prompts the question whether interactions, which induce screening effects, would influence the anomalous Hall conductance or not. As an aside, quantum geometry, a generalization of the Berry curvature, instead of generating AHE, has also been shown to significantly modify superfluid stiffness and other effects in superconducting states [31, 38–45], which we do not address in this work.

In this dissertation, we focus on the effects of interactions on Berry-phase-governed topological responses in three distinct systems: the chiral anomaly in Luttinger liquid (LL), in Weyl semimetals, and the anomalous Hall effect in the phase-disordered regime of chiral superconductors. Specifically, the chiral anomaly in Weyl semimetals and Luttinger liquids is studied in our paper [1], while the theory of the anomalous Hall effect in phase-disordered superconductors is explored in our paper [2]. Before presenting detailed analysis and results, we first review the basic concepts and theoretical framework in the non-interacting case, which provide the background

for understanding how interactions modify these phenomena.

## 1.1 Berry Phase and Topological Phenomena

### 1.1.1 Geometric Phase and Curvature

Berry phase is a geometric phase acquired by a quantum state when the system's parameters (e.g., position, coefficients) are varied adiabatically and cyclically [46]. These parameters are fixed and their values are determined by some external apparatus. Consider a Hamiltonian  $H(\boldsymbol{\lambda})$  that depends on a set of parameters  $\boldsymbol{\lambda} = (\lambda_1, \lambda_2, \dots)$ , with eigenstates  $|n(\boldsymbol{\lambda})\rangle$  satisfying

$$H(\boldsymbol{\lambda})|n(\boldsymbol{\lambda})\rangle = E_n(\boldsymbol{\lambda})|n(\boldsymbol{\lambda})\rangle. \quad (1.1)$$

If the parameters  $\boldsymbol{\lambda}(t)$  are slowly changed along a closed loop  $L$  in parameter space, the instantaneous eigenstate  $|n(\boldsymbol{\lambda}(t))\rangle$  acquires a phase composed of two parts: a dynamical phase and a geometric (Berry) phase,

$$\gamma_n = \oint_L \mathcal{A}_n(\boldsymbol{\lambda}) \cdot d\boldsymbol{\lambda}, \quad (1.2)$$

where the Berry connection  $\mathcal{A}_n(\boldsymbol{\lambda})$  is defined as

$$\mathcal{A}_n(\boldsymbol{\lambda}) = i\langle n(\boldsymbol{\lambda}) | \nabla_{\boldsymbol{\lambda}} | n(\boldsymbol{\lambda}) \rangle. \quad (1.3)$$

This geometric phase is an extra phase that does not depend on the time taken to change the parameters. However, it depends on the path taken through the parameter space.

Berry curvature, which can be viewed as the "field strength" associated with the Berry

connection, is defined as

$$\boldsymbol{\Omega}_n(\boldsymbol{\lambda}) = \nabla_{\boldsymbol{\lambda}} \times \boldsymbol{\mathcal{A}}_n(\boldsymbol{\lambda}). \quad (1.4)$$

Unlike electromagnetism, where magnetic monopoles are forbidden by Maxwell's equations, an analogue of a magnetic monopole can appear in the Berry curvature. However, this is not a real magnetic monopole as in electromagnetism, but rather an abstract concept in the parameter space. This topological property is what connects the Berry phase to topological observables in such systems.

### 1.1.2 Chern Number and Quantized Response

Building on the previous subsection, when the parameter space forms a closed two-dimensional manifold (such as the Brillouin zone torus in a 2D crystal), the integral of the Berry curvature over this manifold defines a topological invariant known as the first Chern number [6]:

$$C_n = \frac{1}{2\pi} \int_{\text{BZ}} d^2k \Omega_n(\mathbf{k}), \quad (1.5)$$

where  $\Omega_n(\mathbf{k})$  is the component of the Berry curvature perpendicular to the 2D Brillouin zone.

Chern number is quantized to integer values and characterizes the topology of the underlying quantum states. Remarkably, it manifests physically as a quantized Hall conductance in units of  $e^2/h$  via the TKNN formula [6], which can be derived from the Kubo formula through linear response theory:

$$\sigma_{xy} = \frac{e^2}{h} \sum_n C_n f_n, \quad (1.6)$$

where  $f_n$  is the occupation number of band  $n$ . This quantization is topologically protected and

robust against disorder or perturbations that do not close the energy gap.

Such topological invariants form the foundation of IQHE and, more generally, the classification of topological insulators and superconductors [3, 4]. Beyond two dimensions, higher-dimensional generalizations exist, such as the second Chern number in four-dimensional quantum Hall systems, which also give rise to quantized topological responses [47].

## 1.2 Chiral Anomaly

The discovery of Weyl and Dirac materials [8, 48, 49] with low energy quasiparticles that are described as a  $(3 + 1)$ D Dirac equation has motivated the study of condensed matter analogs of the chiral anomaly of relativistic fermions in high energy physics. Fundamentally, the chiral anomaly in high energy physics [10, 11] arises from the fact that the electromagnetic response of the regularized charge of  $\text{QED}_{2n}$  with a single Weyl Fermion breaks gauge invariance (i.e. charge conservation) despite the apparent gauge invariance of the action of the Weyl fermion. The gauge invariance can be restored by introducing a second Weyl fermion, which then leads to a chiral symmetry. The chiral symmetry is a  $U(1)$  gauge symmetry similar to the one associated with charge conservation except that it assigns opposite so-called chiral charges to the different Weyl fermions referred to as chiral sectors. In the case of a single Weyl fermion, the chiral current is identical to the total current. The response of such a pair of Weyl fermions can be gauge invariant in addition to being Lorentz invariant though it necessarily breaks conservation of the chiral charge current  $j^{5\mu}$  [10, 11]. The equation for violation of chiral charge current conservation

is the so-called chiral anomaly equation [50]:

$$\partial_\mu j^{5\mu} = (-1)^{n+1} \frac{2e^n}{n!(4\pi)^n} \epsilon^{\mu_1\mu_2\cdots\mu_{2n}} F_{\mu_1\mu_2} \cdots F_{\mu_{2n-1}\mu_{2n}}. \quad (1.7)$$

The chiral symmetry discussed above, which corresponds to conservation of electron density at each Fermi pocket, is not a microscopic symmetry of the Weyl and/or Dirac systems and instead is an emergent IR symmetry [51] that appears after projecting excitations to the low-energy limit. The essential dynamics underlying the chiral anomaly for  $n = 2$  is the one in parallel electric and magnetic fields [52] and can be seen to arise as a consequence of the Berry curvature near the Weyl point. We can quantify the chiral anomaly by projecting the quasiparticles to a shell around the Fermi surface, which is analogous to the regularization discussed in the previous paragraph. This procedure when applied to non-interacting systems predicts a counter-intuitive transfer of charge between the difference Fermi surfaces [8, 53] in response to an electromagnetic field.

### 1.2.1 Chiral Anomaly in 1D Electron Systems

Anomalies can also emerge in 1D condensed matter systems, even in non-interacting models, which is both exciting and intriguing, especially given that Lorentz symmetry is absent in the underlying microscopic models. Moreover, the study of 1D anomalies provides valuable insights that help bridge the understanding to the 3D Weyl case.

A simple but instructive case is the non-interacting one-dimensional electron gas (1DEG), which serves as the foundation for understanding interacting Luttinger liquids (LLs).

Consider the low-energy approximation of non-interacting 1DEG. The Hamiltonian is ex-

pressed in terms of decoupled right- and left-moving fermions:

$$H_{1DEG,approx} = -iv_F \int dx \left( \psi_R^\dagger \partial_x \psi_R - \psi_L^\dagger \partial_x \psi_L \right), \quad (1.8)$$

where  $v_F$  is the Fermi velocity. Obviously, this model possesses a  $U(1)_{\text{charge}} \times U(1)_{\text{chiral}}$  symmetry.

Introducing a slowly varying background gauge field  $A_\mu$  coupled to the charge current leads to a non-trivial response of the chiral current:

$$\partial_\mu j^{5\mu} = \frac{e}{\pi} F_{01}, \quad (1.9)$$

, where  $F_{01}(= E)$  is the external electric field. This is the chiral anomaly equation in 1 + 1D[54].

In order to understand the connection between the Berry phase, the Fermi surface, and the chiral anomaly, we begin with the semiclassical Boltzmann equation. Although the Berry curvature in 1D is trivial, performing this calculation is still valuable, as it serves as a simple version for the more interesting and non-trivial Berry curvature in 3D, which is particularly relevant and meaningful in the study of Weyl semimetals.

The Boltzmann equation for the distribution function  $f(k)$  is given by:

$$\frac{\partial f}{\partial t} + \dot{\mathbf{x}} \cdot \nabla_{\mathbf{x}} f + \dot{\mathbf{k}} \cdot \nabla_{\mathbf{k}} f = 0 \quad (1.10)$$

, where  $\mathbf{x}$  is the position and  $\mathbf{k}$  is the momentum. The equations of motion are given by:

$$\dot{\mathbf{k}} = e\mathbf{E} \quad (1.11)$$

$$\dot{\mathbf{x}} = \mathbf{v}_k + \dot{\mathbf{k}} \times \boldsymbol{\Omega}_k \quad (1.12)$$

, where  $\mathbf{v}_k = \nabla_k \epsilon(k)$  is the velocity and  $\boldsymbol{\Omega}_k = \nabla_k \times \mathcal{A}_k$  is the Berry curvature, with  $\mathcal{A}_k = i \langle u_k | \nabla u_k \rangle$  being the Berry connection.

Since the Berry curvature is zero in 1D, the momentum and position equations are reduced to simpler forms. In the case of a non-interacting system, we assume that the right- and left-moving states are decoupled. This allows us to write the distribution function as:  $f = f_+ + f_-$ , where  $f_+$  is the distribution function for particles moving to the right and  $f_-$  is for particles moving to the left.

For each of these states, we write the corresponding Boltzmann equations:

$$\frac{\partial f_{\pm}}{\partial t} \pm v_F \frac{\partial f_{\pm}}{\partial x} + eE \frac{\partial f_{\pm}}{\partial k} = 0 \quad (1.13)$$

, where  $v_F$  is the Fermi velocity.

We simply define the chiral charge  $\rho_c$  as the difference between the densities of the particles moving to the right and to the left. Then, the chiral charge and the regular charge are

$$\rho_c = \int (f_+ - f_-) \frac{dk}{2\pi} \quad (1.14)$$

$$\rho = \int (f_+ + f_-) \frac{dk}{2\pi} \quad (1.15)$$

Using the property  $\partial f_{\pm}/\partial k = \mp\delta(k)$  and substituting it into the Boltzmann equations, we obtain:

$$\frac{\partial \rho_c}{\partial t} + v_F \frac{\partial \rho}{\partial x} = \frac{eE}{\pi} \quad (1.16)$$

, which is equivalent to Eq.1.9. The derivation process demonstrates the connection between the Fermi surface (including the Berry phase, although it is trivial in 1D) and the chiral anomaly.

When interactions are included, the situation becomes particularly intriguing. In the (1 + 1)D Thirring model, a contact interaction  $\lambda j^{\mu} j_{\mu}$  leads to a renormalization of the anomaly coefficient [54–56]:

$$\partial_{\mu} j^{5\mu} = \left( \frac{1}{1 + \lambda/\pi} \right) \frac{e}{\pi} F_{01}, \quad (1.17)$$

showing that interactions can modify the anomaly, which is often thought to be a topological response. In contrast, the chiral anomaly equation for the 1D edge states of the IQHE remains topological and unrenormalized, even when right- and left-moving particles interact with themselves. This motivates our central question: *How to understand this renormalized 1D anomaly? Is the chiral anomaly robust against interactions in more realistic higher-dimensional systems?*

## 1.2.2 Chiral Anomaly in Weyl Semimetals

Building on the previous subsection where we discussed the 1D case, we now shift our focus to the 3D Weyl semimetals, which are of particular interest for both theoretical study and experimental comparison. In (3 + 1)D Weyl semimetals, the low-energy electronic structure consists of pairs of Weyl nodes with opposite chirality, where the conduction and valence bands touch at isolated points in the momentum space. The effective Hamiltonian near a Weyl node

takes the form:

$$H_{\text{Weyl}} = \pm v_F \boldsymbol{\sigma} \cdot \mathbf{k}, \quad (1.18)$$

where the sign corresponds to the chirality. Applying parallel electric and magnetic fields results in a spectral flow of states between nodes of opposite chirality, leading to the chiral anomaly:

$$\partial_t \rho_c + \nabla \cdot \mathbf{j}_c = \frac{e^2}{2\pi^2} \mathbf{E} \cdot \mathbf{B}. \quad (1.19)$$

This anomaly can also be derived semiclassically from the Berry curvature near the Weyl nodes using the same methods as in the previous section [9, 57] or from Landau's Fermi-liquid theory[58].

The above formulation of the 3D chiral anomaly in solid state systems applies only to non-interacting systems, which leads to the question of whether the chiral anomaly is affected by interactions. In fact, the chiral anomaly in  $(3 + 1)D$  relativistic quantum field theory(i.e. QED<sub>4</sub>) written in Eq. 1.7 is found not to be affected by the addition of interactions in the sense that it receives no radiative corrections [59]. This robustness can be understood in situations where the anomaly can be constrained by a topological term in an action on a higher dimensional space [47, 50, 60]. On the other hand, the chiral anomaly in the  $(1 + 1)D$  Thirring model as introduced in the previous subsection, another relativistic quantum field theory, is found to be renormalized by interactions in Eq.1.17

Given that solid-state systems can support a variety of interaction terms, it is natural to discuss modifications to the chiral anomaly due to interactions [61–63]. For instance, the inclusion of Umklapp scattering explicitly breaks the chiral symmetry even in the IR limit, thus invalidating

the notion of a chiral anomaly. In contrast, the disorder robustness of the chiral anomaly for intra-valley scattering has been established both semiclassically [9] and fully quantum mechanically using the non-linear sigma model [64].

Complicating these discussions is the fact that the chiral charge is only defined in the IR and non-interacting limit, making it difficult to measure as a microscopic variable in solid-state systems. As a result, much of the experimental focus on the chiral anomaly has been focused on secondary manifestations, such as the chiral magnetic effect [8] and the negative magnetoresistance [9]. Although these are relatively convenient to measure, they are known to contain contributions from other mechanisms [65]. Studies of the effect of interactions on anomaly current response signatures, such as the chiral photocurrent [61] and the chiral current [62], have shown a renormalization of these response functions due to interactions.

Interestingly, the detection of the chiral anomaly via non-local transport [66] provides a way to detect spatial variations of the chiral anomaly coefficient without being directly sensitive to the coefficient itself. Moreover, it is possible to find an interaction-robust chiral anomaly in a slab of a four-dimensional second Chern insulator [47, 67] viewed as a three-dimensional lattice system. The difference in charge between the surface states of such a Chern insulator defines a chiral charge, while the second Chern-Simons form of the four-dimensional quantum Hall effect defines the quantized chiral anomaly.

These solid-state examples suggest that the magnitude of the chiral anomaly, in the absence of Lorentz invariance, can depend on both the details of the interaction Hamiltonian and the definition of a chiral charge. To illustrate the latter, an interacting Weyl semimetal can be described as a topological Fermi liquid [37] of non-interacting quasiparticles. In this limit, the chiral anomaly, with the chiral charge defined in terms of quasiparticles, becomes topological

and is not renormalized.

### 1.3 Anomalous Hall Effect

The anomalous Hall effect (AHE) refers to a transverse voltage or current generated in response to an applied longitudinal electric field in the absence of an external magnetic field. Originally observed in ferromagnetic materials, the AHE is now understood to arise from a combination of intrinsic band structure effects and extrinsic scattering mechanisms [13].

Among these, the intrinsic contribution is of particular interest because it is directly related to the Berry curvature of the electronic bands. In semiclassical dynamics, the velocity of a Bloch electron acquires an anomalous correction due to the Berry curvature  $\Omega_k$  as [7]:

$$\dot{\mathbf{r}} = \nabla_{\mathbf{k}}\epsilon(\mathbf{k}) + \dot{\mathbf{k}} \times \Omega_k, \quad (1.20)$$

where  $\dot{\mathbf{k}} = e\mathbf{E}$ . The second term describes a transverse motion leading to an intrinsic Hall current:

$$\mathbf{j} = -e \int_{\mathbf{k}} f_k \dot{\mathbf{r}} \propto \int_{\mathbf{k}} f_k \Omega_k \times \mathbf{E}. \quad (1.21)$$

As we mentioned in Sec.1.1.2, if the material is an insulator, the integral of the Berry curvature over the Brillouin zone gives the Chern number  $C$ , which determines the quantized Hall conductance. Such a material is called a Chern insulator.

To illustrate the connection between Berry phase and anomalous Hall response even in a (semi)metal or semiconductor, we consider the Qi-Wu-Zhang (QWZ) model [68]. The model

Hamiltonian takes the form:

$$H_{QWZ}(\mathbf{k}) = -\mu\sigma_0 + \sin k_x\sigma_x + \sin k_y\sigma_y + [2 + m_0 + \cos k_x + \cos k_y]\sigma_z, \quad (1.22)$$

where  $\sigma_i$  are Pauli matrices,  $\mu$  is the chemical potential, and  $m_0$  is a tunable mass parameter. The band structure of this model hosts a topologically nontrivial phase for certain values of  $m_0$ , characterized by a non-zero Berry curvature.

The intrinsic anomalous Hall conductivity in this model is given by:

$$\sigma_{xy} = -\frac{e^2}{h} \frac{1}{4\pi} \int_{\text{BZ}} d^2k \hat{\mathbf{d}} \cdot \left( \frac{\partial \hat{\mathbf{d}}}{\partial k_x} \times \frac{\partial \hat{\mathbf{d}}}{\partial k_y} \right) f_k, \quad (1.23)$$

where  $\mathbf{d}(\mathbf{k}) = (\sin k_x, \sin k_y, 2 + m_0 + \cos k_x + \cos k_y)$ ,  $\hat{\mathbf{d}} = \mathbf{d}/|\mathbf{d}|$ . The Chern number now has a particularly nice interpretation: it counts the number of times BZ wraps around the sphere defined by  $\hat{\mathbf{d}}$ , and thus an integer. The Chern number is

$$C = \begin{cases} -1 & \text{if } -2 < m_0 < 0, \\ 1 & \text{if } 0 < m_0 < 2, \\ 0 & \text{if } |m_0| > 2, \end{cases} \quad (1.24)$$

which depends on  $m_0$  as expected.

To our interest, when the Fermi level lies within the band, assuming  $m_0 > 0$  and  $\mu > m_0$ , and both much smaller than the band width 4, we can approximate the Berry curvature, Berry

phase, and conductivity as follows:

$$\Omega_q \approx -\frac{m_0}{2(m_0^2 + q^2)^{3/2}}, \quad (1.25)$$

$$\gamma \approx \pi \left(1 - \frac{m_0}{\mu}\right) \quad (1.26)$$

$$\sigma_{xy} \approx \frac{e^2}{2h} \left(1 - \frac{m_0}{\mu}\right) \quad (1.27)$$

, where  $q$  is the momentum vector starting from the point  $(\pi, \pi)$ . The Berry phase and Hall conductivity are the same, apart from a constant factor.

This model quantitatively demonstrates the Berry curvature, governed by the band geometry, and the relationship between the Berry phase and the anomalous Hall response when the Fermi level within the band.

As mentioned earlier, our focus is on understanding the Hall response in a phase-disordered chiral superconductor, particularly just above the Berezinskii-Kosterlitz-Thouless (BKT) transition. In this regime, vortex dynamics and screening effects play crucial roles, and Berry curvature-induced responses may persist or even be modified. This offers an opportunity to explore how topological signatures, stemming from Berry phase phenomena, are encoded in collective degrees of freedom and whether they can be renormalized by interactions.

In fact, chiral superconductivity has been suggested by itself to support an ac Hall response [69, 70]. This chiral response has been conjectured to have several interesting consequences, such as the fractional charge and the angular momentum of vortices [71]. However, a gauge-invariant treatment of screening effects by the background condensate leads to an effective Chern-Simons theory where the chiral conductivity from purely chiral superconductivity at low

wave vectors is suppressed [72, 73]. The evidence for chiral superconductivity in a purely two-dimensional anomalous Hall metal phase [33], where screening effects are reduced and phase-ordered superconductivity is seen motivates us to revisit the question of the chiral response and vortex properties of such phases.

## 1.4 Outline

The following parts of the dissertation is assigned as follows. In Chapter 2, we investigate the chiral anomaly in a one-dimensional interacting fermion system using a mixed anomaly framework. Focusing on a (1+1)D model with emergent Lorentz symmetry, we demonstrate that the chiral anomaly remains robust and unrenormalized by electron-electron interactions when the chiral charge is identified with total momentum. This result contrasts with other definitions of chiral charge in 1D, which can exhibit regularization dependence.

Chapter 3 extends this analysis to three-dimensional Weyl semimetals. By defining a momentum-space chiral charge via the Luttinger volume of each Weyl Fermi pocket, we show that the chiral anomaly in 3D also persists without renormalization in the presence of interactions. We derive an anomaly equation that equates the chiral charge pumping between Fermi surfaces to changes in Fermi-surface volume, establishing an interaction-robust topological response. Furthermore, we propose a pump–probe experiment to measure this effect, providing a practical way to observe the interaction-protected chiral charge transfer between Weyl nodes.

Chapter 4 turns to the anomalous Hall effect (AHE) in a two-dimensional chiral superconductor slightly above its critical temperature, where global phase coherence is lost (a phase-disordered regime). We find that even without long-range superconducting order, a Hall response

endures due to a charge asymmetry between vortices and anti-vortices induced by the Berry phase of the normal-state bands. Using a gauge-invariant effective action formalism and numerical simulations, we show that this vortex-charge-induced Hall current closely matches the Hall conductivity of the normal state. Importantly, we demonstrate that although many-body interactions screen the static charge of each vortex, the time-dependent screening currents restore the Hall response. As a result, the observed dc Hall conductivity in the phase-disordered superconductor aligns with the intrinsic ac Hall conductance of both the superconducting and normal phases, rather than being solely determined by the screened vortex charge itself.

Finally, the Appendices provide technical details and supplementary calculations supporting the main chapters. These include the bosonization derivations for 1D anomalies, clarifications on the relation between physical current and chiral charge, proofs of gauge-invariance in stress–energy tensors, extended analysis of the chiral magnetic effect in kinetic theory, and a second-order Hall response calculation for a Chern insulator. Together, these appendices furnish the theoretical groundwork and additional evidence underpinning the conclusions drawn in Chapters 2-4.

## Chapter 2: Interaction Robustness of Chiral Anomaly in 1D

### 2.1 Regularization Dependence of the Chiral Anomaly

The Tomonaga-Luttinger model [74], which describes low-energy excitations in  $(1 + 1)$ D systems with fermionic excitations, has an emergent Lorentz symmetry. This emergent Lorentz symmetry motivates the study of the chiral anomaly using methods of high-energy physics such as Fujikawa's method, Pauli-Villars regularization, and Feynman diagrams[59, 75, 76].

The action of the Luttinger model,  $S_{LL}$ , is written as  $S_{LL} = S_{LL,0} + S_{LL,int}$  with the Fermi velocity ( $v_F = 1$ ), where

$$S_{LL,0} = \int d^2x i\bar{\Psi}(\not{\partial} + ie\mathcal{A})\Psi, \quad (2.1)$$

is the action associated with the non-interacting fermionic field  $\Psi := (\psi_R, \psi_L)^T$  composed of left and right movers with no spins, and  $A$  is the electromagnetic vector potential. Furthermore,  $\bar{\Psi} = \Psi^\dagger \gamma^0$ , and the Feynman slash notation  $\not{\partial} := a_\mu \gamma^\mu$  is used.  $\gamma^\mu$  in this 1D case has the form:

$$\gamma^0 = \begin{pmatrix} 0 & -i \\ i & 0 \end{pmatrix}, \quad \gamma^1 = \begin{pmatrix} 0 & i \\ i & 0 \end{pmatrix} \quad (2.2)$$

The action  $S_{LL}$  can also include a general local current-current interaction of the form [62]

$$S_{LL,int} = -\frac{1}{2} \int d^2x \lambda_{\mu\nu}^{(2)} j^\mu j^\nu, \quad (2.3)$$

where

$$j^\nu = \bar{\Psi} \gamma^\mu \Psi = (\rho_R + \rho_L, \rho_R - \rho_L) \quad (2.4)$$

is the current 2-vector, and  $\lambda_{\mu\nu}^{(2)}$  are interaction couplings.

The action  $S_{LL}$  has a chiral symmetry  $U_A(1)$  with a parameter  $\beta$  defined by

$$\begin{cases} \psi_R(x) \rightarrow \psi_R(x)' = e^{i\beta(x)} \psi_R(x) \\ \psi_L(x) \rightarrow \psi_L(x)' = e^{-i\beta(x)} \psi_L(x), \end{cases} \quad (2.5)$$

when the argument  $\beta(x)$  is independent of the space and time coordinates  $x$ . In the case of a local transformation, where  $\beta(x)$  varies non-trivially with coordinate  $x$ , the variation of the action  $\delta S_{LL} = S'_{LL,0} - S_{LL,0}$  must be proportional to the derivative  $\partial_\mu \beta$ , thus written as

$$\delta S_{LL} = - \int d^2x j^{5\mu} \partial_\mu \beta, \quad (2.6)$$

which is used to define the chiral current,

$$j^{5\mu} = \bar{\Psi} \gamma^\mu \gamma_5 \Psi \quad (2.7)$$

generated by the transformation where  $\gamma_5 = \gamma^0 \gamma^1$ . The variation of the action (following an integration by parts) considered above suggests the conservation of the chiral current (i.e.  $\partial_\mu j^{5\mu} = 0$ )

along the lines of Noether's theorem in classical mechanics.

The time component of the current  $j^{5,0}$  is a chiral charge density, which can be shown from Eq.2.7,

$$\rho_{c,cb} = \psi_R^\dagger \psi_R - \psi_L^\dagger \psi_L = \rho_R - \rho_L = j, \quad (2.8)$$

where the subscript indicates that this quantity is current-based, with a particularly simple form in the so-called chiral basis for fermions  $\psi_{L,R}$ . However, as we will discuss below, a quantum-mechanical treatment of this action leads to a violation of the conservation law for the chiral current, which is called the chiral anomaly.

The Tomonaga-Luttinger model  $S_{LL}$  can be solved by representing the fermionic fields  $\Psi$  in terms of a bosonic field  $\Phi$ , which is related to the current operator as

$$j^\mu = \frac{1}{\sqrt{\pi}} \epsilon^{\mu\nu} \partial_\nu \Phi, \quad (2.9)$$

through a process known as bosonization [74, 77]. However, the process of bosonization for such gapless models requires regularization to resolve the fate of the chiral current [78]. In the Lorentz-invariant case where  $\lambda_{\mu\nu}^{(2)} = \lambda \eta_{\mu\nu}$ , which is also referred to as the Thirring model [54], normal ordering can be used to regularize divergences provided the bosonization is performed after transforming the action to Euclidean (i.e. Wick rotated) [77]. Since the Lorentz invariance is preserved and essentially becomes rotation in Euclidean space, the chiral current operator based on Eq. 2.7 continues to be a "rotated" version of the conventional current operator, i.e.

$$j^{5\mu} = -\epsilon^{\mu\nu} j_\nu = \frac{1}{\sqrt{\pi}} \partial^\mu \Phi, \quad (2.10)$$

where  $\epsilon^{\mu\nu}$  is the completely anti-symmetric unit tensor. While the charge current  $j^\mu$  in Eq. 2.9 is manifestly divergence-free, as detailed in the Appendix A, the divergence of the chiral current can be written in terms of the classical equation of motion for  $\Phi$  as

$$\langle \partial_\mu j^{5\mu} \rangle = \frac{1}{\sqrt{\pi}} \partial_\mu \partial^\mu \Phi = \frac{1}{1 + \lambda/\pi} \frac{e}{\pi} E. \quad (2.11)$$

where  $E = \partial_0 A_1 - \partial_1 A_0$  is the electric field. This is called the chiral anomaly equation in 1+1D [54]. Furthermore, since the RHS depends on the interaction strength  $\lambda$ , the chiral anomaly is renormalized by interaction [54] in a way that is identical to that obtained directly from the Thirring model using either the Pauli-Villars regularization or the Fujikawa method [62].

Condensed matter systems without microscopic Lorentz invariance allow a more general type of interaction  $\lambda_{\mu\nu}^{(2)} = (g_4 + g_2)\eta_{0\mu}\eta_{0\nu} + (g_4 - g_2)\eta_{1\mu}\eta_{1\nu}$ , while still preserving chiral symmetry. In the absence of Lorentz invariance, one can use a simple "point-splitting" regularization [77] to regulate divergences in  $S_{LL}$ . The point-splitting approach involves replacing the products of operators at the same space-time point  $\rho_{R/L}(x, t)\rho_{R/L}(x, t) \rightarrow \rho_{R/L}(x - \epsilon, t)\rho_{R/L}(x + \epsilon, t)$  with slightly separated points in space at the same time. The correlators of the system can now be computed using a more conventional Hamiltonian operator-based approach [74, 78], which leads to a wave equation for  $\Phi$

$$u^{-1} \partial_t^2 \Phi - u \partial_x^2 \Phi = \frac{eK}{\sqrt{\pi}} E, \quad (2.12)$$

where

$$uK = 1 + \frac{g_4}{2\pi} - \frac{g_2}{2\pi}, \quad u/K = 1 + \frac{g_4}{2\pi} + \frac{g_2}{2\pi} \quad (2.13)$$

(see Appendix A for a review of the derivation) [74].

As reviewed in Appendix A, the bosonization identities [74] can now be applied to the operator definition of the chiral charge density, i.e.,  $\psi_R^\dagger\psi_R - \psi_L^\dagger\psi_L$ , to show that

$$\rho_{c,mb}(:= \rho_R - \rho_L) = j/uK, \quad (2.14)$$

where the subscript indicates that this quantity is momentum-based, which will be explained later. Note that this result for the current differs from Eq. 2.4 and Eq. 2.8 due to the point-splitting regularization, which modifies the definition of currents in order to preserve the charge continuity equation.

Applying this equation of chiral charge to the equation of motion leads to the following chiral anomaly equation:

$$\langle \partial_\mu j_{mb}^{5\mu} \rangle = \frac{1}{\sqrt{\pi}} \partial_t \Pi + \partial_x j_{c,mb} = \frac{e}{\pi} E \quad (2.15)$$

where  $j_{c,mb} = u\rho/K$  is the chiral current, and  $\Pi = \sqrt{\pi}(\rho_R - \rho_L)$  is the canonical conjugate field to  $\Phi(x)$ . We can easily find that the chiral charge in this case directly related to the kinetic momentum. Note that in contrast to the chiral anomaly equation (Eq. 2.11) resulting from a Lorentz-invariant regularization of the TL model, the above chiral anomaly equation has no interaction-based renormalization.

Incidentally, the chiral anomaly equations of the 1D edge for topological integer quantum Hall systems, based on either Eq. 2.11 or Eq. 2.15, are both unrenormalized. This is because in the latter formalism the two edges ( $R$  and  $L$ ) cannot be scattered to each other in the IQHE, the

$g_2$  term,  $\rho_R\rho_L$ , is missing; thus, the Luttinger parameter  $K$  is always 1 and the two chiral charges in Eq. 2.14 and Eq. 2.8 are equivalent.

The above chiral anomaly equation (Eq. 2.15) is clearly different from the relativistic chiral anomaly Eq. 2.11 even in the formally Lorentz-invariant case  $g_4 = 0$  (and  $g_2 = \lambda$ ). Thus, both the chiral anomaly in  $(1 + 1)$  D and the equation of motion for the current  $j$ , even in the presence of formal Lorentz invariance, depend on regularization. This means that one cannot use this formalism to calculate the chiral anomaly for an interacting electron gas because neither regularization can be reliably applied.

### 2.1.1 Application to Interacting Spin-orbit Coupled Fermions

The simplest systems that one may hope to apply these ideas to would be an electron gas with parabolic dispersion and density-density interactions. The density-density interactions lead to the constraints  $g_2 = g_4$  and  $uK = v_F = 1$  in Eq. 2.13 for the bosonized description of the system [74]. Indeed, one can check that this produces the correct equation of motion for the current  $j$  (i.e. Eq. 2.12) based on Galilean-invariance. Thus, the point-splitting regularization rather than the Lorentz-invariant one produces the correct conductivity. However, the chiral charge (i.e., Eq. 2.14) is simply the current density.

The chiral charge  $\rho_c$  can be distinct from the current in a Rashba spin-orbit coupled gas with density-density and spin-spin interactions. A more general way to derive the coefficients  $u, K$  is to directly analyze the equation of motion Eq. 2.12, which can be written as  $(uK)^{-1}\partial_t j + (u/K)\partial_x \rho = (e/\pi)E$ . Taking into account the limits  $\omega \ll q$  and  $\omega \gg q$ , we can interpret  $(u/K)$  as compressibility and  $(uK)^{-1}$  as inertia.

To compute these for the spin-orbit coupled model, consider the Hamiltonian

$$H_{soc}(k) = (k - \alpha\sigma_z)^2 - \alpha^2 + \Gamma\sigma_x. \quad (2.16)$$

For small  $\Gamma$ , the states near the Fermi energy have  $k = \pm 2\alpha$  and are polarized along  $\sigma_z = \pm 1$ . In addition, let us consider a short-ranged interacting term,

$$H_{soc,int} = g_2 \int dx \rho(x)^2 \simeq g_2 \int dx \rho_+(x)\rho_-(x), \quad (2.17)$$

Note that in the small  $\Gamma$  limit,  $\rho_{\pm} \equiv \rho_{L,R}$  in the TL model. Therefore, we can apply the results Eq. 2.13 with  $g_4 = 0$  to this model and derive a non-trivial chiral charge  $\rho_{c,mb}$ , which is different from the current  $j$ , using Eq. 2.14 for this model.

### 2.1.2 Relativistic Anomaly in Condensed Matter Systems

Since many of the low-energy degrees of freedom in condensed matter systems, such as the 1DEG, appear to have Lorentz-invariance based on the bosonized equation of motion Eq. 2.12, one may ask if the Lorentz-invariant anomaly (i.e. Eq. 2.11) applies to such systems in any sense. The results discussed earlier in this section show that different regularizations will generate different results of the chiral anomaly (i.e. Eqs. 2.11, 2.15), some of which are renormalized by interactions and others are not.

This issue can be resolved by refermionization [79], where fermions can be constructed

from a model of bosons. This construction can be shown for the Sine-Gordon model [78, 80]:

$$S_{sg} = \int dt dx \frac{1}{2} \left[ \frac{1}{uK} (\partial_t \Phi)^2 - \frac{u}{K} (\partial_x \Phi)^2 - ug \cos(2\sqrt{\pi}\Phi) \right]. \quad (2.18)$$

The Sine-Gordon model can be obtained as a low-energy description of a 1DEG using bosonization [74] by adding a back-scattering term to the Luttinger-model  $S_{LL}$ , which is written as:

$$S_{LL,bs} = \int dt dx V_0 \cos(2k_F x) \psi^\dagger \psi. \quad (2.19)$$

The Luttinger model  $S_{LL}$  is discussed in Eq. 2.1. While the parameters  $u$ ,  $K$ , and  $g$  depend on the regularization scheme used (similar to the anomaly), the form of the model  $S_{sg}$  is independent of regularization.

Interestingly, the term  $S_{LL,bs}$  explicitly breaks the chiral symmetry (Eq. 2.5) and the spectrum associated with  $S_{sg}$  is gapped for  $1 < K < 2$ . The gap allows one to describe the excited states of the system in terms of solitons and antisolitons over a gapped vacuum [78, 80]. The solitons and antisolitons are fermionic and are described by a massive Thirring model [78].

Furthermore, in the range of parameters  $1 < K < 2$ , the solitons and antisolitons are conserved excitations and can be used to define a soliton-based chiral charge:

$$\rho_{c,sb} = N_s + N_{\bar{s}} \quad (2.20)$$

, where  $N_{s(\bar{s})}$  are the number operator of (anti)solitons. The chiral symmetry of Eq. 2.5 is replaced by the integrability of  $S_{sg}$  which leads to the conservation of the current density despite the absence of an explicit chiral symmetry or momentum conservation.

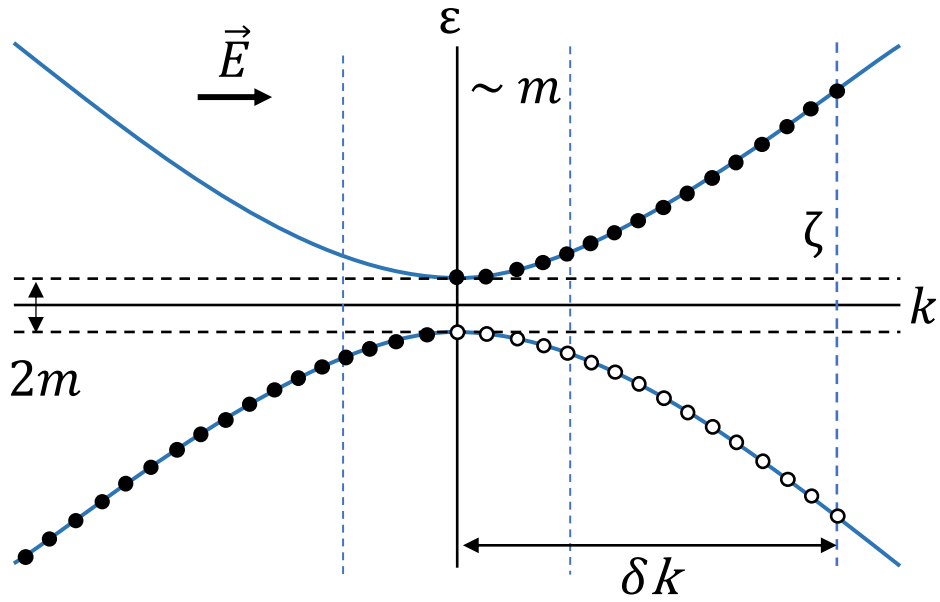


Figure 2.1: Illustration of the chiral anomaly in the Sine-Gordon model. The energy spectrum is sketched as two curves with an energy gap of  $2m$ , where  $m$  is the soliton mass. In the presence of an  $E$ , solitons and antisoliton are generated and are shown by black dots in the top band and white dots in the bottom band, respectively. The range between two dashed lines in the middle corresponds to low-speed moving (anti)solitons. The minimum highest-level momentum of soliton pairs is labeled by  $\zeta$ .

To understand the role of the explicit chiral symmetry breaking term,  $V_0$ , we consider the equation of motion,

$$\partial_t j + u^2 \partial_x \rho + u^2 g K \sin(2\sqrt{\pi}\Phi) = uK \frac{eE}{\pi} \quad (2.21)$$

, where  $j$  is given by Eq. 2.9 and the gap parameter  $g \propto V_0$ . This equation becomes equivalent to the gapless equation of motion in Eq. 2.11 in the limit  $V_0 \rightarrow 0$ .

Furthermore, considering the excitations of the Sine-Gordon model shown in Fig. 2.1, where the gap is proportional to  $m \sim g$ , we see that the limit  $m \sim g \rightarrow 0$  implies that almost all solitons and antisolitons move at speed  $u$ . In this limit, the chiral charge is proportional to the current  $\rho_{c, sb} \simeq j/u$  (see detailed discussion in the Appendix B). The chiral current is related to the chiral charge by the velocity of the modes, we have  $j_{c, sb} \simeq u[N_s - N_{\bar{s}}] \simeq u\rho$  (the final step is a result of the opposite charges of the solitons and antisolitons). Applying this to Eq. 2.21 (taking the limit  $g \rightarrow 0$ ) leads to an anomaly equation,

$$\partial_t \rho_{c, sb} + \partial_x j_{c, sb} = K \frac{eE}{\pi}. \quad (2.22)$$

This equation is essentially equivalent to the relativistic anomaly equation in Eq. 2.11. Note that the role of the mass is rather subtle, since we are using the limit  $g \rightarrow 0$ , which is the same limit considered in Eq. 2.11. However, the finite but vanishingly small  $g$  is needed for the identification of  $\rho_{c, sb}$  as a conserved chiral charge of solitons/antisolitons. This is because, as established earlier in the section, one cannot identify this charge with left/right moving microscopic fermions. The latter identification is dependent on regularization. From an experimental standpoint, the validity of the above equation assumes an electric field that is applied over a rel-

atively short time (i.e. relatively high frequency) relative to the mass  $m \sim g$ . The integrability of the Sine-Gordon model, which leads to the conservation of the chiral charge  $\rho_{c,sg}$  and also remarkably the corresponding physical charge current  $j$ , allows one to measure the chiral charge at a later point to check the validity of the anomaly. In practice, one could simply measure the rescaled current  $j/u$  as the chiral charge. This does not require an actual back-scattering potential. However, to check that this corresponds to a physical density, one would measure the soliton density at long times when the finite mass disperses the wave-packet so that individual solitons and antisolitons are separated. This check requires back-scattering  $V_0$  to create the dispersion of the wave pack and identify the individual charges.

## 2.2 Momentum-based Chiral Anomaly from a Mixed Anomaly Approach

The regularization issues described above can be resolved by defining a chiral charge density in terms of momentum density. The basic idea is to treat the chiral symmetry as an emanant symmetry[81] rather than an emergent symmetry, meaning it emanates from the microscopic translation symmetry. To understand this, let us first review how the mixed anomaly of translation symmetry and  $U(1)$  symmetry is closely analogous to the chiral anomaly  $U(1)$  [82–84].

In the low-energy regime, we can expand the fermionic field operator  $\psi(x, t)$  in a neighborhood of  $\pm k_F$  according to the relation:

$$\psi(x, t) \simeq e^{ik_F x} \psi_R(x, t) + e^{-ik_F x} \psi_L(x, t), \quad (2.23)$$

where  $k_F$  is the Fermi momentum and the right and left fermionic fields  $\psi_R$  and  $\psi_L$  that slowly vary in space and time.

With the help of this preliminary step, the effect of a space translation transformation can be written as

$$\begin{cases} \psi_R(x, t) \rightarrow \psi_R(x, t)' = e^{ik_F a(x, t)} \psi_R(x, t) \\ \psi_L(x, t) \rightarrow \psi_L(x, t)' = e^{-ik_F a(x, t)} \psi_L(x, t). \end{cases} \quad (2.24)$$

Note that we ignore the shift of  $\psi_{R/L}(x + a, t)$  by  $a$  since these fields vary slowly compared to  $k_F$ . These transformations become equivalent to the chiral  $U(1)$  transformation defined in Eq.(2.5) for  $\beta(x) = k_F a(x)$ .

While the total momentum displays properties of a chiral anomaly in systems with discrete translation symmetry [83], systems with continuous translation symmetry allow us to study a local momentum density field, which is analogous to a chiral charge density. The chiral charge density is the Noether current associated with the chiral  $U(1)$  symmetry in the systems described in Sec. 2.1. Similarly, one can identify the low-energy limit of the canonical momentum density  $T^{01}$ , which is the Noether current associated with translation, as the analog chiral charge density for systems with finite bandwidth.

However, unlike anomalous chiral  $U(1)$  symmetry, translation symmetry is preserved under quantization. Thus, the momentum current density  $T^{\mu 1}$  is conserved without any anomaly. Therefore, the anomaly in this case is replaced by a mixed anomaly [83] that arises from the gauge dependence of  $T^{\mu 1}$  under the  $U(1)$  symmetry associated with charge conservation. In the case of continuous translation symmetry, this mixed anomaly can be transformed into a chiral anomaly equation for a locally gauge-invariant analog of the momentum density, as described below.

As a first example, we will start by computing the locally gauge-invariant momentum density, which we will call the kinetic momentum density, in the 1DEG model. The action for the

1DEG model in the presence of an external gauge field in 1+1 is  $S_{1DEG} = S_{1DEG,0} + S_{1DEG,int}$

with

$$S_{1DEG,0} = \int dxdt i\psi^\dagger D_0\psi - \frac{1}{2m}\bar{D}_1\psi^\dagger D_1\psi + \mu\psi^\dagger\psi, \quad (2.25)$$

where  $D_\mu = \partial_\mu + ieA_\mu$  and  $\mu$  is the chemical potential. For simplicity, we take the interacting part of the action as the density-density interaction with the form

$$S_{1DEG,int} = \int dt dx dx' V(x-x')\rho(x)\rho(x'), \quad (2.26)$$

where  $\rho(x) = \psi^\dagger(x)\psi(x)$  is the fermion number density with  $V(x-x')$  being an interaction potential.

As detailed in Appendix C, the stress-energy tensor, which is the Noether current associated with translation, can be calculated considering the variation of the action under translation following Eq. C.2. The spatial dependence of the vector potential  $A_\mu(x, t)$  breaks translation-invariance and leads to a non-zero divergence of the stress-energy tensor

$$\partial_\mu T^{\mu\nu} = e\rho\partial^\nu A_0 - ej\partial^\nu A_1 \quad (2.27)$$

, where  $\rho$  and  $j$  are the charge density and current, respectively. The gauge dependence of  $T^{\mu\nu}$  becomes apparent from the lack of gauge-invariance of the RHS of the divergence of  $T^{\mu\nu}$ .

The gauge-invariance of the RHS can be restored by rewriting Eq. 2.27 as

$$\partial_\mu(T^{\mu\nu} - ej^\mu A^\nu) = ej_\mu F^{\nu\mu} \quad (2.28)$$

, where the notation  $F^{\nu\mu}$  represents the electromagnetic field tensor.

The above equation motivates the definition of a kinetic stress-energy tensor  $K^{\mu\nu}$  as

$$K^{\mu\nu} = T^{\mu\nu} - ej^\mu A^\nu, \quad (2.29)$$

which has a gauge-invariant divergence,

$$\partial_\mu K^{\mu\nu} = ej_\mu F^{\nu\mu}. \quad (2.30)$$

Using the calculated  $T^{\mu\nu}$  in Appendix C, the kinetic momentum density  $K^{01}$  and the kinetic stress  $K^{11}$  are given by the manifestly gauge-invariant form.

$$K^{01} = -i\psi^\dagger D_1\psi \quad (2.31)$$

$$K^{11} = i\psi^\dagger D_0\psi + \frac{1}{2m}\bar{D}_1\psi^\dagger D_1\psi + \left[ \int dx' V(x-x')\rho(x') + \mu \right] \rho(x). \quad (2.32)$$

The electron gas model described by  $S_{1DEG}$  is Galilean-invariant, which corresponds to the  $uK = 1$  case discussed in Sec. 2.1.1, where the chiral charge is exactly equal to the current. Similarly, the chiral charge resulting from  $K^{01}$  which will be discussed in the following is also equal to the current. At the same time, the spin-orbit coupled system discussed in Sec. 2.1.1 requires higher derivative terms to describe. Therefore, we generalize the formalism to include higher spatial derivatives of the fermions with an action that is written as:

$$S_{1DEG,h} = S_{1DEG} - \int dxdt V_h(\psi^\dagger, \psi, D_x\psi, D_x^2\psi, \dots). \quad (2.33)$$

Such an action can describe the spin-orbit coupled dispersion discussed in Sec. 2.1.1 when only the lower-band fermions are considered. The potential  $V_h$  does not contain the time derivative term, since Hamilton is assumed to be time-independent.

The continuity equation of  $K^{\mu\nu}$  is still Eq. 2.30, but  $K^{\mu\nu}$  is modified to

$$K^{\mu\nu} \rightarrow K^{\mu\nu} + C^{\mu\nu}, \quad (2.34)$$

where

$$C^{\mu\nu} = \frac{\partial V_h}{\partial(\partial_\mu A^\rho)} \partial^\nu A^\rho + \left[ \frac{\partial V_h}{\partial(\partial_\mu \partial_\rho A^\rho)} \partial^\nu \partial_\rho A^\rho - \partial_\rho \left( \frac{\partial V_h}{\partial(\partial_\mu \partial_\rho A^\rho)} \right) \partial^\nu A^\rho \right] + \dots \quad (2.35)$$

(See details in Appendix C)

As shown in Appendix C the kinetic momentum  $K^{01}$  written Eq. 2.32 receives no corrections from the higher derivative corrections  $V_h$ , although the expression for  $K^{11}$  is now more complicated. In addition, as detailed in Appendix C, the kinetic stress-energy tensor  $K^{\mu\nu}$  (Eq. C.5) is gauge invariant when the Lagrangian density is gauge-invariant and therefore can be used to define a gauge-invariant chiral charge.

Since  $K^{01}$  has dimensions of momentum, one can convert the kinetic stress-energy tensor to a chiral current using the relation,

$$j_{mb}^{\bar{5}\mu} := K^{\mu 1} / k_F. \quad (2.36)$$

This is consistent with the definition in Eq. 2.14 when applied to the LL case.

The corresponding momentum-based definition of the chiral charge density is

$$\rho_{c,mb} := K^{01}/k_F \quad (2.37)$$

This definition resolves the issue of identifying a nearly conserved chiral charge in a system without having to depend on regularization. The above result shows that in the systems of interest, the momentum density, which we know to be conserved in a system with continuous translation-invariance, can serve as a conserved chiral charge. This is in contrast to the traditional chiral charge in Eq. 2.8, which is only conserved in a TL approximation model, which requires a choice of regularization. Additionally, this definition is roughly consistent with Eq. 2.8 since for a weakly interacting system, we expect the change in momentum  $\delta T^{01} \sim k_F \rho_{c,cb}$ .

Finally, the conservation law for  $j_{mb}^{5\mu}$ , defined according to Eq. 2.36, and derived from Eq. 2.30, gives an anomaly equation, which is written as:

$$\langle \partial_\mu j_{mb}^{5\mu} \rangle = e \frac{n}{k_F} F^{10} = \frac{e}{\pi} E, \quad (2.38)$$

where we have simplified the RHS of Eq. 2.30  $\langle e j_\mu F^{1\mu} \rangle = enE$ . For the last equality, we have used the Luttinger relation [85, 86]  $n = k_F/\pi$  is the average number density, and  $E = F^{10}$  is the external electric field, which is the only non-zero component of the electromagnetic tensor in 1 + 1D. This result is consistent with the non-Lorentz-invariant bosonization result in Eq. 2.15.

In contrast to the Lorentz-invariant renormalized anomaly in Eq. 2.11, this anomaly is not renormalized by interaction. Note that the anomalous non-vanishing of the RHS of Eq. 2.38 in this case arises from the fact that  $K^{1\mu}$  differs from  $T^{1\mu}$ , the conserved canonical stress-energy

tensor, which is not gauge-invariant. Therefore, this represents a mixed anomaly [83] rather than the conventional chiral anomaly arising from regularization."

### 2.2.1 Application: Chiral Charge Conservation between LLs with Different $K$

The momentum-based chiral anomaly has a compelling and practical application in the context of a junction between two LLs with different Luttinger parameters  $K$ . The Hamiltonian can be expressed as

$$H_K = \int dx \frac{u(x)}{2} [K(x)\Pi^2 + K(x)^{-1}(\partial_x\Phi)^2], \quad (2.39)$$

where the boson field  $\Phi$  is defined in terms of the charge density  $\rho = \partial_x\Phi/\sqrt{\pi}$  as in Eq.A.8.  $K(x)$  describes a junction that smoothly varies from  $K_-$  to  $K_+$ . The rest of the bosonization process including the resulting current operator  $j$  remains the same ( $j = -\partial_t\Phi/\sqrt{\pi} = u(x)K(x)\Pi/\sqrt{\pi}$ ) and its conservation law remains the same as in Appendix.A.

Using canonical commutation relations, as before, leads to a slightly more general equation of motion for the field  $\Phi$ :

$$\frac{\partial_t^2\Phi}{u(x)K(x)} - \partial_x \left( \frac{u(x)}{K(x)} \partial_x\Phi \right) = 0. \quad (2.40)$$

Integrating over  $x$  on both sides, the chiral charge conservation law around this junction is obtained:

$$\partial_t Q_c = \partial_t \left( \int dx j/u(x)K(x) \right) = 0, \quad (2.41)$$

where  $Q_c = \int dx \Pi/\sqrt{\pi}$  represents the momentum-based chiral charge (i.e. Eq. 2.14), as opposed to the Lorentz-based definition in Eq. 2.8.

As a notable application, consider a recent experiment [87] that observed a quantized  $e^2/2h$  conductance from a  $\nu_- = 1/3$  fractional quantum Hall edge ( $K_- = 1/3$ ) tunneling into a  $\nu_+ = 1$  integer quantum Hall edge ( $K_+ = 1$ ) in the strong coupling limit. This quantum point contact can be modeled as a quantum wire with a spatially varying Luttinger parameter  $K(x)$  just as discussed above[88]. The scattering pattern at the junction can be determined by using normal and chiral charge conservation. Suppose that the incoming charge packet from the FQH edge carries  $q_{\nu_-,in}$  units of the basic charge  $e$  and moves to the right, the reflected charge packet carries  $q_{\nu_-,rf}$  units and moves to the left, and the transmitted particle carries  $q_{\nu_+,out}$  (integer) units and moves to the IQH edge. Based on conventional charge conservation, we obtain

$$q_{\nu_-,in} = q_{\nu_-,rf} + q_{\nu_+,out}. \quad (2.42)$$

Next, consider the chiral charge,  $Q_c$ , of these three charge packets. The corresponding current operators for each of the packets are  $\tilde{j}_{\nu_-,in}(0) = u_- eq_{\nu_-,in}$ ,  $\tilde{j}_{\nu_-,rf}(0) = -u_- eq_{\nu_-,rf}$ , and  $\tilde{j}_{\nu_+,out}(0) = u_+ eq_{\nu_+,out}$ , respectively. Using the chiral charge definition in Eq. 2.41, we find the corresponding chiral charges of each of the packets to be:  $Q_{c,\nu_-,in} = K_-^{-1} eq_{\nu_-,in}$ ,  $Q_{c,\nu_-,rf} = -K_-^{-1} eq_{\nu_-,rf}$ , and  $Q_{c,\nu_+,out} = K_+^{-1} eq_{\nu_+,out}$ , respectively.

The conservation of chiral charge then leads to the equation:

$$K_-^{-1} q_{\nu_-,in} = -K_-^{-1} q_{\nu_-,rf} + K_+^{-1} q_{\nu_+,out} \quad (2.43)$$

Solving the equations for the conservation of charge and chiral charge yields:

$$q_{\nu-,in} = \frac{K_+^{-1} + K_-^{-1}}{2K_-^{-1}} q_{\nu+,out} \quad (2.44)$$

$$q_{\nu-,rf} = \frac{K_+^{-1} - K_-^{-1}}{2K_-^{-1}} q_{\nu+,out}. \quad (2.45)$$

This indicates that the scattering patterns are restricted to this specific configuration. Consequently, the corresponding dc conductance  $G$  of this Andreev reflection-like process is [89]

$$G = \frac{e^2}{h} T_{K-,K_+} = \frac{e^2}{h} K_- \frac{q_{\nu+,out}}{q_{\nu-,in}} = \frac{2e^2}{h} (K_-^{-1} + K_+^{-1})^{-1}, \quad (2.46)$$

where  $T_{K-,K_+}$  is the transmission coefficient.

Referring back to the experimental settings, with the given  $K$ , we obtain  $q_{1/3,in} = (2/3) q_{1,out}$ ,  $q_{1/3,rf} = (-1/3) q_{1,out}$ , and the dc conductance  $G$  is  $e^2/2h$ . This result is consistent with the measured conductance in experiment [87] and provides an explanation of the predicted quantum Hall transformer conductance [90] using a chiral charge-conserving Andreev reflection-like process.

This chiral charge conservation law (i.e., Eq. 2.41) directly results from the canonical momentum  $\Pi$  conservation. Although we did not initially define the chiral charge in this subsection using microscopic translation symmetry, the bosonization process depends on microscopic details through regularization. Consequently, the effective conservation of canonical momentum in bosonization still originates from the effective microscopic translation symmetry resulting from a smooth potential in the UV description of the QPC, rendering the chiral charge conservation to be an emanant symmetry [81]. Thus, the chiral charge in this case remains "momentum"-based, corresponding to the microscopic translation symmetry. Adding back-scattering terms that break

the effective translation symmetry in the UV could invalidate the chiral charge conservation law.

### 2.3 Discussion and Summary

In 1D case, we begin by addressing the challenges of applying chiral anomaly calculations from relativistic field theories and comparing them with results from bosonization, as presented in Sec. 2.1. These ambiguities in the chiral anomaly equation are resolved by replacing the chiral anomaly with the mixed anomaly between translation and  $U(1)$  charge symmetry [83]. This new equation is qualitatively consistent with the effective action term derived previously through the correspondence between the t'Hooft anomalies and mixed anomalies [84, 91]. We find that the mixed anomaly approach in  $(1 + 1)$ D leads to a chiral charge defined as the kinetic momentum divided by the Fermi wave vector  $k_0$ . This kind of chiral charge has been surprisingly used and measured in  $^3\text{He}$  systems[92]. The electromagnetic force term in the kinetic stress-energy continuity equation corresponds to the anomalous, i.e., chiral symmetry-breaking term.

As a compelling application, we examine the Andreev reflection-like process at the junction between a  $\nu = 1$  IQH edge and a  $\nu = 1/3$  FQH edge. By considering both conventional and chiral charge conservation, we determined the unique scattering pattern, consistent with experimental observations.

Notably, the chiral anomaly equation in this case remains unrenormalized by interactions. However, we also find that an interaction-renormalized Lorentz-invariant anomaly can still be realized in LLs with weak backscattering. Such systems can be approximated by Sine-Gordon models, and the chiral charge in this scenario must be treated as a fermionic representation based on solitons and antisolitons.

## Chapter 3: Interaction Robustness of Chiral anomaly in 3D

The chiral anomaly for non-interacting 3D systems can be understood [8, 52] by focusing on the LL spectra in a magnetic field and applying the 1D results already discussed. However, this decoupling into 1D systems is not preserved in the presence of interactions. Additionally, as discussed in previous sections, the definition of a chiral charge in 1D is ambiguous unless a momentum-based approach to chiral charge is used. On the other hand, 3D Weyl systems away from the Weyl point can be viewed as a topological Fermi liquid [93] where the low energy response is described by free quasiparticles. The chiral charge associated with each Weyl point can be defined in terms of the Luttinger volume of each Fermi pocket without any reference to the regularization required in the 1D case. In Sec. 3.1, we generalize the momentum-based anomaly equation discussed in Sec. 2.2 to the 3D case. In Sec. 3.2, we show that this anomaly equation is equivalent to the anomaly equation based on the Luttinger-volume-based chiral charge. We contrast this in Sec. 3.3 with the direct computation of the change in Luttinger volume using chiral kinetic theory [9]. In Sec. 3.4, we describe how the momentum-based approach continues to apply in the low-temperature Landau level limit beyond the application of chiral kinetic theory. Finally, in Sec. 3.5 we propose a pump-probe measurement of the Luttinger-volume-based chiral anomaly.

### 3.1 Momentum-based Anomaly

In this section, we will assume that the separation between the Weyl points is small compared to the lattice constant so that the dispersion can be approximated by a continuum model [8] with conserved momentum. As will become clear in Sec. 3.4, while the lattice momentum in the  $z$ -direction is important to define the total momentum  $P_z$  in the system, it does not play a role in the chiral anomaly. Additionally, the role of this lattice momentum can be eliminated (regularized) by defining the momentum relative to a trivial insulator that can be defined for the same model.

The momentum-based chiral charge in  $1 + 1$ D i.e., Eq. 2.36 can be generalized to  $3 + 1$ D in a straightforward way as

$$j_{mb}^{5\mu,3D} := K_0^{\mu z} / k_0 \quad (3.1)$$

, where  $2k_0$  is the separation between the Weyl nodes and  $K_0^{\mu z}$  is the kinetic stress-energy tensor associated with the electrons below the Weyl points. We choose the axes  $z$  to be along the direction that joins the two Weyl points.

For the purposes of the validity of Fermi-liquid theory, we will assume that the Fermi level is away from the Weyl point. This means that  $K_0^{\mu z}$  generically differs from  $K^{\mu z}$ , which is the kinetic stress tensor of the topological Fermi liquid [93]. Following the kinetic momentum density approach to the chiral anomaly discussed in Sec. 2.2 for the 1D case, we start with the momentum conservation equation for a charged fluid (as in the  $1 + 1$ D case) in an electric field

assuming the magnetic field along the  $z$ -direction, i.e.

$$\partial_0 \langle K^{0z} \rangle + \partial_i \langle K^{iz} \rangle = \langle \rho \rangle E_z. \quad (3.2)$$

Note that the charge density  $\rho$ , unlike in the 1D case, is not related to  $k_0$ . In fact, the relevant part of the charge density  $\rho$ , here, is the contribution that is linear in  $B$  due to the Streda relation:

$$\lim_{B \rightarrow 0} \left. \frac{\partial \rho}{\partial B} \right|_{\mu} = \frac{e^2}{4\pi^2} Q_z^H. \quad (3.3)$$

, where  $Q_z^H$  is related to the intrinsic Hall conductivity  $\sigma_H^{ab} = (e^2/4\pi^2)\epsilon^{abc}Q_c^H$ . As was shown by Haldane [93], the vector  $Q_c^H$  can be written as an integral over the Berry curvature over the Fermi surface:

$$Q_c^H = \frac{1}{2\pi} \int ds^\mu \wedge ds^\nu \mathcal{F}_{\mu\nu}(\mathbf{k}(\mathbf{s})) k_c(\mathbf{s}), \quad (3.4)$$

where  $\wedge$  is the wedge product, representing the oriented area,  $\mathcal{F}_{\mu\nu}(\mathbf{k}(\mathbf{s}))$  is the Berry curvature tensor, with the Berry curvature  $\Omega(\mathbf{k}(\mathbf{s})) = \mathcal{F}_{\mu\nu}(\mathbf{k}(\mathbf{s})) \hat{s}^\mu \times \hat{s}^\nu$  representing the Berry curvature on the Fermi surface, and  $\mathbf{s}$  parameterizes the Fermi surface. The anomalous Hall conductance is thus a well-defined property of a strongly interacting Fermi liquid.

The above relation also implies that for Weyl points with a net Berry flux, the vector  $Q_z^H$  approaches  $Q_z^H \rightarrow 2k_0$  in the limit of the Fermi energy approaching the Weyl point. When the Fermi energy is away from the Weyl point, one can apply the Streda relation in Eq. 3.3 to the states between the Weyl point and the Fermi surface to calculate the magnetic field-induced

correction to the charge density as

$$\delta\rho_W = \frac{e^2}{4\pi^2}\delta Q_z^H B = \frac{e^2}{4\pi^2}(Q_z^H - 2k_0)B. \quad (3.5)$$

Here,  $\delta\rho_W$  is the  $B$ -dependent correction to the extra density of electrons associated with the Fermi level being away from the Weyl point.

This allows us to identify the electric field-induced change in momentum of the electrons between the Fermi surface and the Weyl point  $K_0^{\mu z}$ :

$$\partial_\mu(\langle K^{\mu z} - K_0^{\mu z} \rangle) = \delta\rho_W E_z = \frac{e^2}{4\pi^2} E_z B \delta Q_z^H. \quad (3.6)$$

Subtracting this change from the total change in momentum (i.e. Eq. 3.2) and applying Eq. 3.3, we get

$$\partial_0\langle K_0^{0z} \rangle + \partial_i\langle K_0^{iz} \rangle = \frac{e^2}{2\pi^2} k_0 E_z B. \quad (3.7)$$

Combining this observation with the definition of a chiral charge in Eq. 3.1 leads to the chiral anomaly equation:

$$\partial_0\langle \rho_{c,mb}^{3D} \rangle + \partial_i\langle j_{c,mb}^{i,3D} \rangle = \frac{e^2}{2\pi^2}(\mathbf{E} \cdot \mathbf{B}) \quad (3.8)$$

We note that we have not explicitly written an expression for the chiral current  $K_0^{iz}$  since it is not necessary to define the chiral anomaly coefficient. However, this is expected to be a direct generalization of Eq. 3.7. We also note that this momentum-based chiral anomaly is unrenormalized as expected, although the momentum  $K_0^{0z}$  and  $k_0$  individually might be renormalized by interactions.

The inclusion of Coulomb interactions between the electrons, in the absence of other trivial Fermi surfaces, constrains the total electron density of the bulk 3D system to be constant instead of the constant chemical potential assumed so far. This results in a correction of the chemical potential in response to the magnetic field  $B$  because of the Streda relation,

$$\delta\mu_B = -\frac{e^2}{4\pi^2} Q_z^H B / N(0), \quad (3.9)$$

since the spectral flow induced change in charge density at constant chemical potential (i.e. Eq. 3.3) is compensated by  $\delta\mu_B$ . This magnetic field-induced change in chemical potential is by itself an interesting variant of the chiral anomaly, since this is another way in which the electromagnetic field can affect the total charge of the Weyl point.

As a result of this change, Eq. 3.5 for the charge density around the Weyl point is modified to

$$\delta\rho_W^{(Coul.)} = \frac{e^2}{4\pi^2} \delta Q_z^H B + N(0) \delta\mu_B = -\frac{e^2}{2\pi^2} k_0 B \quad (3.10)$$

Interestingly, the charge neutrality constraint implies that  $\rho$  in Eq. 3.2 must vanish. Despite this, the application of Eq. 3.6 leads to the conclusion that the chiral anomaly equation Eq. 3.8 is preserved even when the charge-neutral limit is enforced by Coulomb interactions. This is a rather stringent test of the robustness of the anomaly to interactions.

## 3.2 Luttinger Volume-based Chiral Charge

The electric field  $E$  typically changes the momentum of the quasiparticles on the Fermi surface by shifting the Fermi surface, resulting in a momentum contribution  $\delta\rho_W E_z$ . But, as

seen in Eq. 3.6, the change in the Weyl part of the momentum  $K_0^{0z}$  explicitly excludes this piece. Therefore, the change over time,  $\delta K_0^{0z}$ , must arise from an electric field induced transfer of charge between the two Weyl points that are separated by the wave vector  $2k_0$  so that  $k_0^{-1}\delta K_0^{0z} = \delta\rho_{c,mb}^{3D} = \delta\rho_c^{3D}$  is the number of electrons transferred between the Weyl points.

This transfer of charge between the Weyl points has also been derived using chiral kinetic theory [9, 57, 93] and is explicitly written as

$$\frac{\partial\rho_c^{3D}}{\partial t} + \nabla \cdot \mathbf{j}_c^{3D} = \frac{e^2}{2\pi^2}(\mathbf{E} \cdot \mathbf{B}) \quad (3.11)$$

in the low-temperature limit, in which scatterings between two Weyl nodes can be suppressed and neglected.

In fact, this non-conservation of the Weyl point charge  $\rho_c^{3D}$  is the original definition of the chiral anomaly in 3 + 1D [59], which requires regularization. However, in the finite electron density limit discussed here, this chiral charge at the Weyl points  $\rho_c^{3D}$ , which is equivalent to the momentum-based chiral charge  $\rho_{c,mb}^{3D}$ , can naturally be defined and connected to a Fermi-surface property through the Luttinger volume as

$$\rho_{c,FS}^{3D} := \sum_{\alpha=\pm} \gamma_\alpha \int_{FS_\alpha} 1 \quad (3.12)$$

, where  $FS_\alpha$  represents the separate Fermi surfaces around two Weyl nodes, and  $\gamma_\alpha = \pm$  indicates the chirality of the Weyl nodes. Eq. 3.12 represents a form of chiral charge, that is well-defined even for interacting systems where Fermi surfaces are described by  $G^{-1}(k, \omega = 0, \mu) = 0$ , where  $G$  is the single-particle Green's function. The Luttinger volume provides an interaction robust

definition of a chiral charge that does not rely on any form of regularization that is not available in  $1 + 1$ D or in the strong magnetic field limit with only the chiral Landau level being occupied where the chiral anomaly is often discussed [52].

It should be noted that the equivalence of the momentum-based chiral anomaly  $\rho_{c,mb}^{3D}$  and the Fermi-surface-based chiral charge  $\rho_{c,FS}^{3D}$  breaks down when the Fermi surface is at finite temperature and sufficiently far from the Weyl point. This is because at finite temperature  $T$ , the scattering of quasiparticles around the Fermi surface which conserve momentum but not chiral charge as shown in Fig.3.1 will contribute to relaxation of the Fermi-surface-based chiral charge  $\rho_{c,FS}^{3D}$  at rate  $\sim T^2$ . However, such scatterings have no influence on the total momentum; the momentum-based chiral anomaly provides immunity against scattering. The rates of such relaxation processes will be highly suppressed at any finite temperature, as they involve highly correlated multiparticle interactions.

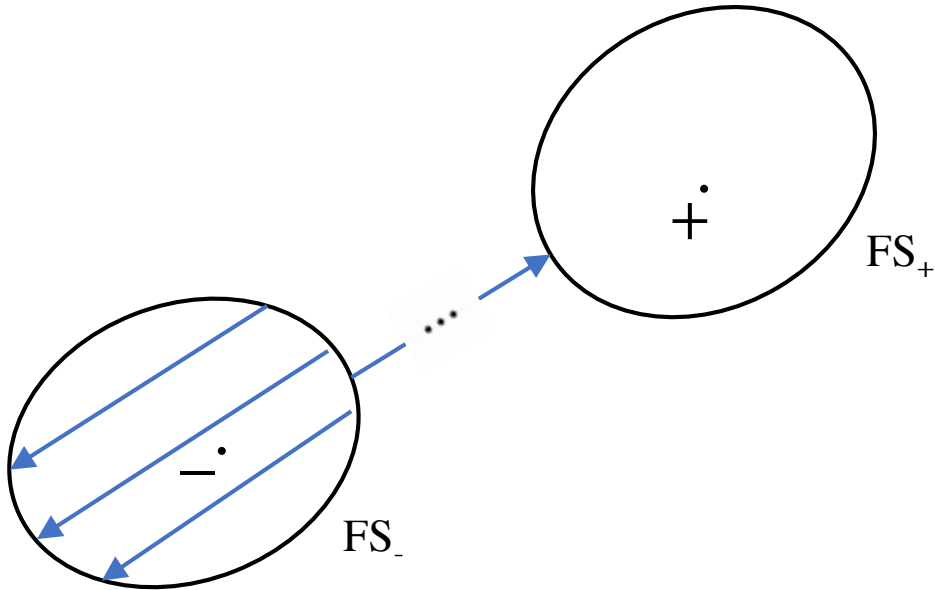


Figure 3.1: Schematic of a scattering pattern around the Fermi surface at finite  $T$ .

On the other hand, momentum can still be affected by intra-Weyl node disorder scatter-

ing, which does not influence  $\rho_{c,FS}^{3D}$ . In the presence of discrete translation symmetry, Umklapp scattering from the lattice will eliminate the momentum-based chiral anomaly. Furthermore, the rates of these relaxation processes are expected to be suppressed in the low-density limit, where the Weyl points are close to each other relative to the Brillouin zone.

### 3.3 Chiral Kinetic Theory

The results of the arguments in Secs. 3.1 and 3.2 can be checked explicitly using the chiral kinetic theory of the quasiparticles [58] of the topological Fermi liquid [93]. This is valid in the limit that the magnetic field is small enough so that the associated cyclotron frequency is much lower than the thermal energy, i.e.,  $\omega_B \ll k_B T$ .

In the Fermi liquid limit, this chiral kinetic theory has been successfully used to understand the properties of topological Fermi liquids [9, 57, 94, 95]. In the following, we will use it to validate the properties of the momentum-based chiral charge as well as the measured chiral charge discussed in Secs. 3.1 and 3.2.

The central equation of kinetic theory is the Boltzmann equation:

$$\frac{\partial f}{\partial t} + \frac{\partial f}{\partial \mathbf{r}} \cdot \dot{\mathbf{r}} + \frac{\partial f}{\partial \mathbf{k}} \cdot \dot{\mathbf{k}} = I_{coll} = -\frac{\delta f}{\tau} \quad (3.13)$$

, where  $f = f(\mathbf{r}, \mathbf{k}, t)$  is the quasiparticle distribution function. The quasiparticles can only change their state and be equilibrated through collisions, which are approximated by the relaxation time approximation with a constant collision frequency  $1/\tau$ .

The equations of motion for quasiparticles in the presence of an anomalous velocity [35]

are written as

$$\dot{\mathbf{k}} = e\mathbf{E} + e\dot{\mathbf{r}} \times \mathbf{B} \quad (3.14)$$

$$\dot{\mathbf{r}} = \mathbf{v}_{\mathbf{k}} + \dot{\mathbf{k}} \times \boldsymbol{\Omega}_{\mathbf{k}} \quad (3.15)$$

, where  $A_{\mathbf{k}} = i \langle u_{\mathbf{k}} | \nabla u_{\mathbf{k}} \rangle$ ,  $\boldsymbol{\Omega}_{\mathbf{k}} = \nabla \times A_{\mathbf{k}}$  is the Berry curvature, and the group velocity  $\mathbf{v}_{\mathbf{k}} = \nabla_{\mathbf{k}} \varepsilon$ .

Due to the Berry curvature term in the above equations, a violation of Liouville's theorem by the RHS of Eq. 3.13 [95] This can be rectified by introducing a phase space density factor  $G_{\mathbf{k}} = (1 + e\mathbf{B} \cdot \boldsymbol{\Omega}_{\mathbf{k}})^2$ , which satisfies an equation of motion[57]

$$\frac{\partial}{\partial t} \sqrt{G_{\mathbf{k}}} + \frac{\partial}{\partial \mathbf{r}} \cdot (\sqrt{G_{\mathbf{k}}} \dot{\mathbf{r}}) + \frac{\partial}{\partial \mathbf{k}} \cdot (\sqrt{G_{\mathbf{k}}} \dot{\mathbf{k}}) = e^2 (\mathbf{E} \cdot \mathbf{B}) \nabla \cdot \boldsymbol{\Omega}_{\mathbf{k}}. \quad (3.16)$$

We can define a conserved phase-space density  $\tilde{f} = \sqrt{G_{\mathbf{k}}} f$  that obeys Liouville's theorem by combining the phase-space density  $\sqrt{G_{\mathbf{k}}}$  with the distribution function  $f$ , which now obeys the conservation law:

$$\frac{\partial}{\partial t} \tilde{f} + \frac{\partial}{\partial \mathbf{r}} \cdot (\tilde{f} \dot{\mathbf{r}}) + \frac{\partial}{\partial \mathbf{k}} \cdot (\tilde{f} \dot{\mathbf{k}}) = e^2 (\mathbf{E} \cdot \mathbf{B}) \nabla \cdot \boldsymbol{\Omega}_{\mathbf{k}} f + \tilde{I}_{coll} \quad (3.17)$$

, where  $\tilde{I}_{coll} = \sqrt{G_{\mathbf{k}}} I_{coll}$ .

Using the above equation of motion for the phase space density  $\tilde{f}$ , we can find the continuity equation for the Luttinger volume-based chiral charge in Sec.3.2 and the kinetic momentum,

$$\mathbf{P} = \int_{\mathbf{k}} \mathbf{k} \tilde{f}, \quad (3.18)$$

in Sec.3.1. The result of the first one (Eq.3.11) has been already discussed in many references and Sec.3.2. The second one, with respect to the kinetic momentum, is written as

$$\frac{\partial}{\partial t} \mathbf{P} + \nabla \cdot \vec{\mathbf{K}} = \frac{e^2}{4\pi^2} (\mathbf{E} \cdot \mathbf{B}) \mathbf{Q}^H + \int_{\mathbf{k}} (e\mathbf{E} + e\mathbf{v}_{\mathbf{k}} \times \mathbf{B}) f. \quad (3.19)$$

, where

$$\vec{\mathbf{K}} = \int_{\mathbf{k}} (\mathbf{v}_{\mathbf{k}} + e\mathbf{E} \times \boldsymbol{\Omega}_{\mathbf{k}} + e(\mathbf{v}_{\mathbf{k}} \cdot \boldsymbol{\Omega}_{\mathbf{k}}) \mathbf{B}) \mathbf{k} f \quad (3.20)$$

, a dyadic tensor, is the stress tensor, and

$$\mathbf{Q}^H = 4\pi^2 \int_{\mathbf{k}} \boldsymbol{\Omega}_{\mathbf{k}} f = \sum_{\alpha} \mathbf{Q}_{\alpha}^H = \frac{1}{2\pi} \sum_{\alpha} \int_{S_{\alpha}} d^2 \mathcal{F} \mathbf{k} \quad (3.21)$$

, which is just the vector associated with the anomalous Hall conductivity in the Streda formula Eq.3.3. The collision term will not contribute if we assume that collisions are elastic. Incidentally, this equation is general for any condensed matter system, and interactions will not be affected.

To obtain the momentum-based chiral anomaly equation from Sec.3.1, we still consider the  $z$ -direction component of the kinetic stress-energy tensor and assume the magnetic field also along  $z$ . Eq.3.19 will be simplified:

$$\frac{\partial}{\partial t} P^z + \nabla \cdot \vec{K}^z = \frac{e^2}{2\pi^2} (\mathbf{E} \cdot \mathbf{B}) Q_z^H. \quad (3.22)$$

Restricting the integrals in Eqs. 3.18 and 3.21 above the Weyl point leads to a variation of the above equation:

$$\frac{\partial}{\partial t} (P^z - P_0^z) + \nabla \cdot (\vec{K}^z - \vec{K}_0^z) = \frac{e^2}{2\pi^2} (\mathbf{E} \cdot \mathbf{B}) \delta Q_z^H, \quad (3.23)$$

where  $P^z$  and  $Q_z^H$  are replaced by  $(P^z - P_0^z)$  and  $\delta Q_z^H = Q_z^H - 2k_0$ , which are the momentum and anomalous Hall contributions of electrons above the Weyl point, respectively. Note that  $P_0^z$  and  $2k_0$  are intrinsic momenta and the anomalous Hall contributions of the Weyl point.

This provides a more quantitative understanding of Eq. 3.6 from Sec. 3.1. Combining Eq. 3.22 with Eq. 3.23 leads us back to the chiral anomaly equation:

$$\frac{\partial}{\partial t} P_0^z/k_0 + \nabla \cdot \vec{K}_0^z/k_0 = \frac{e^2}{2\pi^2} (\mathbf{E} \cdot \mathbf{B}), \quad (3.24)$$

Thus, the analysis of the contribution of the Weyl point to the momenta  $P_0^z$  provides a more microscopic derivation (i.e. in terms of FL quasiparticles) of the anomaly equation Eq. 3.8.

As an aside, the chiral kinetic theory can also compute the chiral magnetic effect (CME).

The current along the  $B$ -direction can be written as [57]

$$\mathbf{j}_{\text{CME}} = e^2 \mathbf{B} \int_{\mathbf{k}} f(\mathbf{v}_{\mathbf{k}} \cdot \boldsymbol{\Omega}_{\mathbf{k}}) = \frac{e^2 \mathbf{B}}{4\pi^2} \Delta\mu, \quad (3.25)$$

where

$$\Delta\mu = \frac{1}{2\pi} \sum_{\alpha} \int_{S_{\alpha}} d^2\mathcal{F} \varepsilon(\mathbf{k}) \quad (3.26)$$

(See details in Appendix D) is the deviation of the chemical potential from an equilibrium state.

Note that since states far away from the Weyl point can contribute to the current, it is important to consider the chiral magnetic current  $\mathbf{j}_{\text{CME}}$  relative to an equilibrium state with vanishing current [96]. If we assume that the electron distribution functions have equilibrium forms in the individual valleys,  $\Delta\mu$  is exactly the chemical potential difference at the Fermi level, and Eq. 3.25

is consistent with references[8, 9]. Eq.3.25 is robust since it depends only on Fermi surfaces.

Hence, the conductivity along the magnetic field direction,  $\sigma_{zz}$ , is modified as[8, 9]

$$\sigma_{zz}(B) = \sigma_{zz}(0) + \frac{e^4 B^2 \tau_a}{4\pi^4 g(\epsilon_F)} \quad (3.27)$$

, where  $g(\epsilon_F)$  is the density of state and  $\tau_a$  is the inter-nodes scattering time. The above conductance depends on the parameters  $\tau_a$  and  $g(\epsilon_F)$ .

On the other hand, the chiral magnetic current  $\mathbf{j}_{CME}$  in terms of  $\Delta\mu$  as given by Eq. 3.25 is universal for a topological Fermi liquid and is not renormalized by interactions. While the above equation for dc conductivity depends on inter-valley scattering at rate  $\tau_a^{-1}$ , one could consider the response to an ac electric field  $E(\omega)$  at frequency  $\omega \gg \tau_a^{-1}$ . In this case, the ac current response should satisfy Eq. 3.25 and lead to a corresponding fluctuation of  $\Delta\mu$  at frequency  $\omega$  provided  $\omega$  is slower than the intra-valley equilibration rate. The chemical potential difference  $\Delta\mu$  can, in principle, be measured by the dissipative optical response at frequency  $\omega_1 \sim \Delta\mu + v_s k_0$ , where  $v_s k_0$  is the minimum phonon frequency of inter-valley scattering from acoustic phonons with sound velocity  $v_s$  and wave vector  $k_0$ , which is the separation of Weyl points. The phonon frequency is a bit difficult to estimate. However, one can consider the change in  $\Delta\mu$  with varying electric field amplitudes to verify the chiral magnetic effect.

## 3.4 Chiral Anomaly in the Landau Level Regime

### 3.4.1 Non-interacting Weyl Model Under a Magnetic Field

The discussion so far has assumed a temperature that is high relative to the small applied magnetic field. However, all the conclusions are carried out equally well at nearly zero temperature.

The low temperature for a non-interacting Weyl system in a magnetic field is described by the chiral Landau level [52]. To illustrate this, we will compute the non-interacting Landau levels for the continuum Weyl toy model [8], which is written as

$$H_{Weyl,R} = (k^2 - k_0^2)\sigma_z + v(k_y\sigma_x - k_x\sigma_y) \quad (3.28)$$

, where  $k^2 = k_x^2 + k_y^2 + k_z^2$  and  $v$  is the Rashba coupling constant. The energy spectrum is indeed the Weyl type in the low-energy regime, which has two touching Weyl points at  $\mathbf{k} = (0, 0, \pm k_0)$  when  $v \neq 0$ .

To study the chiral anomaly, when applying the magnetic field  $B$  along the  $z$ -direction, we calculate the LL spectrum of the Hamiltonian  $H_{Weyl,R}$  in the presence of a magnetic field, as shown in Fig. 3.2. While the magnetic field preserves the angular momentum, the spin-orbit coupling mixes the  $(\sigma_z = 1, n)$  and  $(\sigma_z = -1, n + 1)$  (where  $n$  labels the conventional Landau levels without spin-orbit) and opens a gap in the spectrum. However, one of the Landau levels  $(\sigma_z = -1, n = 0)$  does not have a partner to hybridize and remains gapless. This Landau level, which is referred to as the chiral Landau level, is responsible for the chiral anomaly in an applied

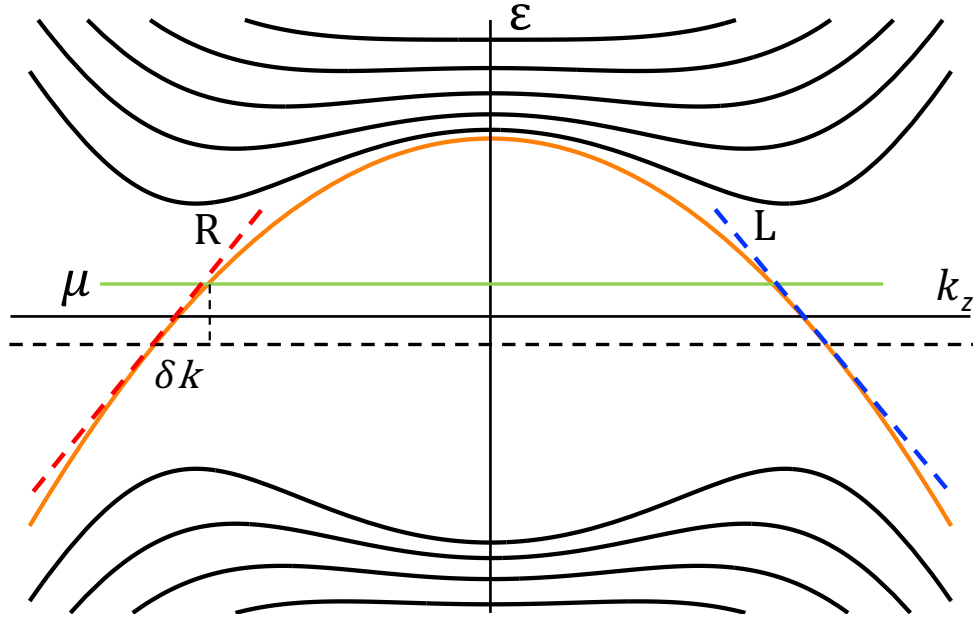


Figure 3.2: Band structure of Weyl model ( $k_0 = 1$ ) in the Sec.3.4 with a small spin-orbit coupling  $v = 1.5$  under the magnetic field  $B = 0.1$ . The chemical potentials are set away from the Weyl nodes, and the low energy states are basically multiply LLs.

electric field within the non-interacting limit [52]. Note that the gap in the non-chiral LLs in Fig. 3.2 actually occurs at negative energies as opposed to the previous calculation of LL spectra of individual Weyl cones [8, 12, 52]. This difference is a manifestation of the Streda formula i.e. Eq. 3.3, which, as discussed in Sec. 3.1 is critical for understanding the chiral anomaly from a momentum conservation perspective.

### 3.4.2 Momentum-based Chiral Charge

The chiral anomaly is conventionally defined, using the argument of Nielsen and Ninomiya [52], as non-conservation of chiral charge can be determined from the LL spectrum in Fig. 3.2 for the non-interacting case where the chemical potential is in the gap of the non-chiral LLs. This argument also leads to a current that appears to be renormalized by interactions [62], which, similar to the 1 + 1D results discussed in Sec. 2.1, depends on the regularization scheme

used for the calculation.

However, the subtleties of defining a chiral charge discussed in Sec. 2.1 arise when only the Fermi level intersects just the chiral LL, and therefore the other LLs are important in defining chiral charge. Therefore, it is beneficial to consider the chiral anomaly away from the Weyl points, where several non-chiral LLs are also occupied. These non-chiral LLs do not contribute to the change in chiral charge in response to an electric field and therefore do not modify the chiral anomaly [8].

These non-chiral LLs do, however, affect the momentum-based definition of chiral charge, since they contribute to momentum change under an electric field. This turns out to be not a problem because, similar to the case discussed in Sect. 3.1, the contribution of non-chiral LLs as well as the electrons in the chiral LL above the Weyl point to the change in momentum can be calculated directly from the density of electrons in the respective LLs. For small magnetic fields corresponding to  $\omega_B \ll E_F$ , this density is given by the FS volume.

Subtracting the momentum contribution of electrons above the gap of the non-chiral LLs leaves only the momentum contribution associated with a transfer of electrons from one Weyl point to the other. This can be estimated to be  $2k_0(B/2\pi)(E_z\delta t)$  where  $E_z\delta t$  is the change in momentum of the electrons and  $B/2\pi$  is the degeneracy per unit area of the chiral Landau level. The factor  $2k_0$  arises from the length of the unoccupied segment (or occupied by holes) of the chiral Landau level in Fig. 3.2. Since  $2k_0$  is the distance between the Fermi points on the chiral LL when the chiral LL crosses the gap of the non-chiral LL, the momentum density can be interpreted as a chiral charge that is consistent with the result of Eq. 3.8. The chiral LL in Fig. 3.2 leaves an ambiguity in the value of  $2k_0$  to be in the range where the chiral LL crosses the gap. This ambiguity drops out in the limit of small  $B$  since the gap also vanishes in this limit.

Fully filled LLs (including a fully filled chiral Landau level) will not contribute to the continuity equation Eq. 3.2. This is because the total crystalline momentum along  $k_z$  generated by a slowly time-varying external electric field  $E_z$  that increases a vector potential  $\delta A_z = E_z \delta T = \Phi_0/L_z$ , changes the momentum on the RHS of Eq.3.2 by a primitive reciprocal lattice vector. Note that the lattice does play an essential role in regularizing the otherwise divergent momentum. However, one would obtain the same result from other regularizations such as by considering the difference in momentum between this chiral system and a variant of Eq. 3.28 with a trivial gap generated by a  $\sigma_x$  term instead of the spin-orbit term.

### 3.4.3 Interaction Effects

The effect of interactions can be included in a Fermi liquid theory in this framework if one goes away from the Weyl point (relative to the cyclotron frequency), i.e.  $E_F \gg \omega_B$ . In this limit and in the presence of a small magnetic field,  $\mathbf{B} = B\hat{\mathbf{n}}$ , the quasiparticles near the FS follow semiclassical orbits (given by Eq. 3.15 with  $\mathbf{E} = 0$ ) which are confined to planes with constant parallel momentum  $\hat{\mathbf{n}} \cdot \mathbf{k} = k$ , with a long scattering lifetime.

The Fermi-surface orbit in  $k$ -space on the FS labeled by  $\alpha$ , has a cross-sectional area  $A_\alpha(k)$  that is set by a quantization condition [97]

$$A_\alpha(k_{F\alpha}^n)l_B^2 - \phi_\alpha(k_{F\alpha}^n) = 2\pi(n + \frac{1}{2}), \quad (3.29)$$

where  $l_B^2 = 1/eB$ , and  $n$  is an integer that labels the Landau orbits (i.e. bands in Fig. 3.2) and  $\phi_\alpha(k)$  is the Berry phase of the quasiparticle on the phase-space orbit at  $k$  on  $FS_\alpha$ . The Landau band in Fig. 3.2 with an extremum closest to the Fermi level represents the pair of Landau orbits

on the FS that is closest to the maximum area orbit at  $k = k_{max}$  of the FS. These are the orbits that contribute to quantum oscillations and are used to determine the size of the Fermi surface [97].

The solution with maximum  $|k|$  is the chiral Landau level, which is a result of the difference in Berry phase  $2\pi C_\alpha = \phi_\alpha(k_1) - \phi_\alpha(k_2)$ , where  $k_1 > k_{max} > k_2$  represents the range of  $k$  of  $FS_\alpha$  and  $C_\alpha = \pm 1$  is the Chern number of Fermi surface around the Weyl point  $\alpha$ . The resulting LL spectrum near the FS is essentially identical to the non-interacting one seen in Fig. 3.2, except that the energy spectrum away from the Fermi energy is ill-defined because of the imaginary part of the self-energy. The response to an external electric field  $E$  in the time period  $\delta t$  is determined by the states near the Fermi energy, which is therefore identical to the non-interacting case discussed in the previous paragraph and is described by Eq. 3.8.

### 3.5 Measuring the Luttinger-volume-based Chiral Anomaly

The quantum oscillations that arise from the extremal Landau bands at  $k = k_{max}$  discussed in the previous subsection can, in principle, be used to detect the Luttinger-volume-based chiral anomaly discussed in Sect. 3.2 by measuring the chiral charge transfer in a pump-probe measurement.

The central idea is to use quantum oscillations to measure the anomaly-induced change in the Fermi wave vector, as is done in magnetotransport (i.e. the Shubnikov-de Hass effect) [97]. This effect relies on the fact that low-frequency longitudinal conductivity would show dips associated with peaks in the density of states (DOS) when the Fermi level crosses a band extremum in Fig. 3.2. This corresponds to an extremal LL being allowed on the FS. For simplicity we will assume that the Fermi surface is nearly spherical near the Weyl point, so that the electron number

density in the Weyl point  $\alpha$ ,  $N_\alpha = A_\alpha(k_{max})^{3/2}/6\pi^{7/2}$ , can be written in terms of the extremal area  $A_\alpha(k_{max})$ .

Our protocol for measuring the Luttinger volume-based chiral anomaly discussed in Sec. 3.2 consists of three steps.

**Step 1:** Choose a magnetic field  $B$  such that the Fermi surface (FS) quasiparticle density of states (DOS) is at a local maximum, as indicated by a minimum in the measured longitudinal conductance. In our model, this corresponds to  $k_{max}$  satisfying Eq. 3.29 for an integer  $n$ .

**Step 2:** Apply a "pump" electric field  $E_z$  for a short time  $\delta t$ , then allow the system to relax for a time  $\tau$ .

**Step 3:** Measure the longitudinal conductance using a "probe" field to check if the conductance is near the minimum value. Repeat step (2) with a different  $\delta t$  until the conductance reaches near the minimum value.

The result of the measurement is  $\Lambda = eE_z\delta t$ , which transfers the system from one conductance minimum to another. For a small magnetic field  $B$ , the change  $\delta k$  in  $k_{max}$  is insignificant, so that we can ignore the Berry phase term and simplify Eq. 3.29 to  $\delta A_\alpha = 2\pi\alpha eB$ . The corresponding change in number density is  $\delta N_\alpha = 4\alpha A_\alpha(k_{max})\delta k/(2\pi)^3 = eB\alpha\sqrt{A_\alpha(k_{max})}/2\pi^{5/2}$ .

Assuming an unrenormalized chiral anomaly and using Eq.3.11, the predicted  $\Lambda$  would be

$$\Lambda_{predict} = eE_z\delta T = \frac{2\pi^2}{e} \frac{\delta(N_+ - N_-)}{B} = 2\sqrt{\frac{A_\alpha(k_{max})}{\pi}}. \quad (3.30)$$

The measured value of  $\Lambda$  determines the Luttinger-volume-based chiral charge transfer between the two Fermi surfaces, which based on results in this section should not be renormalized by interactions or other complexities of the system.

### 3.6 Discussion and Summary

Turning to the 3+1D case, we apply the mixed anomaly technique [83] to Weyl systems, drawing parallels to previous work that maps the t'Hooft anomaly to an effective action term in a mixed anomaly representation [84]. Using the Streda formula, we demonstrate that the anomaly based on the difference in charge density around Weyl pockets is robust and unrenormalized. This is a key distinction from the CME [8], whose manifestations come with various non-universal prefactors that are renormalized by interactions. While some prefactors, like density of states or Fermi velocity, can be determined experimentally, it remains unclear whether the CME is the only contributor to these currents.

For instance, a numerical calculation of the ac Hall conductivity in a non-interacting model of a Weyl material shows a non-zero and non-universal second-order term, even in the absence of interactions (see Appendix E). Additionally, a direct interpretation of the CME in terms of the axion term in effective action [65, 98] suggests a magnetic-field induced current at finite magnetic fields. While such response terms are observed for finite frequency magnetic fields with open boundary conditions [99], and in the form of the gyrotropic magnetic effect [100, 101], they are not observable under physical equilibration [96].

As discussed at the end of Sec. 3.3, an unrenormalized CME relation (i.e., Eq. 3.25) could, in principle, be measured via a pump-probe experiment. However, it is crucial to note that this CME is separate from the anomaly itself, which refers to the violation of charge conservation in an individual Weyl pocket. The anomaly in 3+1D does not suffer from the ambiguities seen in 1+1D and can be defined in terms of the Luttinger volume of the topological Fermi surface [93]. While this measurement is experimentally intricate, we propose a pump-probe measurement that

directly measures the changes in Luttinger volume in response to an electromagnetic field.

It is important to contrast this approach with previous work [83, 84], where the chiral anomaly equations were derived using a mixed anomaly between  $U(1)$  charge and continuous space translation. This requires using a regularization for the kinetic momentum, which is discussed in Sec. 3.4.2, and subtracting off the contribution of the closest gapped insulator. This only makes sense when the Weyl points are close in momentum space relative to the total Brillouin zone, as described in Sec. 3.4. This approach differs from the Chern insulator stack model of a Weyl semimetal [8], and the methodology used here may not apply to that model. On the other hand, the chiral kinetic theory [58] for the charge density in each pocket still predicts a robust quantized change in chiral charge. However, this relies on the full Fermi liquid emergent IR symmetry, which would be broken by finite temperature scattering or Umklapp scattering at the edge of the Brillouin zone. While disorder scattering [8] complicates this entire discussion, the realistic definition of the chiral anomaly must account for the appropriate scaling with disorder [8, 9, 53].

## Chapter 4: Anomalous Hall Effect from Screened Vortex Charge in Phase-Disordered Superconductors

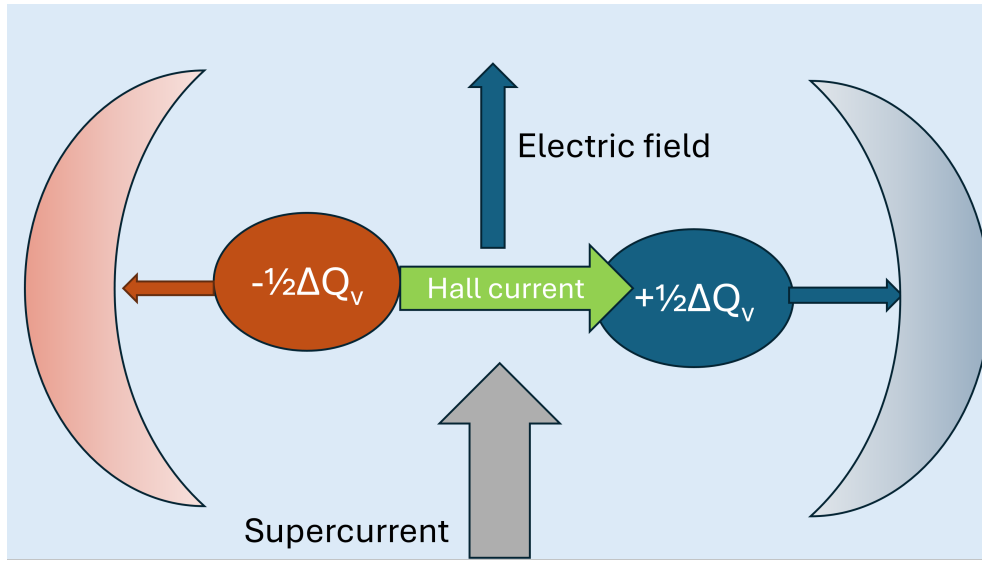


Figure 4.1: Schematic for the origin of anomalous Hall in a 2D superconductor above the BKT transition i.e. so-called phase disordered state. The local supercurrent applies a Magnus force [102] on the vortex-antivortex pair (red and blue discs) in opposite directions. This leads to diffusive motion of the vortices along  $\pm \hat{x}$  [103]. The motion of the vortices corresponds to an electric field along  $y$ , which is the origin of dissipative transport in the phase disordered state. The difference in vortex-anti-vortex charge  $\Delta Q_v = Q_- - Q_+$  that we will numerically show to be related to the normal state anomalous Hall coefficient lead to a Hall current (green arrow) orthogonal to the electric field. We find that many-body screening as well as the far-field phase winding of vortices (shown as the crescents of moving charge) conspire to match the measured dc Hall conductance from vortices to the bulk ac Hall conductance.

As introduced in Chapter 1, recent experiments on tetralayer and pentalayer rhombohedral graphene revealed an robust unconventional superconducting phase characterized by spontaneously broken time-reversal symmetry, of which several observations indicate the chiral nature

[28]. Notably, the normal state of this system exhibits a non-zero anomalous Hall effect at zero applied magnetic field, accompanied by clear magnetic hysteresis. These striking findings naturally raise the question of what mechanism could give rise to such anomalous Hall conductivity, particularly in the absence of long-range phase coherence above the superconducting transition temperature.

In this chapter, we investigate the mechanism behind this anomalous Hall effect [102]. As shown in Fig. 4.1, the difference in charge densities in the cores of vortices and antivortices can lead to an anomalous Hall contribution to the current. We argue that such a contribution can arise from a gauge-invariant effective action of a superconductor [104] that includes a Hall response and numerically check that such a contribution indeed appears in a simple model. We then show using the gauge-invariant response that while the vortex charge is screened by many-body interactions, the dynamical screening cloud (crescents in Fig. 4.1) combine so that the vortex-generated dc Hall conductivity is the same as the ac Hall response.

## 4.1 Effective Action of a Hall Superconductor

To describe a superconductor, we introduce a fluctuating field  $\phi(r, t)$ , which will represent the phase of the symmetry breaking order parameter. The gauge transformation properties of  $\phi$  are such that the shifted gauge potentials  $b_\alpha = A_\alpha - \partial_\alpha \phi$  are gauge-invariant degrees of freedom, which is the essence of gauge fields acquiring mass [104]. For an electronic system similar to tetra-layer graphene assuming screened Coulomb interactions, the field  $\phi$  can be microscopically defined as the phase of a Hubbard-Stratonovich field associated with the pairing interaction and appears as fields  $b_\alpha$  in the effective action following the Hubbard-Stratonovich decomposition.

Expanding this effective action to the lowest order in the fields  $b_\alpha$  in Fourier space  $(q, \omega)$  components  $e^{i(q \cdot r - \omega t)}$ , leads to the expression:

$$S_{sc,eff} = \sum_{q,\omega} b_\alpha(q, \omega) b_\beta^*(q, \omega) K^{(\alpha,\beta)}(q, \omega) \quad (4.1)$$

where  $K^{(\alpha,\beta)}(q, \omega)$  is a Hermitian matrix, that is,  $K^{(\alpha,\beta)*}(q, \omega) = K^{(\beta,\alpha)}(q, \omega)$  for a gapped superconductor. This together with the reality of  $b_\alpha$ , i.e.  $b_\alpha(q, \omega)^* = b_\alpha(-q, -\omega)$  implies that  $S_{sc,eff}$  is non-dissipative.

The ac current (and charge) in the superconductor can be obtained as functional derivatives of the action, i.e.

$$j_\alpha(q, \omega) = \frac{\delta S_{sc,eff}}{\delta A_\alpha^*(q, \omega)} = K^{(\alpha,\beta)}(q, \omega) b_\beta(q, \omega), \quad (4.2)$$

so that  $K^{(\alpha,\beta)}(q, \omega)$  can be viewed as part of the electromagnetic response coefficients of the superconductor [105]. The reality of the current further requires  $K^{(\alpha,\beta)*}(q, \omega) = K^{(\alpha,\beta)}(-q, -\omega)$ .

Expanding  $K^{(\alpha,\beta)}(q, \omega)$  to lowest non-zero order in  $q, \omega$  consistent with these constraints, substituting it into Eq. 4.1 and Fourier transforming to space and time, the effective action  $S_{sc,eff}$  can be written as a gradient expansion:

$$S_{sc,eff} = \int [-C_1 b_0^2 + C_2 b^2 - \{C_3 b - C_4(\hat{z} \times b)\} \cdot \nabla b_0 + C_5(\hat{z} \times b) \cdot \dot{b}]. \quad (4.3)$$

The first two coefficients  $C_1$  and  $C_2$  are superfluid compressibility and stiffness, respectively. In the case  $C_4 = C_5$ , the last two terms Fourier transform to  $b_\alpha^*(q, \omega) \epsilon_{z\alpha\beta} (i q_\beta b_0 - i \omega b_\beta) = i \epsilon_{\alpha\beta\gamma} b_\alpha^*(q, \omega) q_\beta b_\gamma(q, \omega)$  is exactly the Chern-Simons term in the superconductor [69,

73]. Here, we have identified  $q_0 = -\omega$ . Using the definition of an electric field  $\mathcal{E}_\beta(q, \omega) = i\omega b_\beta(q, \omega) - iq_\beta b_0(q, \omega)$ , this term leads to a Hall contribution to the current of Eq. 4.2 given by  $j_{H,\alpha} = -C_5 \epsilon_{z\alpha\beta} \mathcal{E}_\beta = C_5 (\mathcal{E} \times \hat{z})_\alpha$ .

The role of the difference  $(C_4 - C_5)$  for a superconductor will be a central topic in this work. The term proportional to  $C_3$  produces a term in the action  $\nabla\theta \cdot \nabla\partial_t\theta = (1/2)\partial_t[(\nabla\theta)^2]$  that vanishes from being a total derivative. Therefore, we can set  $C_3 = 0$ .

## 4.2 Electromagnetic Response

To understand the physical implication of the coefficients  $C_j$ , let us calculate the ac electromagnetic response as a function of frequency  $\omega$  and wave vector  $q$ . To simplify our analysis, we consider rotationally symmetric systems and assume that the wave vector  $q$  is oriented along the  $x$  direction, which we will refer to as  $L$  (longitudinal or curl-free). The other spatial direction,  $y$ , is perpendicular to  $x$  and will be denoted as  $T$  (transverse or divergence-free), since we are working within a two-dimensional system. Thus,  $L, T$  together with 0 for time will be the values of the indices  $\alpha$  and  $\beta$  in the above equations.

In this notation, the gauge-invariant electric fields that are derived from the generalized vector potential  $b_\alpha$  are written as  $\mathcal{E}_T(q, \omega) = i\omega b_T(q, \omega)$  and  $\mathcal{E}_L(q, \omega) = i\omega b_L(q, \omega) - iq b_0(q, \omega)$ . Due to gauge invariance, the phase fluctuation drops out of the vector  $\mathcal{E}_\alpha$  and is restricted to  $b_0$ . Choosing (for this calculation) a gauge where  $A_0 = 0$  (i.e., radiation gauge),  $b_0 = i\omega\phi$  represents the phase fluctuations.

Applying charge conservation  $\omega j_0 - qj_L = 0$  to the linear response relation Eq. 4.2 determines the phase fluctuation  $b_0 = \frac{q}{C_2 q^2 - C_1 \omega^2} [iC_2 \mathcal{E}_L + (C_4 - C_5)\omega \mathcal{E}_T]$ . Substituting  $b_0$  in the linear

response equation Eq. 4.2 leads to the ac conductivity tensor  $\sigma_{\alpha\beta}(q, \omega)$  for the superconductor.

The longitudinal conductivity tensor produces the well-known result [105]  $\sigma_{LL} = \frac{iC_1C_2\omega}{C_2q^2 - C_1\omega^2}$ , which has a pole associated with the Goldstone phase mode. Similarly, the transverse response to lowest order in  $q, \omega$ , takes the standard form  $\sigma_{TT} = -iC_2/\omega$ , which leads to the Meissner screening response  $j_T = -C_2A_T$  [104]. In the weak pairing limit  $\Delta \ll E_F$ , these conductivities are unchanged from the normal state in the extreme limits  $q \ll \omega$  and  $q \gg \omega$ .

In the former case,  $\sigma_{LL} = \sigma_{TT} = -iC_2/\omega$  is simply the inertial response of the electron gas that leads to the plasmons. The latter case is the static Thomas-Fermi response, which matches the normal response only in the longitudinal case where  $\sigma_{LL} \sim iC_1\omega/q^2$ . Although this may seem unfamiliar at first, the corresponding charge compressibility  $\chi = (q^2/i\omega)\sigma_{LL} = C_1$  allows us to associate  $C_1$  with the charge compressibility for the normal state.

Let us now consider the ac Hall response of such a superconductor [72, 73] arising from  $C_{4,5} \neq 0$ , which turns out to be

$$\sigma_{LT} = -\sigma_{TL} = \frac{C_2C_4q^2 - C_1C_5\omega^2}{C_1\omega^2 - C_2q^2}. \quad (4.4)$$

Although the applied electric field in the dc limit is expected to be screened, a central indicator of chirality of a superconductor is the  $q \ll \omega$  ac Hall response [72, 73], which in our case determines the coefficient  $C_5$ :

$$\sigma_H = \sigma_{LT}(\omega \gg q) = C_5. \quad (4.5)$$

In addition, it was realized that the chiral nature of the superconductor does not contribute to  $C_5$  in

the translationally invariant case [72], although it reappears in multiband superconductors [106]. Explicit computation of the effective action in Eq. 4.1, similar to the case of the normal state, shows that the dominant contribution to  $C_5$  arises from high-energy inter-band matrix elements that are relatively unaffected by correlation and superconductivity. Therefore, we expect  $C_5$  and the ac Hall conductivity for  $q \ll \omega$  to retain the anomalous Hall value in the normal state, which is determined by the Berry curvature of the bands [37].

Let us now consider the other limit, i.e.  $q \gg \omega$ , which is the finite  $q$  static limit. This limit can be understood by combining the conservation relation  $j_0 = -qj_L/\omega = -q\sigma_{LT}\mathcal{E}_T/\omega$  with Faraday's law  $\omega B_T = -q\mathcal{E}_T$ , as the charge response to a flux lattice

$$j_0 = \sigma_{LT}(q \gg \omega)B_T = C_4B_T \quad (4.6)$$

, where  $B_T$  is the amplitude of the magnetic field variation in the flux lattice with period  $q$ . Physically, modulation of charge density  $j_0$  can be viewed as the accumulation of charge in response to the application of a magnetic field. Thus,  $C_4$  is the Streda response coefficient [107], which is proportional to the Hall conductivity  $\sigma_H$  in non-interacting systems [37]. Since  $\sigma_{LT}$  arises from interband transitions that have a smooth frequency dependence near  $\omega \sim 0$ , the coefficient  $C_4$  should match the normal state value. For noninteracting systems, one expects  $C_5 = C_4$ , with both being related to Berry curvature [37]. However, for a flux lattice applied to a normal metal, a large  $N$  or RPA calculation would lead to a screening of charge  $j_0$  by a factor related to  $C_1$ . This would lead to a difference between  $C_4$  and  $C_5$ .

### 4.3 Vortex Charge in an Anomalous Hall Superconductor

The flux lattice discussed in the previous paragraph leads to a supercurrent pattern from the Meissner effect, which resembles a lattice of vortex-antivortex pairs. This motivates the question of whether a vortex, even in the absence of an external magnetic field, would carry a vortex charge.

To understand the vortex charge on a lattice, let us note that a phase vortex can be converted into an anti-vortex by a large gauge transformation:

$$\begin{aligned}\phi(r) &\rightarrow \phi(r) + \Lambda(r) \\ \mathbf{A}(r) \cdot \delta r &\rightarrow \mathbf{A}(r) \cdot \delta r + \Lambda(r + \delta r/2) - \Lambda(r - \delta r/2),\end{aligned}\tag{4.7}$$

where  $\Lambda(r)$  is a smooth function that winds by  $4\pi$  around the center of the vortex. Note that the  $4\pi$  transformation corresponds to a full electron flux quantum (as opposed to a superconducting flux quantum). On a lattice, the magnetic field associated with this vector potential vanishes everywhere except for a flux quantum in one plaquette of the lattice.

Ignoring, for the moment, the limitations of applying  $S_{sc,eff}$  to a point flux, the charge difference between a vortex and anti-vortex can be obtained from the Streda formula Eq. 4.6 to be:

$$\Delta Q_v = C_4 \int dr B_z = 2C_4 \Phi_0,\tag{4.8}$$

where  $\Phi_0$  is the superconducting flux quantum. This suggests a charge difference between vor-

tices and anti-vortices related to the Hall response  $C_4$ , as previously conjectured [71].

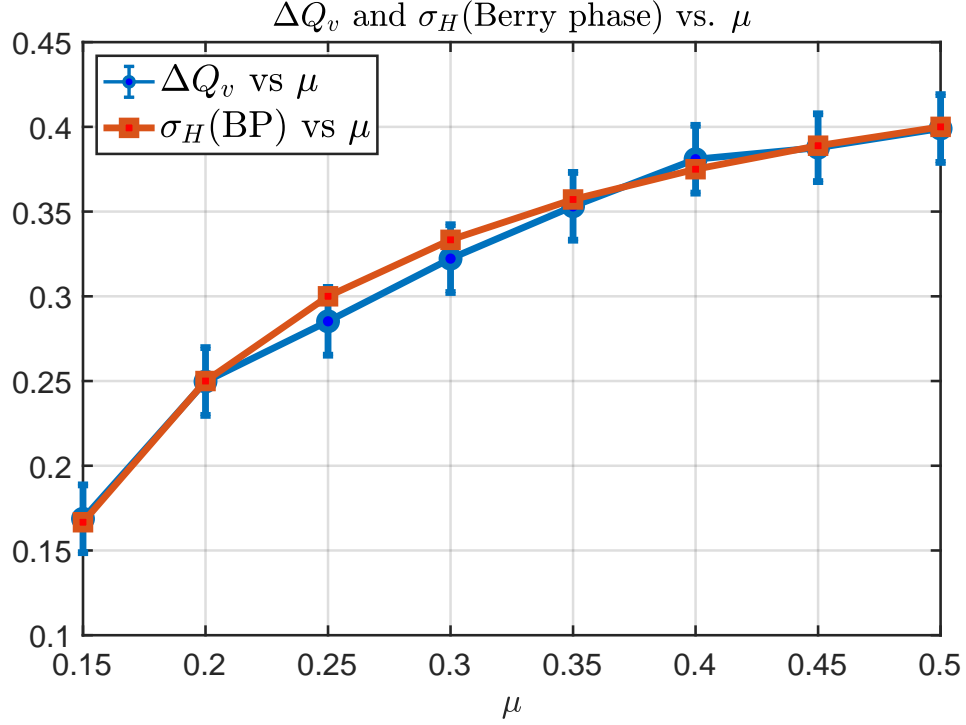


Figure 4.2: The charge difference between the vortex and anti-vortex, defined as  $\Delta Q_v = Q_- - Q_+$ , and the Hall conductivity  $\sigma_H$  related to the Berry Phase are shown as functions of  $\mu$  over the range  $\mu = 0.15$  to  $0.5$ . The  $\Delta Q_v$  data is presented with error bars indicating computational uncertainty. The lattice model features a size of  $N = 200$ , with parameters  $m_0 = 0.1$ ,  $\Delta_0 = 0.05$ , and coherence length  $\xi = 12.0$ .

The subtlety of applying Eq. 4.1 to a point flux motivates us to numerically study the suggestive relationship between the vortex charge and the Berry phase. For this purpose, we employ a model based on a bilayer gapped Dirac model on a square lattice that generates the Chern number in a way similar to multilayer graphene and combine this with  $p_x + ip_y$  superconducting pairing. Specifically, we consider a variation of the QWZ model [68]. The Hamiltonian of each

layer is simply given by Eq. 1.22, as stated here:

$$\begin{aligned}
H_{csc,0}(\mathbf{k}) &= -\mu\sigma_0 \sin(k_x)\sigma_x + \sin(k_y)\sigma_y \\
&+ (2 + m_0 + \cos(k_x) + \cos(k_y))\sigma_z,
\end{aligned} \tag{4.9}$$

where the operators  $\sigma_i$  represent the layer degree of freedom instead of spin. To account for the superconducting pairing, we construct the Bogoliubov-de Gennes (BdG) Hamiltonian:

$$H_{csc,BdG} = H_{csc,0}\tau_z + (\Delta\sigma_{z=1}\tau_+ + h.c.), \tag{4.10}$$

where  $\tau_i$  denotes the Nambu space,  $\sigma_{z=1}$  indicates that the superconducting pairing is applied exclusively to the top layer ( $\sigma_z = 1$ ), and  $\Delta = \Delta_0(k_x + ik_y)$  signifies that the pairing is of the  $p_x + ip_y$  type.

We introduce an (anti-)vortex into the system, we can replace  $\Delta$  with its anti-commutator with the (anti-)vortex operator:

$$\Delta \rightarrow \left\{ \Delta, \hat{V}(\mathbf{r}) \right\} = \Delta_0 \left\{ \hat{k}_x + i\hat{k}_y, e^{\pm i\theta_r} h(r) \right\}, \tag{4.11}$$

where  $\theta_r$  and  $h(r)$  represent the phase and amplitude of the superconducting order parameter, respectively. The  $+$  sign corresponds to a vortex, while the  $-$  sign corresponds to an anti-vortex. Within the (anti-)vortex core, we have  $h(r) \sim (1 - e^{-r/\xi})$ , with  $\xi$  being the coherence length, and  $\theta_r$  possesses a winding number of  $\pm 1$  around the core.

For the numerical computation of the vortex charge in  $H_{csc,BdG}$ , we utilize a lattice model

with a size of  $N = 200$  under periodic boundary conditions, constructing a phase profile  $\theta_r$  that features a vortex at the center and an anti-vortex at the corner. To isolate the vortex, we tweak the phase profile, ensuring that the phase around the center closely resembles an ideal isotropic vortex. We then determine the eigenstates and calculate the total charge around the vortex, denoted  $Q_+$ . A similar procedure is applied to the anti-vortex to obtain its charge,  $Q_-$ . The charge difference between the vortex and the anti-vortex is then defined as  $\Delta Q_v = Q_- - Q_+$ . This analysis is performed at various chemical potentials  $\mu$  and compared with the normal state Hall conductivity,

$$\sigma_H = \frac{1}{2} \left( 1 - \frac{m_0}{\mu} \right) \quad (4.12)$$

, where  $m_0$  is the Dirac mass of Eq. 4.9. The result of the vortex charge versus chemical potential  $\mu$  shown in Fig. 4.2 <sup>1</sup> confirm the expectation that an anomalous Hall superconductor shows that the difference in vortex and antivortex charge  $\Delta Q_v$  creates a charge density response that is essentially unchanged from the Streda-type formula applied to the anomalous Hall metal [37, 107]. The Streda-type response from vortex charges was discussed for chiral  $p$ -wave superconductors [108].

#### 4.4 Hall Response of the BKT Phase

The vortex charge  $\Delta Q_v$  plays a crucial role in describing the Hall effect in the non-superconducting phase at temperatures above the BKT transition. Specifically, let us consider a situation where

---

<sup>1</sup>To verify the convergence of the numerical results, I increased the energy cutoff for each value of  $\mu$  to ensure that the results converge at  $N = 200$ . I also expanded the system size to approximately 300, observing minimal changes (around 0.01). Consequently, the error bars used are based on this observation. Furthermore, I varied the coherence length  $\xi$  to approximately 1.0 and 30.0, finding that the results remained largely unchanged.

$T_{BKT}$ , which is controlled by the superfluid stiffness  $C_1$ , is smaller than the pairing amplitude  $\Delta$  so that for a temperature  $T_{BKT} \ll T \ll \Delta$  the system will be a resistive metal that is described by the action Eq. 4.3. This phase can be described as being in the plasma phase of a Coulomb gas of pairs of vortex-antivortex [102].

The response properties of the Coulomb gas, such as resistivity and the Nernst effect, can be understood in terms of a duality transformation [102] where the supercurrent in the superconductor  $j = \rho_0(\hat{z} \times \tilde{E}_v)$  maps to an electric field  $\tilde{E}_v$  seen by the vortices and the electric field  $E = \Phi_0(\hat{z} \times j_v)$  is given by the vortex current  $j_v$  [109]. Here,  $\rho_0$  and  $\Phi_0$  are the superfluid density and flux quantum, respectively.

As shown in Fig. 4.1, the vortex electric field  $\tilde{E}_v$  encodes the effective Lorentz force or the Magnus force imparted to vortices by a supercurrent [102]. The vortex current  $j_v$  is equivalent to the rate of phase slip generation that leads to a voltage gradient. Both the normal state conductivity and the Nernst effect can be understood by applying these duality relations to the diffusive motion of vortices [70, 109].

In the case of a difference  $\Delta Q_v$  between vortices and anti-vortices, the vortex current  $j_v$  also contributes to the total current, so we must modify the current relation as

$$j = \rho_0(\hat{z} \times \tilde{E}_v) + j_v \Delta Q_v / 2. \quad (4.13)$$

Assuming a diffusive vortex conductivity  $\tilde{E}_v = \sigma_v^{-1} j_v = \Phi_0^{-1} \sigma_v^{-1} (\hat{z} \times E)$  leads to the relation

$$j = \rho_0 \Phi_0^{-1} \sigma_v^{-1} E + \Delta Q_v (\hat{z} \times E) / 2 \Phi_0. \quad (4.14)$$

The first term is the usual Ohmic conductance in a mixed phase superconductor from flux flow [103], while the latter term is the Hall conductivity  $\sigma_H$  that is clearly universally related to the vortex charge difference  $\Delta Q_v$ . Combining with Eq. 4.8, this predicts a dc Hall response  $\sigma_H = C_4$  that appears to differ from the ac Hall response  $C_5$ .

## 4.5 Vortex Charge Screening

The coefficients  $C_4$  and  $C_5$  that appear in the Streda-type response (i.e., Eq. 4.8) and the Hall response Eq. 4.5 are, in principle, different. In fact, these coefficients are different even in the normal state, which serves to determine the value of  $C_{4,5}$  at weak pairing. However, for the weakly interacting limit that we use in our numerical simulations, these coefficients are both given by the Berry curvature according to Eq. 4.12. Including interactions renormalizes  $C_{4,5}$  differently, as can be checked by straightforward calculation in the large  $N$  limit or using the random phase approximation [104].

This can be easily understood from Eq. 4.8, since the coefficient  $C_4$  of the Streda-type charge response should be subject to screening from interactions. The ac Hall response coefficient  $C_5$  is not associated with any charge build-up and should not be screened. In fact, since the coefficient  $C_5$  is related to interband transitions, it can be attributed to the occupation function of fermions, which would be unaffected by weak interactions. However, Eq. 4.14 for Hall conductivity in the BKT phase appeared to strongly depend on the vortex charge  $C_4$ . This leads to an apparent paradox for whether the Hall conductivity in the BKT phase is closer to the normal state value (as was suggested for superconductors in magnetic fields [103]) or is renormalized.

To answer this question, we need to consider carefully the screening process of the vortex

charge when a vortex-antivortex pair is formed. Studying vortex formation systematically is beyond the validity of the formalism in this work. On the other hand, the numerical results in Fig. 4.2 suggest that the vortex charge difference is quite similar to a magnetic flux, whose dynamics can be studied using the effective action in Eq. 4.3. Therefore, we consider the charge response of a flux-antiflux pair, which is represented by an external magnetic field with a Fourier transform  $B(q, t) = 2ie^{-q^2R^2} \sin(vq_x t)\Theta(t)$ , where  $\Theta(t)$  is the Heavisider step function. This external magnetic field corresponds to a pair of fluxes with radius  $R$  moving in opposite directions with velocity  $v$  along  $x$ .

The corresponding electric field from Faraday's law is transverse and written in momentum and frequency space as

$$E_T = \frac{2vq_x e^{-q^2R^2}}{i\omega q[\omega^2 - (vq_x)^2]}. \quad (4.15)$$

Using  $\sigma_{LT}$  from Eq. 4.4 we find that the longitudinal current density  $j_L$ , in addition to the usual ac Hall (i.e.  $\omega \gg q$ ) part  $j_{L,0} = C_5 E_T$  contains an additional "screening" contribution, which is proportional to  $C_4 - C_5$ :

$$\delta j_L = \frac{(C_4 - C_5)c^2 q 2i\omega q_x v e^{-q^2R^2}}{\omega^2 - c^2 q^2 [\omega^2 - (vq_x)^2]}, \quad (4.16)$$

where  $c = \sqrt{C_2/C_1}$  is the velocity of the plasmon.

Fourier transforming this component to the time-domain yields:

$$\delta j_L = 2i(C_4 - C_5)vc^2 q_x q e^{-q^2R^2} \frac{[\cos(cqt) - \cos(vq_x t)]}{c^2 q^2 - v^2 q_x^2}. \quad (4.17)$$

The contribution to the above proportional to  $\cos vq_x t$  combined with the near-field part (i.e. proportional to  $1 - e^{-q^2 R^2}$ ) of  $E_T$  corresponds to the flow of vortex core charge density shown in Fig. 4.1 proportional to  $C_4$ . On the other hand, the contribution to  $\delta j_L$  from  $\cos(cqt)$  contributes to the crescent-shaped charge waves in Fig. 4.1.

The combined result  $\delta j_L$  in the above equation clearly vanishes as  $q, q_x \rightarrow 0$  establishing that the longitudinal current response is determined by  $j_{L,0}$ , which is proportional to the high-frequency ac Hall conductivity  $C_5$ , despite screening reducing the charge at the vortex core to  $C_4$ .

The longitudinal current response in vector form is

$$\mathbf{j}_{L,0} = C_5(\hat{z} \times \mathbf{E}_T) = \frac{2vq_x e^{-q^2 R^2}}{q^2} C_5 \cos(vq_x t) \mathbf{q}. \quad (4.18)$$

Note that while the x component of the current approaches a constant  $j_{L,0,x} \sim 2vC_5$  as  $q_x = q \rightarrow 0$ , the current has a non-trivial dependence on  $q_y/q_x$ , which reflects the angular dependence of the far field that can lead to logarithmic in system size corrections to  $j_{L,0}$ . However, this does not affect the conclusion that the vortex Hall conductivity is determined by the high frequency ac Hall conductivity  $C_5$ .

## 4.6 Discussion and Conclusion

We studied the dc anomalous Hall response of a superconductor slightly above the BKT transition but below the mean-field superconducting gap, where a vortex plasma phase is responsible for dissipative transport. Based on the effective action 4.1, we conjecture, based on an analogy between fluxes and vortices, that the core charge of a vortex and anti-vortex might differ

by an amount proportional to the Streda response coefficient  $C_4$ , which in noninteracting metals is expected to be determined by the Fermi surface Berry phase [37].

In Fig. 4.2, we numerically verify this for a superconducting version of the QWZ model. The coefficient  $C_4$ , however, differs in interacting fermion systems from the ac Hall conductivity  $C_5$ . Using the analogy between fluxes and vortices together with a flux flow model [103] for superconducting transport shown in Fig. 4.1 we showed that the dc Hall conductivity should actually match the ac value  $C_5$ . We expect the effective action Eq. 4.1 with coefficients  $C_{j=1,2,4,5}$  to be a good description of any chiral superconductor including tetra-layer graphene with coefficients that are measurable in the linear response. It would be interesting to compare these coefficients with vortex charge and dc Hall conductivity measurements.

## Appendix A: Details of Bosonization

### A.1 Lorentz-invariance-constrained Chiral Anomaly

Let us now review the chiral anomaly in the relativistic case where we have chosen  $\lambda_{\mu\nu}^{(2)} = \lambda\eta_{\mu\nu}$  so that  $S_{LL}$  is then the Lorentz-invariant Thirring model [54]. In this case, the collective mode velocity  $u$  continues to match the Fermi velocity  $u = v_F = 1$ , and current and density have the same units. The chiral anomaly equation for this so-called Thirring model[54], which was derived using perturbation theory together with a Lorentz-invariant regulator, shows a renormalization. Here we use bosonization to derive the anomaly equation in a way where Lorentz-invariant and non-Lorentz-invariant results can be directly compared.

We consider the Euclidean (i.e. Wick rotated) space-time [77] so that the point-splitting expansion is manifestly rotation (i.e. Lorentz)-invariant in the Wick rotated  $(1 + 1)$ D plane. Using this scheme of normal ordering, the chiral fermionic operators  $\psi_{R,L}(x, t)$  can be written as vertex operators of chiral bosonic operators  $\Phi_{R,L}(x, t)$ , which in turn can be used to define the bosonic field  $\Phi(x, t)$  [77].

Applying the standard bosonization identities in Euclidean space [77] to replace the Fermions in the kinetic term  $S_{1,0}$ , we obtain

$$S_{1,0} = \frac{1}{2K} \int (\partial_\mu \Phi)^2 \tag{A.1}$$

, where  $x_0 = t$  and  $K = 1$ . Similar use of bosonization identities [77] leads to related expressions for the chiral current and the  $U(1)$  charge current, which can be written as

$$j^\mu = \frac{1}{\sqrt{\pi}} \epsilon^{\mu\nu} \partial_\nu \Phi \quad j^{5\mu} = \frac{1}{\sqrt{\pi}} \partial^\mu \Phi, \quad (\text{A.2})$$

where  $\epsilon^{\mu\nu}$  is the completely anti-symmetric unit tensor.

Applying these identities to  $S_{1,int}$  leads to an additional contribution to Eq. A.1, so that the  $K$  factor depends on the interaction strength in the fermionic model as

$$K^{-1} = 1 + \lambda/\pi, \quad (\text{A.3})$$

where  $\lambda = g_2$  and  $g_4 = 0$  due to Lorentz invariance.

The coupling to an external vector potential  $A_\mu$  is included through a term

$$\mathcal{L}_{em} = -e j^\mu A_\mu = -\frac{e}{\sqrt{\pi}} A_\mu \epsilon^{\mu\nu} \partial_\nu \Phi. \quad (\text{A.4})$$

Although the charge current  $j^\mu$  in Eq. A.2 is manifestly conserved, the divergence of the chiral current can be written in terms of the classical equation of motion for  $\Phi$  as

$$\langle \partial_\mu j^{5\mu} \rangle = \partial_\mu \partial^\mu \Phi / \sqrt{\pi} = \frac{1}{1 + \lambda/\pi} \frac{e}{\pi} E. \quad (\text{A.5})$$

where  $E = \partial_0 A_1 - \partial_1 A_0$  is the electric field. This result is obtained by using the expression for the chiral current Eq. A.2 and then combining with Eq. A.1 with Eq. A.4. This shows that the chiral charge, in contrast to the classical result, is not conserved since the right-hand side is non-

zero and is proportional to the electric field  $E$ . This is referred to as the chiral anomaly equation. Furthermore, since the right-hand side depends on the interaction strength  $\lambda$ , the chiral anomaly is renormalized by interactions[54]. This result is identical to that obtained directly from the Thirring model using either the Pauli-Villars regularization or the Fujikawa method [62].

## A.2 Chiral Anomaly with Non-Lorentz-invariant Point-splitting Regularization

Bosonization of the Luttinger model  $S_{LL}$  (from Eq. 2.1 and 2.3) can also be approached from a Hamiltonian perspective that is more appropriate for condensed matter systems that break Lorentz invariance [77]. Historically, this was developed in parallel with the Euclidean formulation in the last subsection. This formalism is simpler because it directly uses operators in a Hamiltonian formalism. The point-splitting in space-time is now replaced by point-splitting in real space. This allows us to use the definition of the chiral charge density in Eq. 2.8 as well as the corresponding equation for the total density as operator equations. In fact, the chiral charge density operators  $\rho_{R,L}$  in  $S_{LL}$  are promoted to operators, which, with the appropriate point-splitting obey the algebra [77]

$$[\rho_a(x), \rho_b(x')] = -\frac{i}{2\pi} a \delta_{ab} \partial_x \delta(x - x'). \quad (\text{A.6})$$

Using the above commutation relation, the TL Hamiltonian can be written entirely in terms

of chiral density operators:

$$\begin{aligned}
H &= \int dx i\bar{\Psi}(\gamma^1\partial_x - i\gamma^0\varphi)\Psi + 2g_2\rho_R\rho_L + g_4(\rho_R^2 + \rho_L^2) \\
&= \int dx (1 + g_4)(\rho_R^2 + \rho_L^2) + 2g_2\rho_R\rho_L + \varphi\rho,
\end{aligned} \tag{A.7}$$

where  $\varphi$  is the electric potential.

We can bosonize the above model using the operator version of Eq. 2.4 for the density operator written as

$$\rho = \rho_R + \rho_L = \frac{1}{\sqrt{\pi}}\partial_x\Phi, \tag{A.8}$$

where  $\Phi$  is the bosonic field. Defining  $\Pi = (\rho_R - \rho_L)\sqrt{\pi}$  as the canonically conjugate field to  $\Phi(x)$ , which is based on the commutation relation in Eq.A.6, the above Hamiltonian can be written in bosonized form [74]

$$H_{1DEG} = \int dx \frac{1}{2} \left( uK\Pi^2 + \frac{u}{K}(\partial_x\Phi)^2 \right) + E\Phi \tag{A.9}$$

, where

$$uK = 1 + \frac{g_4}{2\pi} - \frac{g_2}{2\pi} \tag{A.10}$$

$$u/K = 1 + \frac{g_4}{2\pi} + \frac{g_2}{2\pi} \tag{A.11}$$

and  $E = -\partial_x \varphi$  is the electric field. The current operator  $j$  is now defined as

$$j = -\frac{1}{\sqrt{\pi}} \partial_t \Phi = \frac{1}{\sqrt{\pi}} u K \Pi \quad (\text{A.12})$$

so that it satisfies the continuity equation for the charge.

Note that the two equations Eq. A.8 and Eq. A.12 are direct operator analogs of Eq. 2.4 except that  $j$  is no longer related to  $\rho_{R,L}$  in the same way as an operator. This relation can be used to define the chiral charge in terms of the current operator

$$\rho_{c,mb} = (\rho_R - \rho_L) = \frac{1}{\sqrt{\pi}} \Pi = j/uK = -\frac{1}{\sqrt{\pi}} \partial_t \Phi / uK. \quad (\text{A.13})$$

Applying this definition to the equation of motion for  $\Phi$  (Eq. 2.11) we obtain the chiral anomaly equation:

$$\partial_t \rho_{c,mb} + \partial_x j_{c,mb} = \frac{1}{\sqrt{\pi}} \partial_t \Pi + \partial_x j_{c,mb} = \frac{e}{\pi} E \quad (\text{A.14})$$

where  $j_{c,mb} = u\rho/K$  is the chiral current. Note that in contrast to the chiral anomaly equation (Eq. A.5) resulting from a Lorentz-invariant regularization of the TL model, the above chiral anomaly equation does not have interaction-based renormalization.

As a side note, we note that in the Galilean-invariant case, the Hamiltonian  $H_{1DEG}$  can be written in terms of the current as  $H_{1DEG} = \int dx \pi j^2 / 2uK = \int dx m j^2 / 2n$ , where  $m$  is the mass and  $n = k_F/\pi$  is the average density. Then, we get  $uK = k_F/m = v_F = 1$ . Interestingly, the resulting current  $j = (\rho_R - \rho_L)$  is consistent with the chiral charge, Eq. A.13.

## Appendix B: Current $j$ v.s. Chiral Charge $\rho_{c, sb}$

The relationship between current  $j$  and chiral charge  $\rho_{c, sb}$  naively seems simple, at least when current  $j$  is large enough so that the number of low-speed solitons only is a small portion of the total. However, an extra soliton-antisoliton pair may be produced with zero total momentum, i.e., a soliton appears in the upper right and an antisoliton in the lower left of the energy spectrum (see FIG.2.1). This procedure will not change the total momentum and current, but the number of soliton pairs will increase. Fortunately, it is prohibited due to energy conservation. In this appendix, we demonstrate that the current  $j$  is approximately equal to the chiral charge by considering the charge density profile under a large and instant position-dependent electric field  $E(x)$ .

After applying a large and instant electric field  $E$ , the system will contain high-density solitons and antisolitons. In this high-density gas, the  $\cos$ -term can be neglected to describe the behavior of the solitons. The Hamiltonian can be written as

$$H = \frac{1}{2} \int dx \left[ uK \left( \Pi + \frac{1}{\sqrt{\pi}} eA(x) \right)^2 + \frac{u}{K} (\partial_x \Phi)^2 \right] \quad (\text{B.1})$$

, where the vector potential is

$$A_1(x) = -ET e^{-x^2/2\sigma^2} \frac{L}{\sqrt{2\pi\sigma}} \quad (\text{B.2})$$

,  $E$  is the electric field strength,  $T$  is the action time,  $\sigma$  is the characteristic length of the vector potential, and  $L/\sqrt{2\pi}\sigma$  is a normalization factor. The soliton mass effect can be neglected when  $\sigma \ll h/mu^2$ . Then, we can use the Heisenberg equation to figure out the charge density profile over time  $t$ . The time derivative of the field is

$$\partial_t \Phi = i[H, \Phi] = uK \left( \Pi + \frac{1}{\sqrt{\pi}} eA(x) \right) \quad (\text{B.3})$$

. Then, at the initial time, we have the following conditions:

$$\langle \Phi(x, t = 0) \rangle = 0; \quad \partial \langle \Phi(x, t = 0) \rangle = \frac{uK}{\sqrt{\pi}} eA(x) \quad (\text{B.4})$$

. On the other hand, we can expand the field  $\Phi$  into left and right moving parts, namely,

$$\Phi(x, t) = f(x - ut) + f(x + ut) \quad (\text{B.5})$$

. The function  $f(x)$  can be determined by initial conditions and can be expressed as

$$f(x) = \frac{\sigma}{2\sqrt{2}} KeET \operatorname{erf} \left( \frac{x}{\sqrt{2}\sigma} \right) \frac{L}{\sqrt{2\pi}\sigma} \quad (\text{B.6})$$

, where  $\operatorname{erf}(x)$  is the error function. Hence, the charge density  $\rho(x, t)$  and the current density  $j(x, t)$  are given by

$$\langle \rho(x, t) \rangle = \frac{1}{\sqrt{\pi}} \langle \partial_x \Phi \rangle = \frac{K}{2\pi} eET \left[ e^{-(x-ut)^2/2\sigma^2} - e^{-(x+ut)^2/2\sigma^2} \right] \frac{L}{\sqrt{2\pi}\sigma} \quad (\text{B.7})$$

$$\langle j(x, t) \rangle = -\frac{1}{\sqrt{\pi}} \langle \partial_t \Phi \rangle = \frac{uK}{2\pi} eET \left[ e^{-(x-ut)^2/2\sigma^2} + e^{-(x+ut)^2/2\sigma^2} \right] \frac{L}{\sqrt{2\pi}\sigma} \quad (\text{B.8})$$

. From the above expressions, it is clear that the number  $N_{s(\bar{s})}$  of the right(left) moving charge wave packets ((anti)solitons) is  $KeETL/2\pi$ . After a long time, the solitons and antisolitons will separate in real space and can be easily distinguished by local measurements.

The average current is

$$\langle \bar{j} \rangle = uKeET/\pi = u(N_s + N_{\bar{s}})/L = u\rho_{c, sb} \quad (\text{B.9})$$

as we expected. Hence, we confirm that the average current  $\bar{j}$  and the chiral charge density  $\rho_{c, sb}$  are the same, apart from the characteristic speed  $u$ .

## Appendix C: Kinetic Stress-energy Tensor $K^{\mu\nu}$ and Its Gauge-invariance

In this appendix, we discuss the stress-energy tensor of a general system with a gauge-invariant and minimal-coupled Lagrangian density  $\mathcal{L} = \mathcal{L}(\psi, D_\mu\psi, D_\mu D_\nu\psi, \dots)$ , where  $D_\mu = \partial_\mu + ieA_\mu$ . Simply, the continuity equation can be derived by applying an infinitesimal translation:

$$\partial_\mu T^{\mu 1} = \mathcal{F}^1 \quad (\text{C.1})$$

, where

$$T^{\mu\nu} = -\mathcal{L}\eta^{\mu\nu} + \frac{\partial\mathcal{L}}{\partial(\partial_\mu\psi)}\partial^\nu\psi + \left[ \frac{\partial\mathcal{L}}{\partial(\partial_\rho\partial_\mu\psi)}\partial_\rho\partial^\nu\psi + \frac{\partial\mathcal{L}}{\partial(\partial_\mu\partial_\rho\psi)}\partial_\rho\partial^\nu\psi - \partial_\rho\left(\frac{\partial\mathcal{L}}{\partial(\partial_\rho\partial_\mu\psi)}\partial^\nu\psi\right) \right] + \dots, \quad (\text{C.2})$$

$$\mathcal{F}^\nu = -\frac{\partial\mathcal{L}}{\partial A^\mu}\partial^\nu A^\mu - \frac{\partial\mathcal{L}}{\partial(\partial^\rho A^\mu)}\partial^\rho\partial^\nu A^\mu + \dots. \quad (\text{C.3})$$

This equation can be modified to the gauge-invariant form, which will be proved in the following,

as

$$\partial_\mu K^{\mu\nu} = e j_\mu F^{\nu\mu}, \quad (\text{C.4})$$

(i.e., Eq.2.30), where the kinetic stress-energy tensor  $K^{\mu\nu}$  is written as:

$$K^{\mu\nu} = T^{\mu\nu} - e j^\mu A^\nu + C^{\mu\nu} \quad (\text{C.5})$$

, where

$$C^{\mu\nu} = \frac{\partial \mathcal{L}}{\partial(\partial_\mu A^\rho)} \partial^\nu A^\rho + \left[ \frac{\partial \mathcal{L}}{\partial(\partial_\mu \partial_\rho A^\rho)} \partial^\nu \partial_\rho A^\rho - \partial_\rho \left( \frac{\partial \mathcal{L}}{\partial(\partial_\mu \partial_\rho A^\rho)} \right) \partial^\nu A^\rho \right] + \dots \quad (\text{C.6})$$

In the following, we will show that the kinetic stress-energy tensor  $K^{\mu\nu}$  is naturally gauge-invariant. The basic technique is still the variation method, but in a gauge-invariant approach. Consider the functional expansion of the Lagrangian density  $\mathcal{L}$ , which is

$$\mathcal{L} = \mathcal{L}(\psi(x-a), D_\mu \psi(x-a), D_\mu D_\rho \psi(x-a), \dots) \quad (\text{C.7})$$

, around 0. The variation of it can be written in three parts:

$$\begin{aligned} \delta \mathcal{L} = & - a_\nu \partial^\nu \mathcal{L} \\ & - a_\nu \left[ - \frac{\partial \mathcal{L}}{\partial A^\sigma} \partial^\nu A^\sigma - \frac{\partial \mathcal{L}}{\partial(\partial^\rho A^\sigma)} \partial^\nu \partial^\rho A^\sigma + \dots \right] \\ & + \left[ - \frac{\partial \mathcal{L}}{\partial(D_\mu \psi)} D_\mu (a^\sigma \partial_\sigma \psi) + \dots - \text{liner terms of } a_\nu \right] \end{aligned} \quad (\text{C.8})$$

The first term is the change of the Lagrangian density with the change of the space-time position  $x$ . The second part is the compensation to the change of the vector potential  $A_\mu$  since there is no direct variation of  $A_\mu$  in the functional derivative Eq.C.7. The third part is the first and higher derivative terms. The functional derivative of the first and the third term gives us the

stress-energy tensor  $\partial_\mu T^{\mu\nu}$ . The second one is just the  $\mathcal{F}^\nu$  (Eq.C.3). Hence, we can write the stress-energy tensor as

$$T^{\mu\nu} = -\mathcal{L}\eta^{\mu\nu} - \frac{\delta}{\delta(\partial_\mu a_\nu)} \int d^d x [\mathcal{L}(\psi(x-a), D_\mu\psi(x-a), \dots) - \text{linear terms of } a_\nu]. \quad (\text{C.9})$$

In particular, the expression of the stress-energy tensor of 1DEG (Eq.(2.25),(2.26)) is

$$\begin{aligned} T_{1DEG}^{00} &= \frac{1}{2m} \bar{D}_1\psi^\dagger D_1\psi \\ &\quad + \left[ eA_0 - \int dx' V(x-x')\rho(x') - \mu \right] \rho(x) \\ T_{1DEG}^{10} &= -\frac{1}{2m} (\bar{D}_1\psi^\dagger \partial_t\psi + \partial_t\psi^\dagger D_1\psi) \\ T_{1DEG}^{01} &= -i\psi^\dagger \partial_x\psi \\ T_{1DEG}^{11} &= i\psi^\dagger D_0\psi + \frac{1}{2m} (\bar{D}_1\psi^\dagger \partial_x\psi + \partial_x\psi^\dagger D_1\psi - \bar{D}_1\psi^\dagger D_1\psi) \\ &\quad + \left[ \int dx' V(x-x')\rho(x') + \mu \right] \rho(x) \end{aligned} \quad (\text{C.10})$$

, regardless of whether the Lagrangian density is non-local.

To compare the expression of the tensor  $C^{\mu\nu}$  (Eq.C.6) with the one of the stress-energy tensor  $T^{\mu\nu}$  (Eq.C.9), we also can view the tensor  $C^{\mu\nu}$  as a functional derivative:

$$C^{\mu\nu} = -\frac{\delta}{\delta(\partial_\mu a_\nu)} \int d^d x [\mathcal{L}(\psi(x), D_\mu^-\psi(x), \dots) - \text{linear terms of } a_\nu]. \quad (\text{C.11})$$

, where  $D_\mu^- = D_\mu - ie a_\nu \partial^\nu A_\mu$ .

The functional derivative form of the operator  $-j^\mu A^\nu$  can be derived from the definition of

the current operator, i.e.,  $j^\mu = -\delta L/\delta A_\mu$ . It is

$$-j^\mu A^\nu = -\frac{\delta}{\delta(\partial_\mu a_\nu)} \int d^d x [\mathcal{L}(\psi(x), D_\mu^c \psi(x), \dots) - \text{liner terms of } a_\nu]. \quad (\text{C.12})$$

, where  $D_\mu^c = D_\mu - ieA^\nu \partial_\mu a_\nu$ . It is easy to check by using the chain rule of the functional derivative, i.e.,

$$\begin{aligned} \frac{\delta}{\delta(\partial_\mu a_\nu)} &= \int d^d x' \frac{\delta}{\delta(A^\rho \partial_\sigma a_\rho)} \frac{\delta(A^\rho \partial_\sigma a_\rho)}{\delta(\partial_\mu a_\nu)} \\ &= \frac{\delta}{\delta(A^\rho \partial_\mu a_\rho)} A^\nu. \end{aligned} \quad (\text{C.13})$$

Then, the kinetic stress-energy tensor is finally written as

$$K^{\mu\nu} = -\mathcal{L}\eta^{\mu\nu} - \frac{\delta}{\delta(\partial_\mu a_\nu)} \int d^d x [\mathcal{L}(\psi', D'_\mu \psi', \dots) - \text{liner terms of } a_\nu]. \quad (\text{C.14})$$

, where  $\psi' = \psi - a_\nu \partial^\nu \psi$  and  $D'_\mu = D_\mu - ie(a_\nu \partial^\nu A_\mu + A^\nu \partial_\mu a_\nu)$ . The high-order terms of  $a_\nu$  are neglected in the above expression since they do not contribute.

Since the Lagrangian density is gauge-invariant, we can perform a gauge transformation with the argument  $-iea_\nu A^\nu$ . Therefore, the  $K^{\mu\nu}$  is also equal to

$$K^{\mu\nu} = -\mathcal{L}\eta^{\mu\nu} - \frac{\delta}{\delta(\partial_\mu a_\nu)} \int d^d x [\mathcal{L}(\psi'', D''_\mu \psi'', \dots) - \text{liner terms of } a_\nu] \quad (\text{C.15})$$

, where  $\psi'' = \psi - a_\nu D^\nu \psi$  and  $D''_\mu = D_\mu - ie a^\nu F_{\nu\mu}$ . The linear term here is just  $a_\nu \partial^\nu \mathcal{L}$  since it all comes from the change of the position  $x$ . We notice that the Lagrangian density above in the expression of  $K^{\mu\nu}$  is gauge-invariant under any gauge transformations since the covariant

derivative  $D_\mu$  and the field strength tensor  $F_{\mu\nu}$  have been used in the variation of the field  $\psi$  and the vector potential  $A_\mu$  instead of partial derivatives. Together with the linear terms' gauge invariance, we can conclude that the kinetic stress-energy tensor is naturally gauge-invariant. The concrete expression for the  $K^{\mu\nu}$  up to the second order is

$$\begin{aligned}
K^{\mu\nu} = & -\mathcal{L}\eta^{\mu\nu} + \frac{\partial\mathcal{L}}{\partial(D_\mu\psi)}D^\nu\psi \\
& + \left\{ -ie\frac{\partial\mathcal{L}}{\partial(D^\rho D_\mu\psi)}F^{\nu\rho}\psi \right. \\
& \left. + \left[ \frac{\partial\mathcal{L}}{\partial(D_\rho D_\mu\psi)}D_\rho D^\nu\psi + \frac{\partial\mathcal{L}}{\partial(D_\mu D_\rho\psi)}D_\rho D^\nu\psi - \partial_\rho\left(\frac{\partial\mathcal{L}}{\partial(D_\rho D_\mu\psi)}D^\nu\psi\right) \right] \right\} + \dots
\end{aligned} \tag{C.16}$$

Incidentally, the expression for the  $K^{01}$  term in the generalized 1DEGs can be simplified due to the presence of only one first  $t$ -derivative term in the Lagrangian. Consequently, only the second term on the left side of Eq.C.16 remains non-zero, leading to the simplified form:

$$K^{01} = -i\psi^\dagger D_1\psi. \tag{C.17}$$

## Appendix D: Chiral Magnetic Effect Current in Chiral Kinetic Theory

In this appendix, we will document the procedures for deriving the chiral magnetic effect (CME), i.e. Eq.3.25, in the chiral kinetic theory.

First, the total current in the chiral kinetic theory is obvious to find by definition[57]:

$$\begin{aligned} \mathbf{j} &= \int_{\mathbf{k}} \sqrt{G_{\mathbf{k}}} f \dot{\mathbf{r}} \\ &= \int_{\mathbf{k}} f \mathbf{v}_{\mathbf{k}} + e \mathbf{E} \times \int_{\mathbf{k}} f \boldsymbol{\Omega}_{\mathbf{k}} + e \mathbf{B} \int_{\mathbf{k}} f (\mathbf{v}_{\mathbf{k}} \cdot \boldsymbol{\Omega}_{\mathbf{k}}). \end{aligned} \quad (\text{D.1})$$

Here the first term in Eq.D.1 is the regular current; the second term is the anomalous Hall current; the third term which is along the magnetic field direction is the chiral magnetic current. Therefore, we obtain a comprehensive equation for the chiral magnetic effect (CME) current as follows:

$$\mathbf{j}_{\text{CME}} = e^2 \mathbf{B} \int_{\mathbf{k}} f (\partial_{\mathbf{k}} \varepsilon(\mathbf{k}) \cdot \boldsymbol{\Omega}_{\mathbf{k}}). \quad (\text{D.2})$$

Then, we use the integral by parts and determine that

$$\int_{\mathbf{k}} f (\partial_{\mathbf{k}} \varepsilon(\mathbf{k}) \cdot \boldsymbol{\Omega}_{\mathbf{k}}) = \int_{\mathbf{k}} \nabla_{\mathbf{k}} \cdot (\varepsilon f \boldsymbol{\Omega}_{\mathbf{k}}) - \varepsilon \nabla_{\mathbf{k}} \cdot (f \boldsymbol{\Omega}_{\mathbf{k}}). \quad (\text{D.3})$$

The first term is a boundary term and thus vanishes. The second term can be written as

$$-\int_{\mathbf{k}} \varepsilon \nabla_{\mathbf{k}} \cdot (f \boldsymbol{\Omega}_{\mathbf{k}}) = -\int_{\mathbf{k}} \varepsilon (\nabla_{\mathbf{k}} f) \cdot \boldsymbol{\Omega}_{\mathbf{k}} - \varepsilon f (\nabla_{\mathbf{k}} \cdot \boldsymbol{\Omega}_{\mathbf{k}}). \quad (\text{D.4})$$

At zero temperature, the first term can be expressed as a Fermi-surface integral given that  $\nabla_{\mathbf{k}} f$  is only non-zero on Fermi surfaces:

$$-\int_{\mathbf{k}} \varepsilon (\nabla_{\mathbf{k}} f) \cdot \boldsymbol{\Omega}_{\mathbf{k}} = \frac{1}{(2\pi)^3} \sum_{\alpha} \int_{S_{\alpha}} d^2 \mathcal{F} \varepsilon. \quad (\text{D.5})$$

The second term in Eq.D.4 is non-zero due to the term  $\nabla_{\mathbf{k}} \cdot \boldsymbol{\Omega}_{\mathbf{k}}$  at two Weyl points. However, it will not contribute to the CME current. The reason is that the CME current (Eq.D.1) is the sum of all bands. When we consider the fully occupied lower Weyl band, since  $\nabla_{\mathbf{k}} f$  is always zero, the first term in Eq.D.4 vanishes. The second term for the lower Weyl band is identical to the upper Weyl band except for the opposite sign. Therefore, when accounting for the contributions of all bands to the CME current, the second term in Eq. D.4 will cancel out, leaving only the first term from the upper Weyl band.

Finally, we can express the CME current as

$$\mathbf{j}_{\text{CME}} = \frac{e^2 \mathbf{B}}{4\pi^2} \Delta\mu, \quad (\text{D.6})$$

where

$$\Delta\mu = \frac{1}{2\pi} \sum_{\alpha} \int_{S_{\alpha}} d^2 \mathcal{F} \varepsilon(\mathbf{k}). \quad (\text{D.7})$$

Here Eq.D.6 is a general expression in the zero-temperature limit. If we assume that the electron distribution functions are in equilibrium around each Weyl node, i.e.  $\varepsilon(\mathbf{k}) = \text{const.}$  for  $\mathbf{k} \in S_\alpha$ , we can define the chiral chemical potential, i.e.  $\mu_\alpha$ , and find that  $\Delta\mu$  is exactly the chiral chemical potential difference,  $\mu_R - \mu_L$ . Then, Eq.D.6 is consistent with references[8, 9].

As an illustration, it is straightforward to derive the expression for a simple Weyl semi-material using the energy dispersion  $\varepsilon_\alpha(\mathbf{k}) = \gamma_\alpha v k$  and the Berry curvature  $\Omega_{\mathbf{k}\alpha} = \gamma_\alpha \hat{\mathbf{k}}/2k^2$  around the Weyl nodes  $\gamma_\alpha$  [57]. The obtained result evidently corresponds to Eq. D.6.

### D.0.0.1 Berry Curvature in Fermi liquids

While the topological Fermi liquid [93] as well as the chiral kinetic theory discussed above is defined in terms of Berry curvature on the Fermi surface, Berry curvatures are typically calculated from non-interacting band structures of Fermions. This leads to a question of how to precisely define Berry curvature on a strongly interacting Fermi surface.

Basically, the Berry curvature is defined for non-interacting systems. Shou-cheng Zhang defined invariants for interacting systems with Green functions.[110] The density matrix for quasi-particles at the momentum  $\mathbf{k}$  is defined by  $\rho_{\mathbf{k}} = N_{\mathbf{k}} \int_{\omega \sim \varepsilon_{\mathbf{k}}} d\omega A_{\mathbf{k}}(\omega)$ , where  $A_{\mathbf{k}}(\omega) = \text{Im}[G_{\mathbf{k}}(\omega)]$  is the spectral function matrix.  $N_{\mathbf{k}}$  is a normalization that ensures that  $\rho_{\mathbf{k}}^2 = \rho_{\mathbf{k}}$  and  $\text{Tr}[\rho_{\mathbf{k}}] = 1$  for  $\mathbf{k}$  on the Fermi surface. The density matrix near a non-degenerate Fermi surface can be expanded in terms of a wave-function  $\rho_{\mathbf{k}}(\mathbf{r}, \mathbf{r}') = u_{\mathbf{k}}(\mathbf{r})u_{\mathbf{k}}^*(\mathbf{r}')$  due to the Landau liquid property. This shows that the product

$$\text{Tr}[\rho_{\mathbf{k}}\rho_{\mathbf{k}_1}\rho_{\mathbf{k}_2}] = \langle u_{\mathbf{k}}|u_{\mathbf{k}_1}\rangle\langle u_{\mathbf{k}_1}|u_{\mathbf{k}_2}\rangle\langle u_{\mathbf{k}_2}|u_{\mathbf{k}}\rangle = e^{i\Omega_{\mathbf{k}}\mathcal{A}}, \quad (\text{D.8})$$

where  $\mathcal{A}$  is the area of the triangle. Expanding  $\rho_{\mathbf{k}_j} \simeq \rho_{\mathbf{k}} + (\mathbf{k}_j - \mathbf{k}) \cdot \partial_{\mathbf{k}} \rho_{\mathbf{k}}$ , and we can find the Berry curvature to be  $\Omega_{\mathbf{k}} = Tr[\partial_{\mathbf{k}} \rho \times (\rho \partial_{\mathbf{k}} \rho)]$ . It means the berry curvature on the Fermi surface can be exactly defined by using Green's functions.

## Appendix E: Second-order Term of the ac Hall Conductivity in the Chern Insulator

In this part, rather than directly using the Kubo formula to calculate the ac hall conductivity in Weyl, we will estimate it in the Chern Insulator(CI). Since the Weyl systems can be described as a stack of the Chern insulator, the integral of ac Hall conductivity in CI over one parameter  $k_z$  is just the one in Weyl. However, if we only need to prove that the ac Hall conductivity in Weyl is non-zero and non-universal, the result of the ac Hall conductivity in CI will be sufficient. Indeed, several references have derived a general formula for the ac Hall conductivity  $\sigma_{xy}(\omega)$  of a two-band system in terms of the Berry curvature, using different methods [111–113].

The general Kubo formula for the ac conductivity is

$$\sigma_{xy}(\omega) = \frac{1}{i\omega} \sum_{n \neq 0} \left[ \frac{\langle 0 | J_y | n \rangle \langle n | J_x | 0 \rangle}{\omega + (E_n - E_0)} - \frac{\langle 0 | J_x | n \rangle \langle n | J_y | 0 \rangle}{\omega - (E_n - E_0)} \right] \quad (\text{E.1})$$

, where  $J_i$  is the current operator, the state 0 and  $n$  represents the many-body ground state and

the  $n$ -th excited state. To expand the above expression in series of  $\omega$ , we have

$$\begin{aligned}
\sigma_{xy}(\omega) = & -\frac{i}{\omega} \sum_{n \neq 0} \frac{\langle 0|J_y|n\rangle \langle n|J_x|0\rangle + \langle 0|J_x|n\rangle \langle n|J_y|0\rangle}{E_n - E_0} \\
& + i \sum_{n \neq 0} \frac{\langle 0|J_y|n\rangle \langle n|J_x|0\rangle - \langle 0|J_x|n\rangle \langle n|J_y|0\rangle}{(E_n - E_0)^2} \\
& - i\omega \sum_{n \neq 0} \frac{\langle 0|J_y|n\rangle \langle n|J_x|0\rangle + \langle 0|J_x|n\rangle \langle n|J_y|0\rangle}{(E_n - E_0)^3} \\
& + i\omega^2 \sum_{n \neq 0} \frac{\langle 0|J_y|n\rangle \langle n|J_x|0\rangle - \langle 0|J_x|n\rangle \langle n|J_y|0\rangle}{(E_n - E_0)^4} \\
& + \dots
\end{aligned} \tag{E.2}$$

The first term and all odd order terms vanish, because of the gauge-invariance. Alternatively, it can quickly be seen by rotation-invariance which ensures that the expression should be invariant under  $x \rightarrow y$  and  $y \rightarrow -x$ .

For a simple Chern insulator, the single particle Hamiltonian in the momentum space as

$$H(\mathbf{k}) = \vec{d}(\mathbf{k}) \cdot \vec{\sigma} \tag{E.3}$$

with

$$\begin{aligned}
d_1(\mathbf{k}) &= \sin(k_x); \\
d_2(\mathbf{k}) &= \sin(k_y); \\
d_3(\mathbf{k}) &= 2 - m - \cos(k_x) - \cos(k_y)
\end{aligned} \tag{E.4}$$

, where the  $\vec{\sigma}$  is the Pauli matrices. After simplifying, we can write the DC conductivity as

$$\sigma_{xy} = \frac{e^2}{(2\pi)^2} \int_{\mathbf{T}_2} d^2k \mathcal{F}_{xy} \tag{E.5}$$

and the second-order conductivity as

$$\sigma_{xy}^{(2)}(\omega) = \omega^2 \frac{e^2}{(2\pi)^2} \int_{\mathbf{T}_2} d^2k \frac{\mathcal{F}_{xy}}{(E_+ - E_-)^2} \quad (\text{E.6})$$

with the Berry curvature

$$\mathcal{F}_{xy} = \frac{\partial \mathcal{A}_x}{\partial k_y} - \frac{\partial \mathcal{A}_y}{\partial k_x} \quad (\text{E.7})$$

and the Berry connection

$$\mathcal{A}_i = i \langle -, k | \frac{\partial}{\partial k_i} | -, k \rangle. \quad (\text{E.8})$$

, where the state  $|-, k\rangle$  is the lower energy eigenstate. Actually, the integral in the DC conductivity is related to the Chern number, which is an integer universally. This is just the famous quantized Hall conductivity of the Chern insulator. However, the second-order conductivity cannot be related to the Chern number. In the following, we will show the numerical result of this second-order conductivity. Based on the Hamiltonian of the simple Chern insulator, the Berry curvature can be analytically computed and be written as

$$\mathcal{F}_{\mu\nu} = -\frac{1}{2} \epsilon_{\alpha\beta\gamma} \hat{d}_\alpha \partial_{k_\mu} \hat{d}_\beta \partial_{k_\nu} \hat{d}_\gamma \quad (\text{E.9})$$

with  $\hat{d}_\alpha(\mathbf{k}) = d_\alpha(\mathbf{k})/d(\mathbf{k})$ . Hence, we have the expression for  $\mathcal{F}_{xy}$ ,

$$\mathcal{F}_{xy} = \frac{\cos k_y + \cos k_x [1 + (-2 + m) \cos k_y]}{2 [(-2 + m + \cos k_x + \cos k_y)^2 + \sin^2 k_x + \sin^2 k_y]^{3/2}}. \quad (\text{E.10})$$

The numerical results of the second-order conductivity are shown in Fig.E.1. The second-order conductivity is not zero or quantized. It is non-universal.

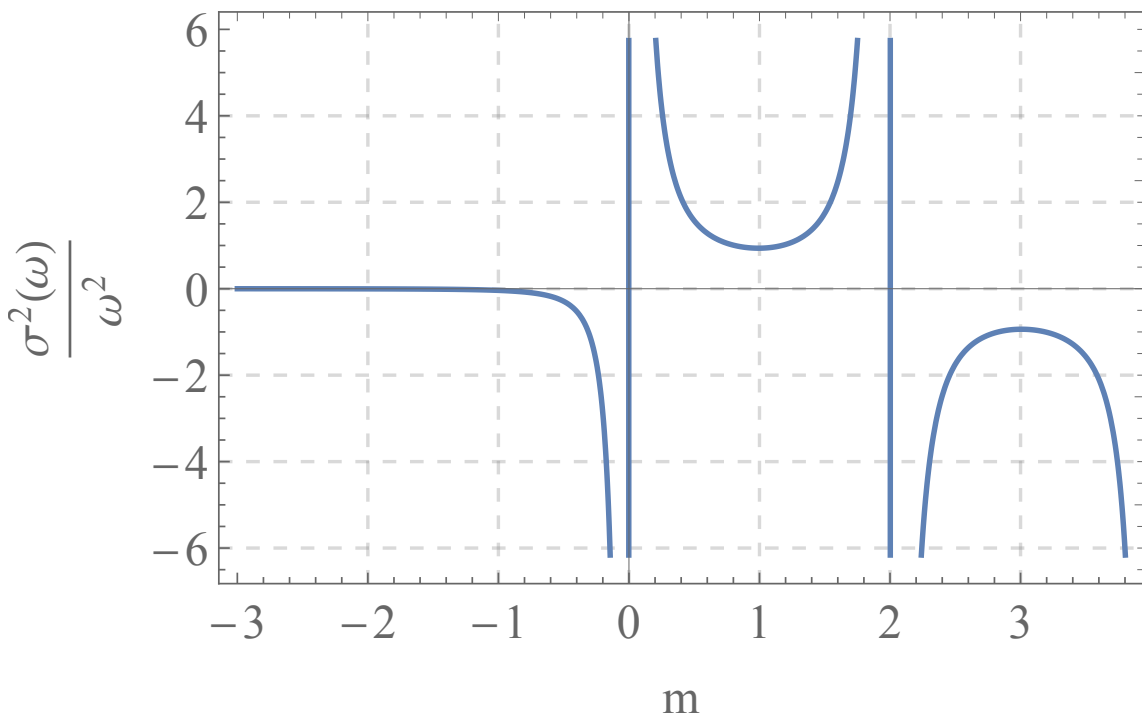


Figure E.1: The second order conductivity  $\sigma_{xy}^{(2)}$  v.s. the parameter  $m$ . It is not quantized and non-universal

## Bibliography

- [1] S. Wang and J. D. Sau, Interaction robustness of the chiral anomaly in weyl semimetals and luttinger liquids from a mixed anomaly approach, [arXiv:2401.09409 \(2024\)](#).
- [2] J. D. Sau and S. Wang, Theory of anomalous hall effect from screened vortex charge in a phase disordered superconductor, [arXiv:2411.08969 \(2024\)](#).
- [3] M. Z. Hasan and C. L. Kane, Colloquium: topological insulators, *Rev. Mod. Phys.* **82**, 3045 (2010).
- [4] X.-L. Qi and S.-C. Zhang, Topological insulators and superconductors, *Rev. Mod. Phys.* **83**, 1057 (2011).
- [5] K. v. Klitzing, G. Dorda, and M. Pepper, New method for high-accuracy determination of the fine-structure constant based on quantized hall resistance, *Phys. Rev. Lett.* **45**, 494 (1980).
- [6] D. J. Thouless, M. Kohmoto, M. P. Nightingale, and M. den Nijs, Quantized hall conductance in a two-dimensional periodic potential, *Phys. Rev. Lett.* **49**, 405 (1982).
- [7] D. Xiao, M.-C. Chang, and Q. Niu, Berry phase effects on electronic properties, *Rev. Mod. Phys.* **82**, 1959 (2010).
- [8] N. P. Armitage, E. J. Mele, and A. Vishwanath, Weyl and dirac semimetals in three-dimensional solids, *Rev. Mod. Phys.* **90**, 015001 (2018).
- [9] D. T. Son and B. Z. Spivak, Chiral anomaly and classical negative magnetoresistance of weyl metals, *Phys. Rev. B* **88**, 104412 (2013).
- [10] S. L. Adler, Axial-vector vertex in spinor electrodynamics, *Phys. Rev.* **177**, 2426 (1969).
- [11] J. Bell and R. Jackiw, A pcac puzzle:  $\pi^0 \rightarrow \gamma\gamma$  in the  $\sigma$ -model, *Il Nuovo Cimento A* **60**, 47 (1969).
- [12] A. Burkov, Weyl metals, *Annu. Rev. Condens. Mat. Phys.* **9**, 359 (2018).
- [13] N. Nagaosa, J. Sinova, S. Onoda, A. H. MacDonald, and N. P. Ong, *Anomalous hall effect*, *Rev. Mod. Phys. Vol. 82*, pp. 1539–1592 (2010).
- [14] Y. Cao, V. Fatemi, A. Demir, S. Fang, S. L. Tomarken, J. Y. Luo, J. D. Sanchez-Yamagishi, K. Watanabe, T. Taniguchi, E. Kaxiras, R. C. Ashoori, and P. Jarillo-Herrero, Correlated insulator behaviour at half-filling in magic-angle graphene superlattices, *Nature* **556**, 80 (2018).

- [15] Y. Cao, V. Fatemi, S. Fang, K. Watanabe, T. Taniguchi, E. Kaxiras, and P. Jarillo-Herrero, Unconventional superconductivity in magic-angle graphene superlattices, *Nature* **556**, 43 (2018).
- [16] M. Yankowitz, S. Chen, H. Polshyn, Y. Zhang, K. Watanabe, T. Taniguchi, D. Graf, A. F. Young, and C. R. Dean, Tuning superconductivity in twisted bilayer graphene, *Science* **363**, 1059 (2019).
- [17] X. Lu, P. Stepanov, W. Yang, M. Xie, M. A. Aamir, I. Das, C. Urgell, K. Watanabe, T. Taniguchi, G. Zhang, A. Bachtold, A. H. MacDonald, and D. K. Efetov, Superconductors, orbital magnets and correlated states in magic-angle bilayer graphene, *Nature* **574**, 653 (2019).
- [18] Z. Hao, A. M. Zimmerman, P. Ledwith, E. Khalaf, D. H. Najafabadi, K. Watanabe, T. Taniguchi, A. Vishwanath, and P. Kim, Electric field-tunable superconductivity in alternating-twist magic-angle trilayer graphene, *Science* **371**, 1133 (2021).
- [19] J. M. Park, Y. Cao, K. Watanabe, T. Taniguchi, and P. Jarillo-Herrero, Tunable strongly coupled superconductivity in magic-angle twisted trilayer graphene, *Nature* **590**, 249 (2021).
- [20] Y. Cao, J. M. Park, K. Watanabe, T. Taniguchi, and P. Jarillo-Herrero, Pauli-limit violation and re-entrant superconductivity in moiré graphene, *Nature* **595**, 526 (2021).
- [21] X. Liu, N. J. Zhang, K. Watanabe, T. Taniguchi, and J. I. A. Li, Isospin order in superconducting magic-angle twisted trilayer graphene, *Nature Physics* **18**, 522 (2022).
- [22] Y. Zhang, R. Polski, C. Lewandowski, A. Thomson, Y. Peng, Y. Choi, H. Kim, K. Watanabe, T. Taniguchi, J. Alicea, F. von Oppen, G. Refael, and S. Nadj-Perge, Ascendance of superconductivity in magic-angle graphene multilayers, [arXiv:2112.09270](https://arxiv.org/abs/2112.09270) (2021).
- [23] J. M. Park, Y. Cao, L. Xia, S. Sun, K. Watanabe, T. Taniguchi, and P. Jarillo-Herrero, Magic-angle multilayer graphene: a robust family of moiré superconductors, [arXiv:2112.10760](https://arxiv.org/abs/2112.10760) (2021).
- [24] G. W. Burg, E. Khalaf, Y. Wang, K. Watanabe, T. Taniguchi, and E. Tutuc, Emergence of correlations in alternating twist quadrilayer graphene, *Nature Materials* **21**, 884 (2022).
- [25] H. Zhou, T. Xie, A. Ghazaryan, T. Holder, J. R. Ehrets, E. M. Spanton, T. Taniguchi, K. Watanabe, E. Berg, M. Serbyn, and A. F. Young, Half- and quarter-metals in rhombohedral trilayer graphene, *Nature* **598**, 429 (2021).
- [26] H. Zhou, T. Xie, T. Taniguchi, K. Watanabe, and A. F. Young, Superconductivity in rhombohedral trilayer graphene, *Nature* **598**, 434 (2021).
- [27] H. Zhou, L. Holleis, Y. Saito, L. Cohen, W. Huynh, C. L. Patterson, F. Yang, T. Taniguchi, K. Watanabe, and A. F. Young, Isospin magnetism and spin-polarized superconductivity in bernal bilayer graphene, *Science* **375**, 774 (2022).
- [28] T. Han, Z. Lu, Y. Yao, L. Shi, J. Yang, J. Seo, S. Ye, Z. Wu, M. Zhou, H. Liu, G. Shi, Z. Hua, K. Watanabe, T. Taniguchi, P. Xiong, L. Fu, and L. Ju, Signatures of chiral superconductivity in rhombohedral graphene, *Nature* **643**, 654 (2025).

- [29] T. Han, Z. Lu, G. Scuri, J. Sung, J. Wang, T. Han, K. Watanabe, T. Taniguchi, H. Park, and L. Ju, Correlated insulator and chern insulators in pentalayer rhombohedral-stacked graphene, *Nature Nanotechnology* **19**, 181 (2024).
- [30] Y.-Z. Chou, J. Zhu, and S. Das Sarma, Intravalley spin-polarized superconductivity in rhombohedral tetralayer graphene, *Phys. Rev. B* **111**, 174523 (2025).
- [31] M. Geier, M. Davydova, and L. Fu, Chiral and topological superconductivity in isospin polarized multilayer graphene, [arXiv:2409.13829](https://arxiv.org/abs/2409.13829) (2024).
- [32] C. Kallin, *Chiral superconductors*, *Reports on Progress in Physics* Vol. 79, p. 054502 (2016).
- [33] M. Kim, A. Timmel, L. Ju, and X.-G. Wen, Topological chiral superconductivity, [arXiv:2409.18067](https://arxiv.org/abs/2409.18067) (2024).
- [34] Z. D. Shi and T. Senthil, Doping a fractional quantum anomalous hall insulator, [arXiv:2409.20567](https://arxiv.org/abs/2409.20567) (2024).
- [35] R. Karplus and J. Luttinger, Hall effect in ferromagnetics, *Phys. Rev.* **95**, 1154 (1954).
- [36] T. Jungwirth, Q. Niu, and A. MacDonald, Anomalous hall effect in ferromagnetic semiconductors, *Phys. Rev. Lett.* **88**, 207208 (2002).
- [37] F. Haldane, Berry curvature on the fermi surface: anomalous hall effect as a topological fermi-liquid property, *Phys. Rev. Lett.* **93**, 206602 (2004).
- [38] S. Peotta and P. Törmä, Superfluidity in topologically nontrivial flat bands, *Nature Communications* **6**, 8944 (2015).
- [39] L. Liang, T. I. Vanhala, S. Peotta, T. Siro, A. Harju, and P. Törmä, Band geometry, berry curvature, and superfluid weight, *Phys. Rev. B* **95**, 024515 (2017).
- [40] J. S. Hofmann, E. Berg, and D. Chowdhury, Superconductivity, pseudogap, and phase separation in topological flat bands, *Phys. Rev. B* **102**, 201112 (2020).
- [41] P. Törmä, S. Peotta, and B. A. Bernevig, Superconductivity, superfluidity and quantum geometry in twisted multilayer systems, *Nature Reviews Physics* **4**, 528 (2022).
- [42] J. Herzog-Arbeitman, A. Chew, K.-E. Huhtinen, P. Törmä, and B. A. Bernevig, Many-body superconductivity in topological flat bands, [arXiv:2209.00007](https://arxiv.org/abs/2209.00007) (2022).
- [43] K. E. Huhtinen, J. Herzog-Arbeitman, A. Chew, B. A. Bernevig, and P. Törmä, Revisiting flat band superconductivity: dependence on minimal quantum metric and band touchings, *Phys. Rev. B* **106**, 014518 (2022).
- [44] D. Mao and D. Chowdhury, Diamagnetic response and phase stiffness for interacting isolated narrow bands, *Proc. Natl. Acad. Sci. U.S.A.* **120**, e2217816120 (2023).
- [45] J. S. Hofmann, E. Berg, and D. Chowdhury, Superconductivity, charge density wave, and supersolidity in flat bands with a tunable quantum metric, *Phys. Rev. Lett.* **130**, 226001 (2023).
- [46] M. V. Berry, Quantal phase factors accompanying adiabatic changes, *Proc. R. Soc. A* **392**, 45 (1984).

- [47] S.-C. Zhang and J. Hu, A four-dimensional generalization of the quantum hall effect, [Science](#) **294**, 823 (2001).
- [48] X. Wan, A. M. Turner, A. Vishwanath, and S. Y. Savrasov, Topological semimetal and fermi-arc surface states in the electronic structure of pyrochlore iridates, [Phys. Rev. B](#) **83**, 205101 (2011).
- [49] K. S. Novoselov, a K Geim, S. V. Morozov, D. Jiang, Y. Zhang, S. V. Dubonos, I. V. Grigorieva, and a a Firsov, Discover of graphene: electric field effect in atomically thin carbon films. [Science](#) **306**, 5696 (2004).
- [50] M. Peskin and D. Schroeder, *An introduction to quantum field theory (frontiers in physics)* (CRC Press, 2015).
- [51] D. V. Else, R. Thorngren, and T. Senthil, Non-fermi liquids as ersatz fermi liquids: general constraints on compressible metals, [Phys. Rev. X](#) **11**, 021005 (2021).
- [52] H. B. Nielsen and M. Ninomiya, The adler-bell-jackiw anomaly and weyl fermions in a crystal, [Phys. Lett. B](#) **130**, 389 (1983).
- [53] A. Burkov, Chiral anomaly and transport in weyl metals, [J. Phys.: Condens. Matter](#) **27**, 113201 (2015).
- [54] H. Georgi and J. M. Rawls, Anomalies of the axial-vector current in two dimensions, [Phys. Rev. D](#) **3**, 874 (1971).
- [55] C. R. Hagen, New solutions of the thirring model, [Il Nuovo Cimento B](#) **51**, 169 (1967).
- [56] S. S. Shei, Anomaly of the axial-vector current in one space and one time dimension, [Phys. Rev. D](#) **6**, 3469 (1972).
- [57] M. A. Stephanov and Y. Yin, Chiral kinetic theory, [Phys. Rev. Lett.](#) **109**, 162001 (2012).
- [58] D. T. Son and N. Yamamoto, Berry curvature, triangle anomalies, and the chiral magnetic effect in fermi liquids, [Phys. Rev. Lett.](#) **109**, 181602 (2012).
- [59] S. L. Adler and W. A. Bardeen, Absence of higher-order corrections in the anomalous axial-vector divergence equation, [Phys. Rev.](#) **182**, 1517 (1969).
- [60] X.-G. Wen, *Quantum field theory of many-body systems: from the origin of sound to an origin of light and electrons* (OUP Oxford, 2004).
- [61] A. Avdoshkin, V. Kozii, and J. E. Moore, Interactions remove the quantization of the chiral photocurrent at weyl points, [Phys. Rev. Lett.](#) **124**, 196603 (2020).
- [62] C. Rylands, A. Parhizkar, A. A. Burkov, and V. Galitski, Chiral anomaly in interacting condensed matter systems, [Phys. Rev. Lett.](#) **126**, 185303 (2021).
- [63] A. Parhizkar, C. Rylands, and V. Galitski, Path integral approach to quantum anomalies in interacting models, [Phys. Rev. B](#) **109**, 155109 (2024).
- [64] J. Lee, J. Pixley, and J. D. Sau, Chiral anomaly without landau levels: from the quantum to the classical regime, [Phys. Rev. B](#) **98**, 245109 (2018).
- [65] P. Goswami, J. Pixley, and S. D. Sarma, Axial anomaly and longitudinal magnetoresistance of a generic three-dimensional metal, [Phys. Rev. B](#) **92**, 075205 (2015).

- [66] S. Parameswaran, T. Grover, D. Abanin, D. Pesin, and A. Vishwanath, Probing the chiral anomaly with nonlocal transport in three-dimensional topological semimetals, [Phys. Rev. X \*\*4\*\*, 031035 \(2014\)](#).
- [67] J. Avron, L. Sadun, J. Segert, and B. Simon, Topological invariants in fermi systems with time-reversal invariance, [Phys. Rev. Lett. \*\*61\*\*, 1329 \(1988\)](#).
- [68] X.-L. Qi, Y.-S. Wu, and S.-C. Zhang, Topological quantization of the spin hall effect in two-dimensional paramagnetic semiconductors, [Phys. Rev. B \*\*74\*\*, 085308 \(2006\)](#).
- [69] V. M. Yakovenko, Theory of the high-frequency chiral optical response of a  $p_x + ip_y$  superconductor, [Phys. Rev. Lett. \*\*98\*\*, 087003 \(2007\)](#).
- [70] V. Mineev, Broken time-reversal symmetry in the superconducting state of  $\text{Sr}_2\text{RuO}_4$ , [Phys. Rev. B \*\*76\*\*, 212501 \(2007\)](#).
- [71] J. Goryo, Vortex with fractional quantum numbers in a chiral p-wave superconductor, [Phys. Rev. B \*\*61\*\*, 4222 \(2000\)](#).
- [72] R. M. Lutchyn, P. Nagornykh, and V. M. Yakovenko, Gauge-invariant electromagnetic response of a chiral  $p_x + ip_y$  superconductor, [Phys. Rev. B \*\*77\*\*, 144516 \(2008\)](#).
- [73] R. Roy and C. Kallin, Collective modes and electromagnetic response of a chiral superconductor, [Phys. Rev. B \*\*77\*\*, 174513 \(2008\)](#).
- [74] T. Giamarchi, *Quantum physics in one dimension* (Oxford university Press, 2007).
- [75] K. Fujikawa, Path integral for gauge theories with fermions, [Phys. Rev. D \*\*21\*\*, 2848 \(1980\)](#).
- [76] A. Diaz, W. Troost, P. V. Nieuwenhuizen, and A. V. Proeyen, Understanding fujikawa regulators from pauli-villars regularization of ghost loops, [Int. J. Mod. Phys. A \*\*04\*\*, 3959 \(1989\)](#).
- [77] M. Stone, *Bosonization* (World Scientific, 1994).
- [78] S. Coleman, Quantum sine-gordon equation as the massive thirring model, [Phys. Rev. D \*\*11\*\*, 2088 \(1975\)](#).
- [79] J. Von Delft and H. Schoeller, Bosonization for beginners—refermionization for experts, [Annalen der Physik \*\*510\*\*, 225 \(1998\)](#).
- [80] S. Mandelstam, Soliton operators for the quantized sine-gordon equation, [Phys. Rev. D \*\*11\*\*, 3026 \(1975\)](#).
- [81] M. Cheng and N. Seiberg, Lieb-schultz-mattis, luttinger, and 't hooft - anomaly matching in lattice systems, [SciPost Phys. \*\*15\*\*, 051 \(2023\)](#).
- [82] M. Oshikawa, Commensurability, excitation gap, and topology in quantum many-particle systems on a periodic lattice, [Phys. Rev. Lett. \*\*84\*\*, 1535 \(2000\)](#).
- [83] G. Y. Cho, C. T. Hsieh, and S. Ryu, Anomaly manifestation of lieb-schultz-mattis theorem and topological phases, [Phys. Rev. B \*\*96\*\*, 195105 \(2017\)](#).
- [84] C. Wang, A. Hickey, X. Ying, and A. Burkov, Emergent anomalies and generalized luttinger theorems in metals and semimetals, [Phys. Rev. B \*\*104\*\*, 235113 \(2021\)](#).
- [85] J. M. Luttinger, Fermi surface and some simple equilibrium properties of a system of interacting fermions, [Phys. Rev. \*\*119\*\*, 1153 \(1960\)](#).

- [86] K. B. Blagoev and K. S. Bedell, Luttinger theorem in one dimensional metals, *Phys. Rev. Lett.* **79**, 1106 (1997).
- [87] L. A. Cohen, N. L. Samuelson, T. Wang, T. Taniguchi, K. Watanabe, M. P. Zaletel, and A. F. Young, Universal chiral luttinger liquid behavior in a graphene fractional quantum hall point contact, *Science* **382**, 542 (2023).
- [88] S. N. Thomas and J. D. Sau, Quantum hall transformer in a quantum point contact over the full range of transmission, [arXiv:2406.17778](https://arxiv.org/abs/2406.17778) (2024).
- [89] N. P. Sandler, C. C. de Chamon, and E. Fradkin, Andreev reflection in the fractional quantum hall effect, *Phys. Rev. B* **57**, 12324 (1998).
- [90] D. B. Chklovskii and B. I. Halperin, Consequences of a possible adiabatic transition between  $\nu = 1/3$  and  $\nu = 1$  quantum hall states in a narrow wire, *Phys. Rev. B* **57**, 3781 (1998).
- [91] T. L. Hughes and Y. Wang, Gapless fermionic systems as phase-space topological insulators: nonperturbative results from anomalies, *Phys. Rev. B* **110**, L121119 (2024).
- [92] T. D. Bevan, A. J. Manninen, J. B. Cook, J. R. Hook, H. E. Hall, T. Vachaspati, and G. E. Volovik, Momentum creation by vortices in superfluid  $^3\text{He}$  as a model of primordial baryogenesis, *Nature* **386**, 689 (1997).
- [93] F. D. Haldane, Berry curvature on the fermi surface: anomalous hall effect as a topological fermi-liquid property, *Phys. Rev. Lett.* **93**, 206602 (2004).
- [94] C. Duval, Z. Horváth, P. A. Horváthy, L. Martina, and P. C. Stichel, Berry phase correction to electron density in solids and "exotic" dynamics, *Mod. Phys. Lett. B* **20**, 373 (2006).
- [95] D. Xiao, J. Shi, and Q. Niu, Berry phase correction to electron density of states in solids, *Phys. Rev. Lett.* **95**, 137204 (2005).
- [96] M. Vazifeh and M. Franz, Electromagnetic response of weyl semimetals, *Phys. Rev. Lett.* **111**, 027201 (2013).
- [97] N. W. Ashcroft and N. D. Mermin, *Solid state physics* (Cengage Learning, 2022).
- [98] Y. Chen, S. Wu, and A. Burkov, Axion response in weyl semimetals, *Phys. Rev. B* **88**, 125105 (2013).
- [99] Y. Alavirad and J. D. Sau, Role of boundary conditions, topology, and disorder in the chiral magnetic effect in weyl semimetals, *Phys. Rev. B* **94**, 115160 (2016).
- [100] J. Ma and D. Pesin, Chiral magnetic effect and natural optical activity in metals with or without weyl points, *Phys. Rev. B* **92**, 235205 (2015).
- [101] S. Zhong, J. E. Moore, and I. Souza, Gyrotropic magnetic effect and the magnetic moment on the fermi surface, *Phys. Rev. Lett.* **116**, 077201 (2016).
- [102] P. Minnhagen, The two-dimensional coulomb gas, vortex unbinding, and superfluid-superconducting films, *Rev. Mod. Phys.* **59**, 1001 (1987).
- [103] J. Bardeen and M. Stephen, Theory of the motion of vortices in superconductors, *Phys. Rev.* **140**, A1197 (1965).

- [104] A. Altland and B. D. Simons, *Condensed matter field theory* (Cambridge university press, 2010).
- [105] J. R. Schrieffer, *Theory of superconductivity* (CRC press, 2018).
- [106] P. Brydon, D. S. Abergel, D. Agterberg, and V. M. venko, Loop currents and anomalous hall effect from time-reversal symmetry-breaking superconductivity on the honeycomb lattice, *Phys. Rev. X* **9**, 031025 (2019).
- [107] P. Streda, Theory of quantised hall conductivity in two dimensions, *J. Phys. C: Solid State Phys.* **15**, L717 (1982).
- [108] D. Ariad, Y. Avishai, and E. Grosfeld, How vortex bound states affect the hall conductivity of a chiral  $p_x \pm ip_y$  superconductor, *Phys. Rev. B* **98**, 104511 (2018).
- [109] S. Raghu, D. Podolsky, A. Vishwanath, and D. A. Huse, Vortex-dynamics approach to the nernst effect in extreme type-ii superconductors dominated by phase fluctuations, *Phys. Rev. B* **78**, 184520 (2008).
- [110] Z. Wang and S. C. Zhang, Simplified topological invariants for interacting insulators, *Phys. Rev. X* **2**, 031008 (2012).
- [111] Y. Yao, L. Kleinman, A. H. MacDonald, J. Sinova, T. Jungwirth, D.-s. Wang, E. Wang, and Q. Niu, First principles calculation of anomalous hall conductivity in ferromagnetic bcc fe, *Phys. Rev. Lett.* **92**, 037204 (2004).
- [112] S. Tewari, C. Zhang, V. M. Yakovenko, and S. Das Sarma, Time-reversal symmetry breaking by a  $(d + id)$  density-wave state in underdoped cuprate superconductors, *Phys. Rev. Lett.* **100**, 217004 (2008).
- [113] S. S. Pershoguba and V. M. Yakovenko, Optical control of topological memory based on orbital magnetization, *Phys. Rev. B* **105**, 064423 (2022).